DOE/ER-0046/20

Damage Analysis and Fundamental Studies

Quarterly Progress Report
October-December 1984

February 1985

U.S. Department of Energy
Office of Energy Research
Office of Fusion Energy
Washington, DC 20545
B&R No. AT-15-02-03-04

NOTICE

Printed in the United States of America
Available from
National Technical Information Service
U.S. Department of Commerce
5285 Port Royal Road
Springfield, VA 22161

NTIS price codes
Printed copy: A06
Microfiche copy: A01

DOE/ER-0046/20
uc-20-2oc

Damage Analysis and Fundamental Studies

Quarterly Progress Report
October-December 1984

February 1985

U.S. Department of Energy
Office of Energy Research
Office of Fusion Energy
Washington, DC 20545
B&R No. **AT-15.02-03-04**

FOREWORD

This report is the twenty-eighth in a series of Quarterly Technical Progress Reports on *Damage Analysis and Fundamental Studies* (DAFS), which is one element of the Fusion Reactor Materials Program, conducted in support of the Magnptic Fusion Energy Program of the U.S. Department of Energy (DOE). The first eight reports in this series were numbered DOE/ET-0065/1 through 8. Other elements of the Fusion Materials Program are:

- Alloy Uevelopment for Irradiation Performance (ADIP)
- Plasma-Materials Interaction (PMI)
- Special Purpose Materials (SPM).

The DAFS program element is a national effort composed of contributions from a number of National Laboratories and other government lahoratories, universities, and industrial laboratories. It was organized by the Materials and Radiation Effects Branch, DOE/Office of Fusion Energy, and a Task Group on *Damage Analysis and Fundamental Studies,* which operates under the auspices of that branch. The purpose of this series of reports is to provide a workinq technical record of that effort for the use of the program participants, the fusion energy program in general, and the DOE.

This report is orqanized along topical lines in parallel to a Program Plan of the same title so that activities and accomplishments may he followed readily, relative to that Program Plan. Thus, the work of a given laboratory may appear throughout the report. A chapter has been added on Reduced Activation Materials to accommodate work on a topic not included in the early program plan. The Contents is annotated for the convenience of the reader.

This report has been compiled and edited by N. E. Kenny under the guidance of the Chairman of the Task Group on *Damage Analysis and Fundamental Studies,* D. G. Doran, Hanford Engineerinq Development Laboratory (HEDL). Their efforts, those of the supporting staff of HEOL, and the many persons who made technical contributions are gratefully acknowledged. T. C. Reuther, Fusion Technologies Branch, is the DOE counterpart to the Task Group Chairman and has responsibility for the DAFS program within DOE.

G. M. Haas, Chief
Fusion Technologies Branch
Office of Fusion Energy

CONTENTS

CONTENTS (Cont'd)

CHAPTER 1

IRRADIATION TEST FACILITIES

RTNS-II IRRADIATIONS AND OPERATIONS

C.M. Logan and D. W. Heikkinen
Lawrence Livermore National Laboratory

1.0 Objective

The objectives of this work are operation of RTNS-II (a 14-MeV neutron source facility), machine development, and support of the experimental program that utilizes this facility. Experimenter services include dosimetry, handling, scheduling, coordination, and reporting. RTNS-II is supported jointly by the U.S. and Japan and is dedicated to materials research for the fusion power program. Its primary use is to aid in the development of models of high-energy neutron effects. Such models are needed in interpreting and projecting to the fusion environment, engineering data obtained in other spectra.

2.0 Summary

Irradiations were performed on 13 different experiments during this quarter. The new materials lab has been completed. Target vacuum system modifications were begun on the right and left machines. Clint Logan will be transferring from RTNS-II in January 1985. Dale Heikkinen has been appointed Acting Manager as of January 7, 1985. The Fifth U.S.-Japan Steering Committee meting was held December 13, 1984 in Tokyo, Japan.

3.0 Program

Title: RTNS-II operations (WZJ-16)
Principal Investigator: C. M. Logan
Affiliation: Lawrence Livermore National Laboratory

4.0 Relevant DAFs Program Plan Task/Subtask

TPSK II.A.2,3,4.
TASK II.B.3,4
TPSK II.C.1,2,6,11,18.

5.0 Irradiation - C. M. Logan, D. W. Heikkinen and M. W. Guinan

During this quarter, irradiations (both dedicated and add-on) were done for the following people.

Experimenter	P OR A*	Sample Irradiated
R. Smither (ANL)	A	Al - the $^{27}Al(n,2n)^{26}Al$ cross section near threshold
D. Heikkinen (LLNL)	A	Nb - dosimetry calibration
N. Yoshida (Kyushu) H. Matsui (Tohoku) K. Abe (Tohoku) M. Kiritani (Hokkaido) H. Takahashi (Hokkaido) S. Ishino (Tokyo) A. Kohyama (Tokyo) K. Miyahara (Tokyo) Y. Shimomura (Hiroshima) H. Yoshida (Kyoto) C. Kinoshita (Kyushu) E. Kuramoto (Kyushu)	P	Metals - displacement damage & mechanical properties. Irradiation at 475°C and 550°C
H. Matsui (Tohoku) and M. Guinan (LLNL) M. Kiritani (Hokkaido) H. Takahashi (Hokkaido) H. Kayano (Tohoku) K. Abe (Tohoku)	P	Metals - cascade and microstructural damages - low temperature experiment

Experimenter	P or A*	Sample Irradiated
Matsui/Guinan Cont'd. A. Kohyama (Tokyo) S. Nanao (Tokyo) H. Kawanishi (Tokyo) M. Iseki (Nagoya) Y. Shimomura (Hiroshima) N. Yoshida (Kyushu) E. Kuramoto (Kyushu)		
R. Haight (LLNL)	A	Ni - Activation for dosimetry intercomparison
N. Smith (LLNL)	A	^{121}Sb & ^{123}Sb - Activation products for calibration of detectors
N. Yoshida (Kyushu)	A	Cu, Fe & Au - Long term rearrangement of cascade defects
N. Yoshida (Kyushu)	A	Au, Cu, Ni, Mo and Fe - Observe three dimensional structure of an individual cascade
Y. Shimomura (Hiroshima)	A	Cu, Au, Ag, Ni and Mo - Structure of cascade damage
C. Kinoshita (Kyushu) K. Shinohara (Kyushu) M. Kiritani (Hokkaido) K. Okamura (Tohoku) T. Iseki (TIT) M. Iseki (Nagoya) H. Matsui (Nagoya) K. Saka (Nagoya) S. Iwmta (Osaka) M. Nakagawa (Kyoto) K. Futagami (Miyazaki)	P	Ceramics - Cascade structure and their stability
P. Pawlikowski (LLNL) G. Coleman (LLNL)	P	(n,2n) cross section
H. Matsui (Nagoya)	A	Li_2O - Radiation damage
M. Kiritani (Hokkaido)	A	Au, Al, Fe, Ni, Cu and SS Mechanical properties and deformtion structure

*P - primary, A = Add-on

5.1 RTNS-II Stat - M. D. W. Heikkinen

The vertical turbo pumps in the target rooms are being replaced with Balzer's turbo pumps as part of the vacuum system modification.

The left machine's target controller has been upgraded and now operates under LSI-11 control.

A new ion source control panel was installed on the right mchine.

The target differential pumps have been included on the emergency power system.

The target chilled water system has undergone extensive maintenance and the bypass system is being upgraded.

6.0 Future Work

Irradiations will be continued for Pawlikowski/Coleman (LLNL), D. Heikkinen (LLNL), P. Cannon (HEDL), C. Snead (BNL)/M. Guinan (LLNL) and R. Flukiger (Karlsruhe)/M. Guinan (LLNL). Also during this period, irradiations for M. Guinan (LLNL), R Borg (LLNL), J. Huang/M. Guinan (LLNL), R. Hartman (Northrop), M. Nakazawa (Tokyo), S. Iwasaki (Tohoku), H. Heinisch (HEDL)/H. Matsui (Tohoku)/N. Yoshida (Kyushu) and E. Kuramoto (Kyushu) will be initiated.

The modifications to both neutron source vacuum System and to the target chilled water system will extend into the next quarter.

CHAPTER 2

DOSIMETRY AND DAMAGE PARAMETERS

SPINEL IRRADIATIONS IN THE OMEGA WEST REACTOR

L. R. Greenwood (Argonne National Laboratory)

1.0 Objective

To characterize neutron irradiation experiments in terms of neutron fluence, spectra, and damage parameters (dpa, gas generation, transmutation).

2.0 Summary

Dosimetry measurements and damage calculations have been completed for several short irradiations of spinel in the Omega West Reactor at Los Alamos National Laboratory. The longest irradiation had a fluence of 7.8 x 10^{18} n/cm^2 producing 3.8 x 10^8 neutron rads in spinel. The status of all other experiments is summarized in Table I.

TABLE I

STATUS OF DOSIMETRY EXPERIMENTS

	Facility/Experiment	Status/Comments
ORR	- MFE 1	Completed 12/79
	- MFE 2	Completed 06/81
	- MFE 4A1	Completed 12/81
	- MFE 4A2	Completed 11/82
	- MFE 48	Completed 04/84
	- TBC 07	Completed 07/80
	- TRIO-Test	Completed 07/82
	- TRIO-I	Completed 12/83
	- Hf Test	Completed 03/84
	- JP Test	Samples Sent 06/84
HFIR	- CTR 32	Completed 04/82
	- CTR 31, 34, 35	Completed 04/83
	- T2, RB1	Completed 09/83
	- T1, CTR 39	Completed 01/84
	- CTR 40-45	Completed 09/84
	- CTR 30, 36, 46	Samples Received 11/84
	- RB2, T3	Samples Received 11/84
	- CTR 47-56	Irradiations in Progress
	- JP 1-8	Irradiations in Progress
Omega West	- Spectral Analysis	Completed 10/80
	- HEDL1	Completed 05/81
	- HEDL2	Samples Sent 05/83
	- LANL 1	Completed 08/84
EBR II	- X287	Completed 09/81
IPNS	- Soectral Analysis	Completed 01/82
	- LANL1 (Hurley)	Completed 06/82
	- Hurley	Completed 02/83
	- Coltman	Completed 08/83

3.0 Program

Title: Dosimetry and Damage Analysis
Principal Investigator: L. R. Greenwood
Affiliation: Argonne National Laboratory

4.0 Relevant OAFS Program Plan Task/Subtask

Task II.A.I Fission Reactor Dosimetry

5.0 Accomplishments and Status

Dosimetry measurements and damage calculations have been completed for three short irradiations of spinel ($MgAl_2O_4$) by William Coghlan (Arizona State University1 and Frank Clinard (Los Alamos National Laboratory) using the Omega West Reactor (OWR) at LANL. This reactor has been studied previously and measurements in core position 4-F have been reported earlier.[1] The present irradiations were conducted in the hydraulic rabbit tube near the center of the reactor in core position 3E. The longest irradiation lasted 7.55 hours on June 15, 1984, with an accumulated exposure of 59.61 MWH. For this experiment, Fe, Ni, Ti, 0.1% Co-Al, 80% Mn-Cu, and Al dosimeters were used. The measured activation rates are listed in Table II. These activities were then used to adjust the neutron spectrum measured previously1 usinq the STAY'SL computer code. The adjusted flux and fluence values are listed in Table III. The spectrum is shown in Fig. 1 and compared to our previously measured spectrum in core position 4F.[1] As can be seen, the flux in the rabbit tube is considerably higher, partly due to less attenuating material and partly due to an apparent flux gradient in the reactor.

TABLE II

ACTIVATION RATES IN THE OMEGA WEST REACTOR
(Rabbit tube - 59.6 MWH - Norm. to 8 MW)
Values accurate to 2% unless noted.

Reaction	Activation Rate (atom/atom-s)
$^{59}Fe(n,\gamma)^{59}Fe$	1.38 x 10-10
$^{59}Co(n,\gamma)^{60}Co$	4.46 x 10-9 (dilute Co)
$^{63}Cu(n,\gamma)^{64}Cu$	5.23 x 10-10 (±10%)
$^{54}Fe(n,p)^{54}Mn$	3.31 x 10-12
$^{58}Ni(n,p)^{58}Co$	4.27 x 10-12
$^{46}Ti(n,p)^{46}Sc$	4.58 x 10-13
$^{47}Ti(n,p)^{47}Sc$	7.80 x 10-13
$^{48}Ti(n,p)^{48}Sc$	1.26 x 10-14
$^{54}Fe(n,\gamma)^{51}Cr$	3.75 x 10-14 (±3%)
$^{27}Al(n,\alpha)^{24}Na$	2.40 x 10-14 (±5%)
$^{55}Mn(n,2n)^{54}Mn$	1.02 x 10-14

TABLE III

FLUX AND FLUENCE VALUES FOR THE OMEGA WEST REACTOR
Rabbit tube flux normalized to 8 MW; fluence for 59.6 MWH

Energy	Flux (x 1013 n/cm2-s)	Fluence (x 10^{18} n/cm2)
Total	28.0	7.50
Thermal (<.5 eV)[a]	16.0	4.29
0.5 eV - 0.1 MeV	5.61	1.51
>0.1 MeV	6.35	1.71

[a]The 2200 m/s flux is about 25% lower.

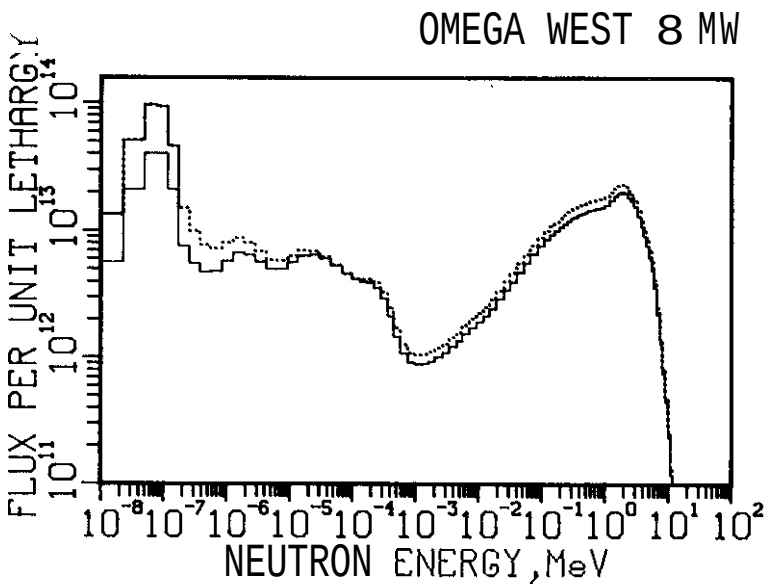

FIGURE 1. Comparison of adjusted neutron spectra for the rabbit tube in position 3E (dotted line) and the furnace in position 4F (solid line) of the Omega West Reactor.

Damage parameters were then calculated using the SPECTER2 computer code and the results are listed in Table IV. In this case we simply added up the various components of spinel. This procedure is not really correct and a different formulation of secondary displacements should be used, as discussed by Parkin and Coulter.3 However, since the elements in spinel are not so widely separated in mass, our linear approximation is fairly good in the present case.

TABLE IV

DAMAGE FOR SPINEL ($MgAl_2O_4$)

Material	Rads ($\times 10^8$)	DPA[a] ($\times 10^{-3}$)	H, appm ($\times 10^{-3}$)	He, appm ($\times 10^{-3}$)
Mg	1.67	2.51	1.24	3.24
Al	4.84	2.19	4.54	0.70
O	3.65	1.77	0.029	9.67
Spinel-neutron	3.76	2.00	1.49	6.19
gamma	136.			
Total	139.8			

[a]SPECTER assumes displacement energies of 25, 27, and 30 eV for Mg, Al, and O, respectively; the same values were also assumed for spinel.

Calculations of the total dose must also include gamma heating. Unfortunately, this rate is not very well known in the OWR and we have assumed a value of 5 W/g, a rather high value compared to other materials reactors. Using this value, the gamma dose exceeds the neutron dose, as listed in Table IV.

Two shorter irradiations were also conducted for 2 hours (15.93 MWH) and 4 hours (31.88 MWH) on July 23, 1984. In these experiments Only a nickel dosimetry wire was used and the results were scaled to the previous run as shown in Table V.

TABLE V

ACTIVITIES, FLUENCES, AND DAMAGE RATES FOR THE OMEGA WEST REACTOR
(Two irradiations in the rabbit tube on July 23, 1984)

Sample	$^{58}Ni(n,p)$ Activity ($\times 10^{-12}$ at/at-s)	Fluence >.1 MeV ($\times 10^{17}$ n/cm^2)	Spinel ($MgAl_2O_4$) DPA ($\times 10^{-3}$)	He, appm ($\times 10^{-3}$)	Rads (Si)[a] ($\times 10^{8}$)
1 (4 hr)	3.95	8.46	0.99	3.06	1.86
2 (2 hr)	4.36	4.66	0.55	1.69	1.03
June 15	4.27	17.1	2.00	6.19	3.76

[a]High gamma heating at 5 W/g will produce 7.2 $\times 10^9$ rads in 4 hours and 3.6 $\times 10^9$ rads in 2 hours.

6.0 References

1. L. R. Greenwood, Damage Analysis and Fundamental Studies Quarterly Progress Report, DOE/ER-0046/6, pp. 17-28, August 1981.

2. L. R. Greenwood, SPECTER: Neutron Damage Calculations for Materials Irradiations, ANL/FPP-TM197, in press.

3. D. M. Parkin and C. A. Coulter, J. Nucl. Mater. 103, 1315-1318 (1981).

7.0 Future Work

Further short irraditions may be conducted in the OWR. A paper is now being drafted describing these measurements.

Dosimeters have been received from the CTR 30, 36, 46, T3, and RB2 irradiations in HFIR and analysis is now in proqress.

8.0 Publications

None.

UPDATING OF THE SPECTER RND DOSFILE COMPUTER CODES

L. R. Greenwood (Argonne National Laboratory)

1.0 Objective

To standardize procedures for the calculation of damage parameters and for the reporting of dosimetry and damage data via computer codes which may be easily accessed by the fusion community.

2.0 Summary

The SPECTER and DOSFILE computer codes have been updated on the National Magnetic Fusion Energy Computer. Procedures are reviewed for running these codes.

3.0 Program

Title: Dosimetry and Damage Analysis
Principal Investigator: L. R. Greenwood
Affiliation: Argonne National Laboratory

4.0 Relevant DAFS Program Plan Task/Subtask

Task II.A.6 Dosimetry Standardization
Task II.B.1 Calculation of Defect Production Cross Section

5.0 Accomplishments and Status

5.1 Introduction

Two computer codes are resident on the National Magnetic Fusion Energy Computer (NMFEC) at Lawrence Livermore National Laboratory. The purpose of this section is to review procedures whereby anyone with access to the CRAY computer can easily obtain and run these codes. SPECTER[1,2] is a comprehensive program for the calculation of damage parameters including displacements-per-atom (dpa), gas production (H, He), total dose (Kerma), and recoil atom energy distributions. The code contains master libraries of damage functions. Users need only specify a neutron spectrum and irradiation time. The code will then provide spectral-averaged damage parameters.

DOSFILE[2] is a program which records dosimetry and damage data from all fusion materials irradiations. For each irradiation, the file contains an identification and history, measured activities, input and output neutron flux spectra from STAY'SL,[3] flux and fluence summaries, covariance data, and damage calculations from SPECTER. Users may select desired information using a list of key words for the irradiation and for the type of data desired.

5.2 SPECTER

Users of the NMFEC can easily obtain and run the SPECTER computer code. A COSMOS file has been created which will obtain all necessary files from FILEM, run the code, and send the output to your **hox.** The necessary files can be obtained with a simple COPY comnand from my public file directory 15060.111. ?he COSMOS file is called COSPECT. Please note that **if** you desire a permanent copy of the code in your space, then you must run a FILEM job; otherwise, you will need to recopy the program from my space when you want to run SPECTER.

Once you have obtained the necessary files, you can imnediately run a test case by simply typino:

cosmos **cospect** site = **xxx** **box** = yyy

This command will run a job using an input file called SPIN and an output file called SPOUT. To verify proper operation of the code, you can compare the **new** output with the old version of SPOUT in my directory. Please note that the COSMOS file COSPECT contains a FILEM command to retrieve the files from your space. **If** you want to run more than one job, then this command is not needed. You can either create a new COSMOS file or simply run the job by typinq XSPECT and then using a NETOUT command to send SPOUT to your **box.**

In order to run SPECTER, you need only create a new input file SPIN patterned after my sample file. The input is, as follows:

Line #	Description
1.	Title (80 characters)
2.	ITYP, ISIG, IGP, IPKA, ACNM, TIME (4I2,2F10.4) ITYP = 0 normally; = 2 **if** input from STAY'SL ISIG = 0 normally; = **1** to print dpa cross sections IGP = 0 **if** group differential flux = **1** **if** true differential flux = 2 **if** true group flux IPKA = 0 to calculate recoils (PKA); = **1** to kill ACNM = **1** normally (**will** renormalize input) TIME = irradiation time (seconds) or any desired normalization factor
3.	NPT (I3) = number of flux-energy points
4.	Energies (7E10.3) low to high in MeV
5.	Fluxes (7E10.3) flux values
6.	Covariance matrix (7E10.3) (from STAY'SL)

Notes: 1. If group fluxes are specified, then you must enter one extra energy point to define tne upper bin limit.

2. The covariance file is synnetric so only half of the values need he entered. Each line starts with the diagonal term.

Recoil spectra calculations require some extra explanations. Since the recoil files (PKA) are quite large, the routine version of SPECTER only considers the net recoil spectrum. However, **it** is possible to run SPECTER so that recoil spectra are calculated for each type of nuclear reaction. In order to do this, you must change the call link statements in SPECTER (lines 25 and 26) to select a group of subelements for the calculation and then recompile SPECTER before running. That is, change from PKA and SIGD to PKAX and SIGDX where X is a number from **1** to **4** designating a group of subelements (H to F, Na to Ca, Ti to Mo, and Ag to Pb). This situation is somewhat awkward; however, the large size of the recoil files makes **it** prohibitive to have all of the recoil data in a single file. On the other hand, **we** believe that most users of SPECTER will not want to obtain recoil spectra (IPKA = **11** and that many of the others will be satisfied **with** the standard file PKA without the need for examining the recoil contributions from individual reactions. Please note that most users need not make any changes in the codes or procedures.

5.3 DOSFILE

Procedures for running the DOSFILE are similar to those for SPECTER. First, copy my public files 15060.dos into your space and file them **if** you desire a permanent copy. To run a test case, simply type in:

```
cosmos    codos    site = xxx    box = yyy
```

This cosmos procedure will obtain the files from FILEM, run the job using my sample input DOSIN, and send the output DOSOUT to your box.

To run your own job, simply create a new file called DOSIN, then type the same cosmos comnand as before. Please note that if you plan to run multiple jobs, then the FILEM commands are not needed in codos. The input file is, as follows:

Line #	Description
1.	num (I2) number of names on line 2
2.	names (a5, 1x) key words from Table I
3.	ntp (I2) number of types on line 4
4.	types (a3, 1x) key words from Table II

TABLE I

IRRADIATIONS CONTAINED IN DOSFILE*

Irradiation	Key Word	Irradiation	Key Word
HFIR-CTR31	HFR31	ORR-MFE1	ORMF1
HFIR-CTR32	HFR32	ORR-MFE2	ORMF2
HFIR-CTR34	HFR34	ORR-MFE4A1	OR4A1
HFIR-CTR35	HFR35	ORR-MFE4A2	OR4A2
HFIR-CTR39	HFR39	ORR-MFE4B1	ORR4B
HFIR-CTR40/41	HFR40	ORR-TRIO1	TRIO1
HFIR-CTR42/43	HFR42	ORR-SPECTRAL	ORRLP
HFIR-CTR44/45	HFR44	ORR-TBC07	ORRT7
HFIR-T1	HFRT1	ORR-TRIO TEST	TRIOT
HFIR-T2	HFRT2	RTNS II 30 CM	RTS30
HFIR-RB1	HFRB1	TRIGA-VIENNA	TRIGA
OWR-SPECTRAL	OMWSP	HFBR-VT15-2	HFBR2
OWR-HEDL1	OMWH1	HFBR-VT15-3	HFBR3
OWR-LANL1	OMWL1	CP5-CONVERTER	CP5FC
EBRII-X287	EB287	IPNS-VTE-REF	IPN9C

*HFIR = High Flux Isotope Reactor (ORNL)
ORR = Oak Ridge Research Reactor (ORNL)
OWR = Omeqa West Reactor (LANL)
IPNS = Intense Pulsed Neutron Source (ANL-E)
CP5 = Chicago Pile 5 (ANL-E)
EBRII = Experimental Breeder Reactor II (ANL-W)
HFER = High Flux Beam Reactor (BNL)
RTNSII = Rotatinq Target Neutron Source II (LLNL)

TABLE II

DATA TYPES IN DOSFILE

Key Word	Description
idn	identification, history, gradients, references
act	measured activities, uncertainties, self-shielding, covers
fli	input flux spectrum (STAY'SL)
flo	output flux spectrum (STAY'SL)
fcv	output flux covariance matrix (symmetric)
fsm	summary of flux and fluence data
dam	damage parameters (dpa, He-SPECTER)

The key words in Tables I and II are used to select a particular irradiation and type of data. If you want to see all entries on the file, then both lines 2 and 4 can simply say "all".

The output file is intended to be self-exulanatory with plain-english titles and references to published reports. The activities and fluxes are designed for use with the STAY'SL[3] code for spectral adjustment. The simple structure of the code is intended to allow users to easily scan the data files. Using a text editor, more knowledgable users could easily construct special files for data correlations.

5.4 Conclusions

Users of the SPECTER and DOSFILE computer codes are urged to contact the author (FTS 972-4351) with any comments, suggestions, or problems.

6.n References

1. L. R. Greenwood, SPECTER: Neutron Damage Calculations for Materials Irradiations, ANL/FPP-TM197, in press.

2. L. R. Greenwood, J. Nucl. Mater. 122, 1011-1016, 1984.

3. F. G. Perey, Least-Squares Dosimetry Unfolding: The Program STAY'SL, ORNL/TM-6062 (1977); modified by L. R. Greenwood (1979).

7.0 Future Work

Both the SPECTER and DOSFILE codes will be routinely updated as new data becomes available. The SPECTER code has also been sent to the Radiation Shielding and Information Center at Oak Ridge National Laboratory.

8.0 Publications

See references 1 arid 2.

HELIUM PRODUCTION IN REACTOR-IRRADIATED COPPER AND TITANIUM, AND EVIDENCE FOR A COPPER THREE-STAGE REACTION

D. W. Kneff, B. M. Oliver, R. P. Skowronski (Rockwell International), and L. R. Greenwood (Argonne National Laboratory)

1.0 Objective

The objectives of this work are to apply radiometric plus helium accumulation neutron dosimetry to the measurement of neutron fluences and energy spectra in mixed-spectrum fission reactors utilized for fusion materials testing, and to measure helium generation rates of materials in these irradiation environments.

2.0 *Summary*

Helium generation measurements have been performed for Cu and Ti samples irradiated in the High Flux Isotopes Reactor (HFIR) experiments CTR31 and CTR32, and in the Oak Ridge Research Reactor (ORR) experiment MFE2. The results are widely discrepant with helium generation calculations based on ENDF/B-V cross section evaluations. The copper samples from the HFIR irradiations contain an excess of helium that increases nonlinearly with fluence. These results, plus correlated discrepancies in ^{65}Zn reaction rates measured for the irradiated copper samples, suggest the presence of a thermal neutron three-stage reaction process in copper. This is expected to impact the interpretation of damage effects in copper-based materials irradiated to high neutron fluences ($>10^{22}$ neutron/cm^2).

3.0 Programs

Title: Helium Generation in Fusion Reactor Materials/Dosimetry and Damage Analysis
Principal Investigators: D. W. Kneff and H. Farrar IV/L. R. Greenwood
Affiliation: Rockwell International/Argonne National Laboratory

4.0 Relevant OAFS Program Plan Task/Subtask

Task II.A.1	Fission Reactor Dosimetry
Task II.A.4	Gas Generation Rates
Subtask II.A.5.1	Helium Accumulation Monitor Development

5.0 Accomplishments and Status

Helium generation measurements have been made for copper and titanium samples irradiated in the mixed-spectrum reactors ORR and HFIR, and the results have been compared with calculations based on the unfolded reactor neutron spectra and the ENDF/B-V evaluated nuclear data file. These measurements are part of a joint Rockwell-Argonne National Laboratory (ANL) program to measure total helium production rates over the range of fission reactor neutron spectra and fluences used for fusion materials testing, and to use the results to integrally test helium production cross section evaluations used in damage calculations. For copper, comparisons of the helium measurements with calculations, and with radiometric counting data, suggest the presence of a thermal neutron three-stage reaction process that produces significant extra helium at high neutron fluences.

5.1 Helium Measurements

Most of the new copper and titanium results are for bare wire segments from experiments ORR-MFE2, HFIR-CTR31, and HFIR-CTR32. These measurements extend the experimental results previously reported for copper

and titanium from the fusion materials irradiation experiments ORR-MFE4A2[1] and EBRII-X287.[2] The samples were incorporated in these irradiations for both helium accumulation and radiometric dosimetry measurements. The samples are listed in Tables 1 and 2, respectively. The activation gamma counting was performed at ANL using Ge(Li) spectroscopy. The samples were then etched, segmented, and analyzed by high-sensitivity gas mass spectrometry[3] at Rockwell International for their irradiation-generated helium concentrations. Multiple specimens from each sample location were analyzed for helium, with good reproducibility, The absolute uncertainty in each helium analysis was ±1-2%. The results are summarized in Column 4 of Tables 1 and 2.

One copper sample from each irradiation, and multiple samples of titanium from each sample location, were also analyzed for ^{3}He. The 3He, which can be formed from the decay of tritium often found in reactor environments, would be expected to be present in the titanium samples, as titanium is a good tritium getter. The 3He concentration in each copper sample was found to be less than 0.1 appb (10^{-9} atom fraction), while that in the titanium samples was found to range from 1.6 appb (CTR31 sample Ti-1) to 600 appb (MFE2 sample Ti-3).

Additional helium analyses were also performed on Cu and Ti samples which were irradiated in ORR-MFE4A2 within miniature platinum capsules. These capsules were previously etched and sheared to measure the helium release from the samples into the capsule void, as described in a previous report.[1] Those results indicated a relatively large (~3.5-6%) helium release from the Cu and Ti samples. which was assumed to be a diffusion effect. The new measurements were for etched and unetched segments of the encapsulated samples, plus the platinum encapsulating material. These results indicate that the high helium release measured during shearing was probably the result of high temperatures within each capsule during irradiation, produced by poor thermal conduction between the sample and the capsule wall. The observed temperature effects were not present for the unencapsulated samples, and other evidence indicates that the unencapsulated samples did not suffer measurable helium loss during irradiation. The preliminary helium production measurements for the bare MFE4A2 Cu and Ti samples[1] were therefore adjusted, and the final results are included in Tables 1 and 2. The results for etched sample segments from the copper (Cu-Y4) and titanium (Ti-M5, V51 capsules are also included. Note that the temperature effects have no effect on helium measurements for an unsheared capsule.

5.2 Comparisons with Calculations and Evidence for a Copper Three-Stage Reaction

The calculated ^{4}He concentrations for the irradiated samples are given in Column 5 of Tables 1 and 2. They are based on the unfolded neutron spectra and the ENDF/B-V cross section files. These calculations have been summarized in previous reports describing the individual irradiations.[4-6]

Comparisons between the measured and calculated helium concentrations in the Cu and Ti samples are given in Column 6 of Tables 1 and 2, where the calculated/experimental (C/E) ratios are given. For titanium (Table 2) the ratios are generally constant, but about 240% higher than the calculated values. This indicates a need to revise the ENDFIB-V files for helium generation in titanium at fission reactor neutron energies, as pointed out in previous reports.[1,2]

For copper (Table 1), the C/E values are not constant. but decrease with increasing fluence at high neutron fluences. This can be seen by comparing the C/E ratios with the thermal neutron fluences at the individual sample locations. as tabulated in Column 7 of Table 1. The helium production rates appear to be increasing rapidly above a thermal neutron fluence of about 10^{22} neutrons/cm^2. This was not observed in the ORR samples, which were irradiated to lower total neutron fluences. A correlated effect is also observed in the gama counting of the copper samples following irradiation. Radioactive ^{65}Zn, produced from ^{63}Cu through the thermal neutron reaction sequence

$$^{63}Cu(n,\gamma)^{64}Cu \rightarrow {}^{64}Zn(n,\gamma)^{65}Zn,$$

has been found to be significantly less abundant than expected in the high-fluence HFIR samples.

The evidence from the helium and radiometric measurements of the copper samples suggest that the C/E discrepancies are due to two sources. First, the ENDFIB-V cross section files underpredict the $Cu(n,X\alpha)$ helium production in a fission reactor neutron spectrum by about 35-40%. This is observable in the ORR comparisons. Second, the extra helium produced at high fluences appears to be due to the fallowing three-stage reaction process with thermal neutrons:

$$^{63}Cu(n,\gamma)^{64}Cu \rightarrow {}^{64}Zn(n,\gamma)^{65}Zn(n,\alpha)^{62}Ni.$$

TABLE 1

HELIUM PRODUCTION MEASUREMENTS FOR COPPER IRRADIATED IN ORR AND HFIR

Experiment	Sample	Core Height[a] (cm)	4He Concentration Measured (appm)[b]	4He Concentration Calculated[c] (appm)[b]	Calculated/Measured (C/E)	Thermal Fluence (10^{22} n/cm^2)
ORR-MFE2	Cu-1	+14.32	1.24	0.80	0.65	0.31
	cu-2	+ 7.49	1.52	0.97	0.64	0.38
	cu-4	+ 0.76	1.68	1.06	0.63	0.44
	cu-3	- 6.16	1.82	1.10	0.61	0.47
ORR-MFE4A2	cu-Y4	- 3.65 inner	1.97	1.31	0.66	0.47
	cu-5	- 5.40 inner	2.02	1.31	0.65	0.47
	cu-8	- 5.41 outer	2.16	1.38	0.64	0.52
	cu-4	-13.82 outer	2.03	1.30	0.64	0.49
	Cu-1	-13.97 inner	1.88	1.22	0.65	0.45
HFIR-CTR32	cu-3	+ 5.20	5.77	2.90	0.50	1.58
HFIR-CTR31	Cu-1	+21.86	6.78	3.30	0.49	1.91
	cu-3	+ 5.20	21.08	5.97	0.28	3.19
	cu-5	-11.47	14.95	5.33	0.36	2.57

(a) Distance above core midplane
(b) Atomic parts per million (10^{-6} atom fraction)
(c) Based on ENDF/B-V; see Refs. 4-6. The ORR-MFE2 calculations (Ref. 4) have been adjusted for gradients between the fusion materials experiment locations and the helium dosimetry tube.

TABLE 2

HELIUM PRODUCTION MEASUREMENTS FOR TITANIUM IRRADIATED IN ORR AND HFIR

Experiment	Sample	Core Height[a] (cm)	^{4}He Concentration Measured (appm)[b]	^{4}He Concentration Calculated[c] (appm)[b]	Calculated/Measured (C/E)
ORR-MFE2	Ti-1	'14.32	0.78	1.95	2.50
	Ti-2	+ 7.49	0.94	2.31	2.46
	Ti-3	- 6.16	1.09	2.67	2.44
ORR-MFE4A2	Ti-M5	- 3.02 inner	1.16	2.75	2.38
	Ti-5	- 4.22 inner	1.16	2.75	2.38
	Ti-8	- 4.22 outer	1.23	2.94	2.40
	Ti-V5	-12.23 inner	1.12	2.57	2.29
	Ti-4	-12.62 outer	1.18	2.90	2.45
	Ti-1	-12.78 inner	1.13	2.71	2.40
HFIR-CTR32	Ti-3	+ 4.57	2.17	5.28	2.43
HFIR-CTR31	Ti-1	+21.23	2.52	5.93	2.35
	Ti-3	+ 4.57	4.29	10.30	2.40
	Ti-5	-12.10	3.90	8.98	2.30

(a) Distance above core midplane
(b) Atomic parts per million (10^{-6} atom fraction)
(c) Based on ENDFIB-V; see Refs. 4-6. The ORR-MFE2 calculations (Ref. 4) have been adjusted for gradients between the fusion materials experiment locations and the helium dosimetry tube.

Investigation of other possible reaction mechanisms, including impurity interactions. indicates that this three-stage reaction is the only likely candidate to produce helium at the observed levels as a nonlinear function of neutron fluence.

Three cross sections relevant to this three-stage helium production mechanism are not known: $^{65}Zn(n,\alpha)$ dnd the process-competing reactions $^{64}Cu(n,\gamma)$ and $^{65}Zn(n,\gamma)$. Calculations performed for the full three-stage reaction sequence, using a series of values for the $^{64}Cu(n,\gamma)$ cross section, show that all three spectrum-integrated cross sections can be determined from the irradiated copper samples. The $^{64}Cu(n,\gamma)$ cross section can be deduced from the $^{65}Cu/^{63}Cu$ isotopic ratios in the irradiated samples, and the other two cross sections can then be determined from the helium and gama-counting measurements. The initial calculations indicate that the $^{65}Zn(n,\alpha)$ cross section is on the order of 3 barns. **Work** is in progress to measure the final copper isotopic ratios in several of the irradiated samples, and the helium and radiometric measurements are being extended to cover additional copper samples irradiated in HFIR experiments CTR30 and CTR32, and ORR experiment MFE4B. The CTR30 samples will extend the neutron fluence range upwards by another factor of two.

The HFIR results presented in Table 1 demonstrate the importance of measuring the helium generation in samples where accurate gas production data are required. The helium produced by the three-stage process at high thermal neutron fluences ($\geq 10^{22}$ n/cm^2) could have a significant impact on the interpretation of damaae effects in irradiation studies of comer-based materials. For example. initial calculations indicate that this process will produce an estimated 50 appm extra helium in copper at a thermal neutron fluence of $b \times 10^{22}$ n/cm^2.

6.0 References

1. B. M. Oliver, D. W. Kneff, and R. P. Skowronski, "Helium Generation Measurements for Ti and Cu from ORR," in Damage Analysis and Fundamental Studies. Quarterly Progress Report April-June 1984, DOE/ER-0046/18, U.S. Department of Energy, 18 (1984).

2. B. M. Oliver, D. W. Kneff, and R. P. Skowronski, "Helium Generation Measurements for EBR-II and ORR," in Damage Analysis dnd Fundamental Studies, Quarterly Progress Report January-March 1984, DOE/ER-0046/17, U.S. Department of Energy, 14 (1984).

3. B. M. Oliver, J. G. Bradley. and H. Farrar IV, "Helium Concentration in the Earth's Lower Atmos phere," Geochim. Cosmochim. Acta, **48**, 1759 (1984).

4. t. R. Lreenwood, "Fission Reactor Dosimetry," in Damage Analysis and Fundamental Studies, Quarterly Progress Report April-June 1981, DOE/ER-0046/6, U.S. Department of Energy, 17 (1981).

. R. Greenwood, "Dosimetry and Damage Analvsis for the MFE4A Soectral Tailorina Experiment in ORR," in Udmage Analysis and Fundamental Studies.. Quarterly Progress Report October-December 1982, DOE/ER-0046/12, U.S. Department of Energy, 14 (1983).

6. L. R. Greenwood, "Fission Reactor Dosimetry - HFIR - CTR 31, 32, 34, and 35," in Damage Analysis and Fundaniental Studies, Quarterly Progress Report April-June 1983, DOE/ER-0046/14, U.S. Department of Energy, 9 (1983).

7.0 Future Work

Helium measurements, activation measurements, and isotopic ratio measurements are in progress for additional copper samples irradiated in the mixed-spectrum reactors ORR and HFIR. The results will be used to derive spectrum-integrated cross sections for those reactions needed to quantify the copper three-stage reaction process. These cross sections can then be used to predict helium generation in copper for high-fluence irradiations,

8.0 Publications

None.

CHAPTER 3

REDUCED ACTIVATION MATERIALS

CROSS SECTIONS FOR REDUCED ACTIVATION STUDIES

F. M. Mann (Hanford Engineering Development Laboratory)

1.0 Objective

To provide nuclear physics support for the development of reduced activation materials.

2.0 *Summary*

A new library was created based on the Evaluated Nuclear Data File (ENDFIB-V), the Activation Library from the Lawrence Livermore National Laboratory (ACTL), on special evaluations from the Los Alamos National Laboratory and the Hanford Engineering Development Laboratory, and from systematics calculations. This library contains reaction cross sections for 337 isotopes and for about 6000 reactions. At least 14 reactions [including (n,gamma), (n,2n), (n,p), and (n,alpha)] are given for each isotope. Table 1 provides a summary of the reactions included as well as the source of the cross sections.

3.0 Program

Title: Irradiation Effects Analysis
Principal Investigator: D.G. Doran
Affliation: Hanford Engineering Development Laboratory

4.0 Relevant OAFS Program Plan Task/Subtask

Not in program plan.

5.0 Accomplishments and Status

5.1 Introduction

To predict the activity of proposed fusion reactor materials, cross sections for the many different possible reactions are needed. The libraries[1-3] used in the past have been incomplete because the number of needed reactions is very large. Not only are reactions needed from the isotopes initially making up the material, but reactions are also needed which lead to long-lived radioactive products through multi-step processes and which can burn out the radioactive products.

5.2 Isotopes Included

All the major and minor constituents of the major fusion reactor materials are included. In addition, all unstable isotopes with a half-life greater than 5 years and with an atomic mass of less than 220 amu are included. All isotopes which lead to such a radioactive product are also in the library. Finally isotopes which have shorter half-lives but which are in a nuclide region of high interest or which would allow a complete treatment of an element were included. Thus over 90% of the stable isotopes are included (only certain isotopes of Se, Te, Xe, Dy, and Yb are missing). Figure 1 shows the iron island of the Chart of the Nuclides as an example of the isotope coverage.

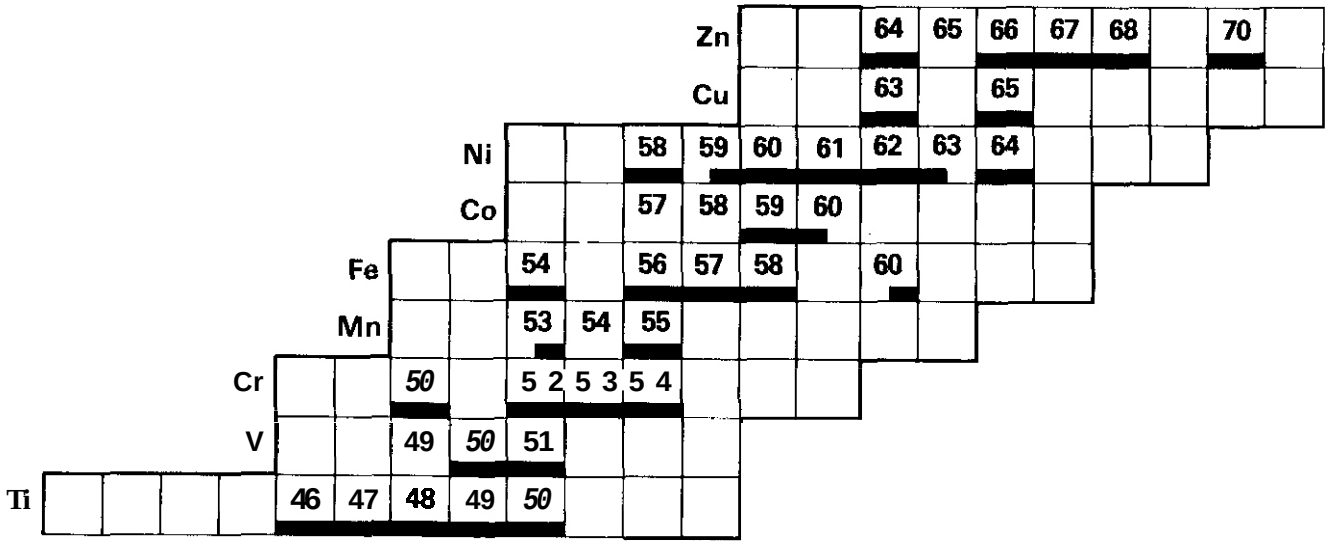

FIGURE 1. The Iron Island of the Chart of the Nuclides Showing the Isotopes Having Cross Sections (those having a number in the box) and Those Having Decay Data (isotopes having a box). The bar at the bottom of each box indicates the half-life of the isotope (a full bar indicating a stable isotope, a partial bar on the right indicating a half-life greater than 1000 years, a bar on the left indicating a half-life between 5 and 1000 years, while no bar indicates a half-life less than 5 years).

5.3 Source of Evaluations

Not only it is neccesary that the isotope base be complete, but so also must the reaction content of the library be complete. Thus the systematics code THRESH2,[4] modified to produce cross sections to 40 MeV, was used to calculate (n,2n),(n,3n),(n,p),(n,d),(n,np),(n,t),(n,nd),(n,nt),(n,2p),(n,he-3), (n,alpha),(n,n he-3). and (n,n alpha) reactions. Although the code fairly accurately predicts (n,2n) reactions, it often produces cross section values for reactions involving charged particles which are incorrect by over a factor of 2. The code also has no ability to calculate (n,gamma) cross sections, an important source of activation. Thus the ENDF/B-V[5] (Evaluated Nuclear Data File, version 5.2), maintained by the Cross Section Evaluation Working Group, was used to update the THRESH2 calculations whenever possible. If evaluations were unavailable from ENDF/B (or if the processing of such cross sections did not merit the effort), cross sections from the 1984 version of the Lawrence Livermore National Laboratory Activation Library[2] (ACTL) were used. As both the ENDF/B and ACTL evaluations only exist to 20 MeV, the THRESH2 values were used after 20 MeV but normalized to the evaluated library value at 20 MeV. In a few cases (for example, important activation reactions from iron above 20 MeV or reactions involving tritium), special evaluations have been performed by the Los Alamos National Laboratory[6] or by the Hanford Engineering Development Laboratory. Finally there were some cross sections [mainly (n,gamma) or cross sections to isomeric states] where no data exist. Values for these cross sections were taken from the cross section for the ground state (which may in fact be the cross section for the ground and isomeric state) or from the cross section for the same reaction from a neighboring nucleus where an evaluation had been done.

5.4 Cross Section Library

Table 1 presents the contents of the reaction cross section library with the source of the cross sections shown. The library has cross sections in an ENDFIB-V file 3 format (with the addition of a preceding title card) for neutron energies from 1.0e-5 eV to 40 MeV [20 MeV in the case of (n,gamma)]. The cross sections are maintained as a set of Cray files on the National Magnetic Fusion Energy Computer Center's (NMFECC) mass storage system.

6.0 References

1. T.Y. Sung and W.F. Vogelsang, "Decay Chain Data Library for Radioactivity Calculations," UWFDM-171, University of Wisconsin (1976).

2. M.A. Gardner and R.J. Howerton, "ACTL: Evaluated Neutron Activation Cross Section Library - Evaluation Techniques and Reaction Index," UCRL-50400, Vol. 18, Lawrence Livermore National Laboratory (Oct. 1978).

3. F.M. Mann, "Transmuation of Alloys in MFE Facilities as Calculated by REAC [A Computer Code System for Activation and Transmutation)," HEQL-TME 81-37, Hanford Engineering Development Laboratory (1982).

4. S. Pedrlstein, "Nuclear Cross Sections and Their Uncertainities Obtained from Nuclear Systematics," Proc. Conf. Nuclear Cross Sections and Technology, CONF-7511469, Washington, O.C. (March 1975).

5. R. Kinsey, Compiler, "ENDF/B Summary Documentation (ENDF-201)," 3rd Edition (ENDF/B-V), BNL-NCS-17541, Brookhaven National Laboratory (1979). Version V.2 was released in 1982-3.

6. E.D. Arthur and P.G. Young "Evaluated Neutron-Induced Cross Section for ^{54,56}Fe to 40 MeV," LA-8626-MS, Los Alamos National Laboratory (1980)

7.0 Future Work

The point-wise cross sections will be processed into a 63 group structure for use in the revised REAC activation code system. New activation "limits" will then he calculated to guide material scientists in their design of reduced activation materials. Also one group cross section values for the STARFIRE (and possibly other) conceptual designs will be generated and published.

TABLE 1

CONTENTS OF HEDL ACTIVATION LIBRARY (OEC. 1984)

334 Isotopes 5941 Reactions

Isotope	n,n*	n,2n	n,3n	n,na	n,np	n,nd	n,nt	n,nh	n,4n	n,g	n,p	n,d	n,t	n,h	n,a	n,2p
H 1	x	x	x	x	x	x	x	x	x	e	x	x	x	x	x	x
H 2	x	e	x	x	x	x	x	x	x	e	x	x	x	x	x	x
H 3	x	e	x	x	x	x	x	x	x	x	x	x	x	x	x	x
He 3	x	x	x	x	*	x	x	x	x	a	e	e	x	x	x	x
He 4	x	*	x	x	*	*	x	x	x	x	x	*	x	x	x	x
Li 6	x	*	x	x	*	a	*	x	x	e	te	x	te	x	x	x
Li 7	x	te	x	te	*	x	x	x	x	e	x	e	x	x	x	x
Be 9	x	ta	t	t	t	t	t	t	x	e	te	e	e	x	te	t
Be 10	x	t	t	t	t	t	t	t	*	g	t	*	*	*	t	*
B 10	x	t	t	t	t	x	*	*	x	e	te	te	t	t	te	t
B 11	x	te	t	t	t	t	t	t	•	e	te	*	e	*	te	t
C 12	x	t	t	x	t	*			*	e	te	te	t	t	te	t
C 13	x	t	t	t	t	t	t	t	*	g	t	*	*		t	t
C 14	x	t	t	t	t	t	t	t	*	g	t	*	*	*	t	t
N 14	x	te	t	t	t	t	*			e	te	te	te	t	te	t
N 15	x	te	t	te	te	t	t	t	*	e	te	e	e	*	te	t
O 16	x	ta	t	ta	ta	t	t	t	*	e	te	te	t	t	te	t
O 17	x	te	t	te	te	t	t	t	*	e	te	e	*	*	te	
O 18	x	t	t	t	t	t	t	t	*	g	t		*	*	t	
F 19	x	te	t	ta	ta	t	t	t	*	e	te	ta	ta	t	te	t
Ne 20	x	t	t	t	t	t	t	t	*	g	t	t	t	t	t	
Ne 21	x	t	t	t	t	t	t	t	*	g	t	t	t	t	t	
Ne 22	x	t	t	t	t	t	t	t	*	g	t				t	
Na 22	x	t	t	t	t	t	t	t	*	g	t	t	t	t	t	t
Na 23	x	te	t	ta	ta	t	t	t	•	e,y	te	t	t	t	te	t
Mg 24	x	ta	t	t	ta	t	t	t	*	a	te	t	t	t	ta	t
Mg 25	x	ta	t	t	t,y	t	t	t		a	ta	t,y	t	t	ta	
Mg 26	x	ta	ta	t	t	t,y	t	t	*	a	ta	*	*,y		ta	
Al 26	x,t	t	t,t	t	t	t	t	t	*	g	t	t	t	t,y	t	
Al 27	x	te,g	t	t	t	t	t	t	*	e	te	te	te	t	te,y	
Si 28	x	t	t	t	t	t,t	t	t	*	a	ta	t	t,t	t	ta	
Si 29	x	ta	t	ta	ta	t	t,t	t	*	a	ta	t	t	t	ta	t
Si 30	x	ta	ta	ta	ta	t	t	t	•	a	ta	*	*	*	ta	
Si 32	x	t	t	t	t	t	t	t	*	g	t	t	t	t	t	
P 31	x	te	t	t	te	t	t	t	*	e	te	t	t	t	te	t
S 32	x	ta	t	t	ta	t	t	t	*	a	te	t	ta	t	ta	t
S 33	x	ta	t	ta	ta	t	t	t	*	a	ta	ta	t	t	ta	t
S 34	x	ta	t	ta	ta	t	t	t	*	a	ta	a	*	*	ta	t
S 36	x	ta	ta	ta	t	t	t	t	*	a	t	t	t	t	t	
Cl 35	x	ta,ta	t	ta	ta	t	t	t	*	a	ta	t	t	t	ta	
Cl 36	x	ta	t,t	ta	ta	t	t	t	*	a	ta	t	t	t	ta	
Cl 37	x	ta	ta	ta	ta	t	t	t	*,*	a	ta	t	t	t	ta	t
Ar 36	x	ta	t	t	t	t,t	t	t	*	a	ta	t	t,t	t	ta	
Ar 38	x	ta	t	t	t	t	t	t	*	a	ta,y	t	t	t	ta	
Ar 39	x	ta	ta	t	t,t	t	t	t		a	ta	t,t	t	t	ta	
Ar 40	x	ta	ta	t	t	t,t	t	t	*	a	ta	t	t,t	t	ta	
Ar 42	x	ta	ta	t	t	t	t	t	*	a	t	t	t	t	t	
K 39	x	ta,ta	t	t	t	t	t	t		a	ta	t	t	t	ta	t,y
K 40	x	ta	t,t	t	t	t	t	t	*	a	ta	t	t	t,y	ta	t
K 41	x	ta	ta	t	t	t	t	t,t	*,y	a	ta	t	t	t	ta,t	t
Ca 40	x	ta	t	ta	ta	t,t	t	t	*	a	ta	t	t,t	t	ta	t
Ca 41	x	ta	t	ta	ta	t	t,t	t		a	ta	t	ta	t	ta	
Ca 42	x	ta	t	ta	ta	t	t	t	*	a	ta	t	t	t	ta	
Ca 43	x	ta	t	ta	t	t	t	t	*	a	ta	ta	t	t	ta	t
Ca 44	x	ta	t	t	t	t	t	t		a	ta	ta	t	t	ta	t
Ca 45	x	ta	t	t	t	t	t	t	*	a	ta	ta	t	t	ta	t
Ca 46	x	ta	t	t	t	t	t	t	*	a	ta	t	t	t	ta	t
Ca 48	x	ta	t	t	t	t	t	t	*	a	ta	t	t	t	t	*
sc 45	x	ta,ta	t	t	t	t	t	t	*,*	a,y	ta	t	t	t	ta	t

TABLE I (cont'd)

Isotope	n,n*	n,2n	n,3n	n,na	n,np	n,nd	n,nt	n,nh	n,4n	n,g	n,p	n,d	n,t	n,h	n,a	n,2n
Ti 44	x	t	t	t	t	t,t	t	t	*	g	t,t	t	t,t			
Ti 46	x	ta	t	ta	ta	t,t	t	t	*	a	te,y	t	th,g			
Ti 47	x	ta	t	ta	te	t	t,t	t	*	a	te	ta,y	t	t	ta	t
Ti 48	x	ta	t	ta	te,y	th	th	t	*	a	te	t	th,y	t	te	t
Ti 49	x	ta	t	ta	ta	t,y	t	t	*	a	ta	t	t	t	ta	t
Ti 50	x	ta	ta	ta	ta	t	t,y	t	*	a	ta	t	t	t	te	
V 49	x	ta	t	ta	ta	t	t	t,t	*	a	ta	t	t	t	ta,ta	t
V 50	x	ta	t	ta,y	ta	t	t	t	*	a	ta	t	t	t	ta	t
V 51	x	te	t	te	te	t	t		*	e	te	te	te	t	te	t
Cr 50	x	te	t	te	ta	t	t	t	*	a	ta	t	t	t	te	t
Cr 52	x	te	t	te	te	t	t	t	*	g	ta	t	t	t	te	t
Cr 53	x	te	t	te	ta	t	t	t	*	g	ta	t	t	t	te	t
Cr 54	x	te	te	t	ta	t	t	t	*	a	ta	t	t	t	ta	t
Mn 53	x	ta,ta	t	ta	ta	t	t	t	**	a	ta	t	t	t	ta	t
Mn 54	x	ta	t,t	ta	ta	t	t	t	*	a	ta	t	t	t	ta	t
Mn 55	x	te	te	te	te	t	t	t	*,*	e	te	te	*	te	te	t
Fe 54	x	l,y	t,g	1	1	th,g	th	t	x	e	1	t	th,g	t	1	t
Fe 55	x	ta		ta	ta	t	t,t	t	*,*	a	ta	t	t	t	ta	t
Fe 56	x	1	1	1	1	th	th	t	l,y	g	l	t	th	t	1	t
Fe 51	x	t	ta	t	ta	t	t	t		a	ta	t	t	t	t	t
Fe 58	x	t	t	t	ta	t	t	t	*	e	ta,g	t	t	t	ta	t
Fe 60	x	ta	ta	t	t	t,t	t	t	*	a	t	t	t,t	t	t	x
Co 51	x	ta	t	t	ta	t	t	t	*.*	g,g	ta	t	t	t	t	t
Co 59	x	ta,ta	t	te	te	t	t	t	*,*	ea,ea	te	te	te	te	te	t,t
Co 60	x,t	ta	ta, ta	ta	ta	t	t	t	*	a	td	t	t	t,t	ta	t
Ni 58	x	te	t	t	ta	th	th	t	*	e	ta,ta	t	th	t	te	t
Ni 59	x	t	t	t	t,t	t	t	t	*	e	te	t,t	t	t	te	t
Ni 60	x	te	t	t	t	t,t	t	t	*	g	ta,ta	t	t.t	t	t	t
Ni 61	x	t	t	t	ta,ta	t	t,?	t	•	g	ta	t,t	t	t	t	t
Ni 62	x	t	t	t	ta	t,t	t	t	*	e	ta.ta	t	t,t	t	te	t
Ni 63	x	ta	ta	ta	ta,g	t	t	t	*	a	ta	t,t	t	t	ta	t
Hi 64	x	ta	t	ta	ta	t,t	t	t	*	a	ta	t	t,t	t	ta	x
Cu 63	x	ta	t	ta	ta	t	t	t,t	*	a	te	t	t	t	te,t	t
Cu 65	x	te	ta	ta	ta	t	t	t,t	*	a	ta	t	t	t	ta,a	t
Zn 64	x	t	t	t	t	t	t	t	*	g	t	t	t	t	t	t
Zn 65	x	t	t	t	t	t	t	t	*	g	t	t	t	t	t	t
In 66	x	t	t	t	t	t	t	t	*	g	t	t	t	t	t	t
Zn 61	x	t	t	t	t	t	t	t	*	g	t	t	t	t	t	t
Zn 68	x	t	t	t	t	t	t	t	*	9.9	t,t	t	t	t	t	t
Zn 10	x	t,t	t	t	t	t,t	t	t	*	g,g	t,t	t	t,t	t	t	*
Ga 69	x	t	t	t	t	t	t	t	*	g	t,t	t	t	t	t	t,t
Ga 71	x	t	t	t	t	t,t	t	t,t	*	a	t,t	t	t,t	t	t,t	t,t
Ge 68	x	t	t	t	t	t	t	t	*	g	t	t	t	t	t	t
Ge 70	x	t	t	t	t	t	t	t	*	g	t	t	t	t	t	t,t
Ge 72	x	t	t	t	t	t	t	t,t	*	g	t	t	t	t	t,t	t,t
Ge 73	x	t	t	t,t	t	t	t	t	*	g	t	t	t	t,t	t	t
Ge 74	x	t	t	t	t	t	t	t,t	*	g,g	t,t	t	t	t	t,t	t
Ge 76	x	t,t	t	t	t	t,t	t	t	*	g,g	t	t	t,t	t	t	t
As 15	x	t	t	t	t	t	t	t		a	t,t	t	t	t	t	t,t
Se 78	x	t,t	t	t	t	t	t	t,t	*	9.9	t	t	t	t	t,t	t,t
Se 79	x,t	t	t,t	t,t	t	t	t	t	*	g	t	t	t	t,t	t	t
Se 80	x	t,t	t	t	t	t	t	t,t	*,*	g,g	t	t	t	t	t,t	t,t
Br 79	x,t	t	t,t	t	t	t,t	t	t	*,*	g,g	t,t	t	t,t	t	t	t
Br 81	x	t,t	t,t	t	t	t,t	t	t	*	g,g	t,t	t	t,t	t	t	t
Kr 78	x	t	t	t	t,t	t	t	t	*	g,g	t	t,t	t	t	t	t,t
Kr 80	x	t,t	t	t	t,t	t	t,t	t,t	*	g,g	t,t	t,t	t	t	t,t	t,t
Kr 81	x,t	t	t,t	t,t	t,t	t,t	t	t	*	g	t	t,t	t,t	t,t	t	t
Kr 82	x	t,t	t	t	t	t,t	t,t	t,t	*,*	g,g	t,t	t	t,t	t	t,t	t,t
Kr 83	x,t	t	t,t	t,t	t,t	t	t,t	t	*,*	g	t	t,t	t	t,t	t	t
Kr 84	x	t,t	t	t	t	t,t	t	t,t	*,*	g,g	t,t	t	t,t	t	t,t	t,t
Kr 85	x,t	t	t,t	t,t	t,t	t	t,t	t	*,*	g	t	t,t	t	t,t	t	t
Kr 86	x	t,t	t	t	t	t,t	t	t,t	*,*	g	t	t	t,t	t	t,t	t
Rb 85	x	t,t	t	t	t	t,t	t	t,t	*,*	g,g	t,t	t	t,t	t	t,t	t,t
Rb 81	x	t,t	t	t	t	t,t	t	t,t	*,	g	t	t	t,t	t	t,t	t

TABLE 1 (cont'd)

Isotope	n,n*	n,2n	n,3n	n,na	n,np	n,nd	n,nt	n,nh	n,4n	n,g	n,p	n,d	n,t	n,h	n,a	n,2p
Sr 84	x	t,t	t	t	t	t,t	t,t	t,t	*,*	g,g	t,t	t	t,t	t	t,t	t,t
Sr 86	x	t,t	t	t	t	t,t	i	t,t	*	g,g	t,t	t	t,t	t	t,t	t,t
Sr 87	x,t	t	t,t	t,t	t,t	t	t,t	t	* *	Q	t	t,t	t	t,t	t	t
Sr 88	x	t,t	t	t	t	t,t	t	t,t	* *	g	t	t	t,t	t	t,t	t
Sr 90	x	t	t	t	t	t	t	t	* *	Q	t,t	t	t	t	t	t
Y 88	x	ta,t	t,t	t,t	ta,t	t	t,t	t	* *	g,g	ta	t,t	t	t,t	t	t
Y 89	x,t	ta	t,t	t	ta	t,t	t	t,t	* *	a,g	ta	t	t,t	t	t,t	t
Zr 90	x,y	te,g	t	t	ta,y	t	t,t	t,t	* *	g	te,g	ta,y	t	t	te,g	
Zr 91	x	te,y	ta,g	t,t	ta,g	t,y	t	t		a	te,g	ta,g	t,y	t	te	
Zr 92	x	te	ta,y	t	ta,g	t,t	t,y	t	* *	a	te	ta,g	t,t	t	te	t
Zr 93	x	ta	ta	t	t	t,t	t,y	t	* *	a	ta,t	t	t,t	t	ta	
Zr 94	x	te	ta	ta	t,y	t	t,t	t	* *	a	te	t,y	t	t	te	
Zr 96	x	te	t	t	t	t	t,y	t	* *	g	t,t	t	t	t	te	t
Nb 91	x,t	ta,t	t,t	t,t	t,t	t,t	t	t	* *	a,a	ta	t,t	t,t	t,t	t	t,t
Nb 92	x,t	t,ta	t,t	t	t	t,t	t,t	t,t		a,g	ta	t	t,t	t,t	t,t	t,t
Nb 93	x,a	ta,ta	ta,ta	te,ta	t	t	t,y	t,t	*,y	a,g	ta	t	t	t,y	te,g	t
Nb 94	x,t	ta,t	t,ta	t,t	t	t	t	t,t		a,g	ta	t	t	t	t,t	t,t
Mo 92	x	ta,g	t	t	t,ta	t,y	t,t	t,t	*,*	a,g	ta,ta	ta,ta	t,y	t,y	ta,g	t
Mb 93	x,t	ta	t,t	t,y	t,t	t,t	t,t	t,t	* *	a	ta,t	t,ta	t,t	t	ta,t	t
Mo 94	x	ta,ta	ta		ta,g	t,t	t,t	t	* *	a	ta,g	ta,g	t,ta	t	ta	t
Mo 95	x	ta	ta,g	ta	t,t	t,t	t,t	t	* *	a	ta,g	t,t	t,t	t	ta	t
Mo 96	x	ta	ta	ta	t,t	t,t	t,t	t	* *	a	ta	t,t	t,t	t	ta	t
Mo 97	x	ta	ta	t	t	t,t	t,t	t	* *	a	ta,y	t	t,t	t	ta	t
Mb 98	x	ta	ta	t	t,y	t	t,t	t	* *	a	ta,g	t,t	t	t	ta	t
Mo100	x	ta	t	t	t,t	t,t	t	t	* *	a	ta,g	t,t	t,t	t	ta	t
Tc 97	x,t	t,t	t,t	t,t	t	t	t	t,t	* *	g	t	t	t	t,t	t,t	
Tc 98	x	t,t	t,t	t,t	t	t	t	t,t	* *	g,g	t	t	t	t	t,t	
Tc 99	x,t	t	t,t	t,t	t	t	t	t	,	Q	t	t	t	t,t	t	
Ru 96	x	t	t	t	t,t	t,t	t,t	t,t	*	g	t,t	t,t	t,t	t	t,t	
Ru 98	x	t	t	t	t,t	t,t	t,t	t	*	Q	t	t,t	t,t	t	t	t
Ru 99	x	t	t	t	t	t,t	t,t	t	*	g	t,t	t	t,t	t	t	t
Ru100	x	+	t	t	t,t	t	t,t	t		Q	t	t,t	t	t	t	
Ru101	x	t	t	t	t	t,t	t	t	*	g	t	t	t,t	t	t	
Ru102	x	t	t	t	t	t	t,t	t	*	g	t,t	t	t	t	t	t
Ru104	x	t	t	t	t	t	t	t	* *	g	t	t	t	t	t	
Rh103	x,t	t,t	t,t	t,t	t	t	t	t		g,g	t	t	t	t	t	
Pd102	x	t	t	t	t,t	t,t	t,t	t	•	g	t,t	t,t	t,t	t	t	
Pd104	x	t	t	t	t,t	t,t	t,t	t	*	g	t,t	t,t	t,t	t	t	
Pd105	x	t	t	t	t,t	t,t	t,t	t	*	g	t,t	t,t	t,t	t	t	t
Pd106	x	t	t	t	t,t	t,t	t,t	t	*	g,g	t,t	t,t	t,t	t	t	t
Pd107	x,t	t	t	t	t,t	t,t	t,t	t	*	g	t	t,t	t,t	t	t	t
Pd108	x	t,t	t	t	t	t,t	t,t	t		g	t,t	t	t,t	t	t	t
Pd110	x	t,t	t	t	t	t,t	t	t	*,*	g	t,t	t	t,t	t	t	t,t
Ag107	x,t	ta,ta	ta,t	t,t	t	t	t	t,t	* *	a,a	t,t	t	t	t,t	t,t	t,t
Ag108	x,t	ta,t	ta,t	t,t	t,t	t	t	t,t	* *	a,g	t	t,t	t	t,t	t,t	t
Ag109	x,t	ta,ta	ta,t	t,t	t	t,t	t	t,t	*	a,a	ta,t	t	t,t	t	t,t	t,t
Cd106	x	t	t	t	t,t	t,t	t,t	t		g	t,t	t,t	t,t	t	t	t
Cd108	x	t	t	t	t,t	t,t	t,t	t	•	g	t,t	t,t	t,t	t	t	t,t
Cd110	x	t	t	t	t,t	t,t	t,t	t,t	*	g,g	t,t	t,t	t,t	t	t,t	t,t
Cd111	x,t	t	t	t,t	t,t	t,t	t,t	t		Q	t,t	t,t	t,t	t,t	t	t
Cd112	x	t,t	t	t	t,t	t,t	t,t	t,t	•	g,g	t	t,t	t;t	t	t,t	t,t
Cd113	x,t	t	t,t	t,t	t	t,t	t,t	t	* *	Q	t,t	t	t,t	t,t	t	
Cd114	x	t,t	t	t	t,t	t	t,t	t,t	* *	9.9	t	t,t	t	t	t,t	
Cd116	x	t,t	t	t	t,t	t	t,t	t,t	* *	g,g	t,t	t,t	t	t	t,t	
In113	x,t	t,t	t,t	t,t	t	t,t	t	t,t	* *	g,g	t,t	t	t.t	t.t	t,t	t
In115	x,t	t,t	t,t	t,t	t	t,t	t	t	,	g,g	t,t	t	t;t	t;t	t	t
Sn112	x	t	t	t	t,t	t,t	t,t	t	•	g,g	t,t	t,t	t,t	t	t	t,t
Sn114	x	t,t	t	t	t,t	t,t	t,t	t,t		g	t,t	t,t	t,t	t	t,t	t,t
Sn115	x	+	t,t	t,t	t,t	t,t	t,t	t	*•	g	t,t	t,t	t,t	t,t	t	t
Sn116	x	t	t	t	t,t	t,t	t,t	t,t	,	g,g	t,t	t,t	t,t	t	t,t	t,t
Sn117	x,t	t	t	t,t	t,t	t,t	t,t	t	*	Q	t,t	t,t	t,t	t,t	t	t
Sn118	x	t,t	t	t	t,t	t,t	t,t	t,t	*	g,g	t,t	t,t	t,t	t	t,t	t,t
Sn119	x,t	t	t,t	t,t	t,t	t,t	t,t	t	*,*	g	t,t	t,t	t,t	t,t	t	t
Sn120	x	t,t	t	t	t,t	t,t	t,t	t,t		Q,Q	t.t	t,t	t.t	t	t,t	t,t
Sn121	x,t	t	t,t	t,t	t,t	t,t	t,t	t	*,*	g	t;t	t,t	t;t	t,t	t	t
Sn122	x	t,t	t	t	t,t	t,t	t,t	t,t	* *	g,g	t,t	t,t	t,t	t	t,t	*,*
Sn124	x	t,t	t	t	t,t	t,t	t,t	*,*		g,g	t,t	t,t	t,t			*

4BLE 1 (cont'd)

Isotope	n,n*	n,2n	n,3n	n,na	n,np	n,nd	n,nt	n,nh	n,4n	n,g	n,p	n,d	n,t	n,h	n,a	n,2p
Sb121	x	t,t	t	t,t	t	t,t	t	t,t	***	g,g	t,t	t	t,t	t,t	t,t	t,t
Sb123	x	t,t	t	t,t	t	t,t	t	t,t	* *	g,g	t,t	t	t,t	t,t	t,t	t,t
Te122	x	t,t	t	t	t	t,t	t	t,t	*'*	g,g	t,t	t	t.t	t	t,t	t,t
Te123	x,t	t	t,t	t,t	t,t	t	t,t	t	*	g	t	t,t	t	t,t	t	t
Te124	x	t,t	t	t	t	t,t	t	t,t	*(*	g,g	t,t	t	t,t	t	t,t	t,t
Te125	x,t	t	t,t	t,t	t,t	t	t,t	t	*	g	t	t.t	t	t.t	t	t
1 127	x	t	t	t	t	t,t	t	t,t	*	g	t,t	t	t,t	t	t,t	t,t
! 129	x	t	t	t	t	t.t	t	t,t	*	g,g	t,t	t	t,t	t	t,t	t,t
Xe129	x,t	t	t,t	t,t	t	t	t	t	*'*	g	t	t	t	t.t	t	t
Xe130	x	?,t	t	t	t	t	t	t,t		g,g	t,t	t	t	t	t,t	
Xe131	x,t	t	t.t	t.t	t,t	t	t	t	*'*	g	t	t,t	t	t,?	t	
Xe132	x	t,t	t	t	l	t,t	t	t,t		g,g	t.t	t	t,t	t	:,t	
Cs133	x,t	t	t	t	t	t,t		t,t	*	g,g	t;t	t	t,t	t	t,t	t,t
Cs134	x,t	t	t	t,t	t,t	t	t,t	t		g,g	t	t,t	t	t,t	t	t,t
Cs135	x,t	t,t	t	t	t	t,t	t	t,t	*'*	9.9	t,t	t	t,t	t,t	t.?	t,t
Cs137	x	t,t	t,t	t,t	t	t,t	t	t,t	*	g,g	t	t	t,t	t	t,t	t,t
Ba130	x	t.t	t	t	t	t	t	t,t	* *	9.4	t	t	t	t	t,t	t,t
Ba132	..	t,t	t	t	t	t	t	t,t	*	g,g	t	t	t	t	t,t	t,t
Ba133	x,t	t	t,t	t,t	t	t	t	t	* *	g	t	t	t	t,t	t	t
Ba134	x	t.t	t	t	t	t	t	t,t	*	g,g	t,t	t	t	t	t,t	t,t
Ba135	x,t	t	t,t	t,t	t,t	t	t	t	* *	g,g	t.t	t,t	t	t,t	t	
Ba136	x,t	t,t	-	t	t,t	t,t	t	t,t	*	g,g	t;t	t,t	t,t	t	t,t	
Ba137	x,t	t,t	t,t	t.t	t,t	t,t	t,t	t	* *	g	t	t,t	t,t	t,t		
Ba138	x	t,t	t,t	t	t	t,t	t,t	t,t	*	g	t.t	t	t.t	t	t.t	t
La137	x	t	t	t	t,t	t,t	t	t,t	*	9	t,t	t,t	t;t	t,t	t,t	t,t
La138	x	t	t	t.t	t,t	t.t	t,t	t,t	*	a	t	t.t	t,t	t,t	t,t	t
La139	x	t	t	t;t	t	t;t	t,t	t,t	•	Y	t	t	t.t	t	t,t	t,t
La140	x	t	t	t,t	t	t	t,t	t	*	g	t	t	t	t,t	t	t
Ce136	x	t,t	t	t	t	t	t	t,t	* *	g,g	t	t	t	t	t,t	t,t
Ce138	x	t.t	t	t	t	t	t	t,t		9.9	t	t	t	t,t	t,t	t,t
Ce140	x	t,t	t	t,t	t	t	t	t,t	* *	g	t	t	t	t	t,t	t
Ce142	x	t	t	t	t	t	t	t	* *	g		t	t	t	t	t
Pr141	x	t	t	t	t	t,t	t	t	* *	9.3	t	t	t,t	*	t	t
Nd142	x	t,t	t	t	t	t	t	t,t	*	g	t,t	t	t	t	t,t	t
Nd143	x	t	t,t	t,t	t,t	t	t	t	* *	g	t	t,t	t	t	t	t
Nd144	x	t	t	t	t	t,t	t	t	*	9	t,t	t	t,t	t		t
Nd145	x	t	t	t	t,t	t	t,t	t	*	g	t	t,t	t	t	t	t
Nd146	x	t	t	t	t	t,t	t	t		9	t	t	t,t	t	t	t
Nd148	x	t	t	t	t	t	t	t	*	g	t,t	t	t	t		t
Nd150	x	t	t	t	t	t,t	t	t	*	9	t	t	t,t	t	t	t
Pm144	x	t	t	t	t	t	t,t	t		g	t	t	t	t,t	t	t
Pm145	x	t	t	t	t	t	t	t,t	*	3	t	t	t	t	t,t	t,t
Pm146	x	t	t	t,t	t	t	t	t	*	g	t	t	t	t,t	t	t
Pm147	x	t	t	t	t	t	t	t,t		g,g			t	t	t,t	t
Sm144	x	t,t	t	t	t	t	t	t.t	* *	g	t	t	t	t	t,t	
Sm145	x	t	t,t	t,t	t	t		t	*	g	t	t	t	t	t	
Sm146	x	t	t	t	t	t	t	t	*	g	t	t		t	t	t
Sm147	x	t	t	t	t	t	t	t	*	g	t	t	t	t	t	t
Sm148	x	t	t	t	t	t	t	t	*	g	t,t	t	t	t	t	t
Sm149	x	t	t	t	t,t	t	t	t	*	g	t	t,t	t	t	t	t
Sm150	x	t	t	t	t	t,t	t	t	*	g	t	t	t,t	t	t	t
Sm151	x	t	t	t	t	t	t,t	t	*	9	t	t	t	t	t	t
Sm152	x	t	t	t	t	t	t	t	*	g	t,t	t	t	t	t	t
Sm154	x	t	t	t	t	t,t	t	t		g	t,t	t	t,t	t	t	
Eu149	x	t	t	t	t	t	t	t	*	9.9	t	t	t	t	t	
Eu150	x.t	t	t	t	t	t	t	t	*	g	t	t	t	t,t	t	
Eu151	x	t,t	t	t	t	t	t	t,t	*	9.9	t	t	t	t	t,t	t
Eu152	x,t	t	t,t	t,t	t	t	t	t	* *	g	t	t	t		t	t
Eu153	x	t.t	t	t	t	t	t	t	*	g,g	t	t	t	t	t	t,t
Eu154	x,t	t	t,t	t	t	t	t	t		g	t	t	t	t,t	t	t
Eu155	x	t,t	t	t	t		t	t,t	*,*	g	t	t	t	t	t,t	t,t

TABLE 1 (cont'd)

Isotope	n,n*	n,2n	n,3n	n,na	n,np	n,nd	n,nt	n,nh	n,4n	n,g	n,p	n,d	n,t	n,h	n,a	n,2p
Gd148	x	t	t	t	t	t	t	t	**	g	t	t	t	t	t	t
Gd150	x	ta	t	t	t	t	t	t	*	a	t,t	t	t	t	t	t
Gd151	x	ta	t	t	t,t	t	t	t	*	a	t	t,t	t	t	t	t
Gd152	x	t	t	t	t	t,t	t	t	*	g	t,t	t	t,t	t	t	t
Gd154	x	t	t	t	t	t,t	t	t	*	g	t,t	t	t,t	t	t	t
Gd155	x	t	t	t	t,t	l	t,t	t	*	g	t	t,t	t	t	t	t
Gd156	x	t	t	t	t	t,t	t	t	*	g	t	t	t,t	t	t	t
Gd157	x	t	t	t	t	t	t,t	t	*	g	t	t	t	t	t	t
Gd158	x		t	t		t	t	t	*	g	t	t	t	t	t	t
Gd160	x	t	t	t	t	t	t	t	* *	g	t	t	t	t	t	x
Tb157	x	t,t	t	t	t	t	t	t,t	*	9.9	t	t	t	t	t,t	t
Tb158	x,t	t	t,t	t,t	ι	t	t	t	* *	g	ŧ	t	t	t	l	
Tb159	x	t,t	t	t	t	t	t	t	,	g	t	t	t	t	t	
Dy154	x	t	t	t	t	t,t	t,t	t	*	g	t,t	t	t,t	t	t	t
Dy158	x	t	t	t	t	t,t	ŧ	t	*	g	t,t	t	t,t	t	t	t
Dy160	x	t	t	t	t	t,t	t	t	*	g	t	t	t,t	t	t	t
Dy161	x	t	t	t	t	t	t,t	t	* *	g	t	t	t	t	t	t
Ho163	x,t	t,t	ta,t	t	t	t	t	t	* *	a,a	ta	t	t	t	t	t
Ho165	x	ta.ta	ta,t	t	t	t	t	t	* *	a,a	ta,t	t	t	t	t	t
Ho166	x,t	ta	ta,t	t	t,t	t	t	t	*	a	ta	t,t	t	t	t	t
Er162	x	t	t	t	t,t	t,t	t,t	t	*	g	t,t	t,t	t,t	t	t	
Er164	x	t	t	t	t,t	t,t	t,t	t	*	g	t,t	t,t	t,t	t	t	t
Er166	x	t	t	t	t	t,t	t,t	t	*	g,g	t,t	t	t.t	t	t	t,t
Er167	x,t	t	t	t	t,t	t	t,t	t	*	g	t	t,t	t	t,t	t	t
Er168	x	t,t	t	t	t	t,t	t	t,t	* *	g	t	t	t,t	t	t,t	t
Er170	x	l	t	t	t	t	t	l	*	g	t,t	t	t	t	t	t
Tm169	x	t	t	t	t	t,t	t	t,t	* *	g	t	t	t,t	t	t,t	t
Lu175	x	ta,ta	ta	t	t	t	t	t	*	a,a	t	t	t	t	t	t
Lu176	x,t	ta	ta,ta	t	t	t	t	t	*	a,a	t,t	t	t	t	t	t
Hf174	x	t	t	t	t	t,t	t,t	t	*	g	t,t	t	t,t	t	t	
Hf176	x	t	t	t	t	t,t	t	t	*	9.9	t,t	t	t,t	t	t	t
Hf177	x,t	t	t	t	t,t	t	t,t	t	*	g,g	t,t	t,t	t	t	t	t.t
Hf178	x,t	t,t	t	t	t,t	t,t	t	t	*	g,g	t,t	t,t	t,t	t,t	t	t;t
Hf179	x,t	ta,t	ta,g	t	t,t	t,t	t,t	t,t	* *	a,g	ta	t,t	t,t	t,t	t,t	t
Hf180	x,t	ta,t	ta,t	t,t	t	t,t	t,t	t,t	* *	a	ta	t	t,t	t	t,t	*
Hf182	x,t	t	t,t	t	x	t	t	x	*	g	x	x	t	x	x	
Ta180	x,t	t	t,t	t,t	t,t	t,t	t,t	t,t	* *	g	t,t	t,t	t,t	t,t	t,t	
Ta181	x	ta,ta	te	ta,g	t,t	t,t	t,t	t,t	*	a,a	te	t,t	t,t	t	t,t	t
W 180	x	ta,g	ta	t	t	t,t	t	t,t	* *	a	ta,g	t	t,t	t,t	t,ta	t,t
W 182	x	te	ta	t,t	t	t,t	t	t,t	*	a,g	te,g	t	t,t	t.t	ta,ta	t
W 183	x,t	ta	te	t,ta	te,g	l	t,t	t,t	*	a	te	t,t	l	l	ta,g	t,t
W 184	x	ta,g	ta	t,t	te	t,t	t	t	* *	a,g	te	t	t,t	t.,t	te	t
W 186	x	te,g	ta	t,t	te	t	t	t	* *	a	te	t	t	t	te	*
Re185	x	ta,ta	ta	t	t	t,t	t	t,t		a,g	ta,t	t	t,t	t	t,t	t
Rei86	x,t	ta	ta,ta	t,t	t,t	t	t,t	t	* *	a	ta	t,t	t	t	t	t
Re187	x	ta,t	ta	t	t	t,t	t	t	* *	a,a	ta	t	t,t	t	t	t
Os184	x	t,t	t	t	t	t,t	t	t	* *	g	t,t	t	t,t	t	t	t,t
Os186	x	t	t	t	t	t,t	t	t,t	*	g	t,t	t	t,t	t	t,t	t,t
Os187	x	t	t	t,t	t,t	t	t,t	t		g	t	t,t	t	t,t	t	t
Os188	x	t	t	t	t	t,t	t	t.t	*	g,g	t.t	t	t.t	t	t,t	t
Os189	x,t	t	t	t,t	t,t	t	t,t	t	*	9.9	t	t,t	t	t	t	
Os190	x,t	t,t	t	t	t	t,t	t	t	* *	9.9	t,t	t	t,t	t	t	
Os192	x,t	t,t	t,t	t	t	t,t	t	t	* *	g	t	t	t,t	t	t	t
Os194	x	t	t,t	t	x	x	x	x	,	g	x	x	x	x	x	x
Ir191	x,t	t,t	t	t	t,t	t,t	t	t,t	*	g,g	t,t	t,t	t,t	t	t,t	t,t
Ir192	x,t	t,t	t,t	t,t	t,t	t,t	t.t	t	* *	9.9	t,t	t,t	t,t	t,t	t	t
Ir193	x,t	t,t	t,t	t	t,t	t,t	t;t	t,t	,	9.9	t	t,t	t,t	t	t,t	t
Pt190	x	t	t	t	t	t	t	t	*	g	t,t	t	t	t	t	t,t
Pt192	x	t	t	t	t,t	t,t	t	t,t	*	g,g	t,t	t,t	t,t	t.t	t,t	t,t
Pt193	x,t	t	t	t,t	t,t	t,t	t,t	t,t	*	g	t,t	t,t	t,t	t;t	t,t	t,t
Pt194	x	t,t	t	t,t	t,t	t,t	t,t	t,t		g,g	t,t	t,t	t,t	t,t	t,t	t

TABLE 1 (cont'd)

Isotope	n,n*	n,2n	n,3n	n,na	n,np	n,nd	n,nt	n,nh	n,4n	n,g	n,p	n,d	n,t	n,h	n,a	n,2p
Pt195	x,t	t	t,t	t,t	t,t	t,t	t,t	t,t	*,*	g	t,t	t,t	t,t	t	t,t	t
Pt196	x	t,t	t	t,t	t,t	t,t	t,t	t	* *	g,g	t,t	t,t	t,t	t	t	t
Pt198	x	t,t	t	t	t,t	t,t	t,t	t		g,g	t	t,t	t,t	t	t	t
Au197	x,t	ta,ta	ta,t	t,t	t	t,t	t	t,t	*,*	a,g	ta,t	t	t,t	t,t	ta,t	t,t
Hg194	x	t,t	t	t	t,t	t	t,t	t	* *	g,g	t	t,t	t	t	t	t,t
Hg196	x	t,t	t	t	t,t	t	t,t	t,t	* *	g,g	t,t	t,t	t	t	t,t	t,t
Hg198	x	t,t	t	t	t,t	t,t	t,t	t	*	g,g	t,t	t,t	t,t	t	t,t	t,t
Hg199	x,t	t	t,t	t,t	t,t	t,t	t,t	t	* *	g	t	t,t	t,t	t,t	t	t
Hg200	x	t,t	t	t	t	t,t	t,t	t,t	*	g	t,t	t	t,t	t	t,t	t,t
Hg201	x	t	t,t	t,t	t,t	t	t,t	t	* *	g	t	t,t	t	t,t	t	t
Hg202	x	t	t	t	t	t,t	t	t,t	*	g	t	t	t,t	t	t,t	t
Hg204	x	t	t	t	t	t	t	t	*	g	t	t	t	t	t	x
11203	x	t	t	t	t	t	t	t,t		g	t	t	t	t	t,t	t
Tl205	x	t	t	t	t	t	t	t	*,*	g,g	t	t	t	t	t	t
Pb202	x,t	t,t	t	t	t	t	t	t,t		g,g	t	t	t	t	t,t	t
Pb204	x,t	ta,t	ta,t	t	t	t	t	t	* *	a	t	t	t	t	t	t
Pb205	x	ta,t	ta,t	t	t	t	t	t		a	t	t	t	t	t	t
Pb206	x	ta	ta,t	t	t	t	t	t	* *	a,g	t,t	t	t	t	t	t
Pb207	x,t	ta	ta	t	t,t	t	t	t	* *	a	t,t	t,t	t	t	t	t
Pb208	x	ta,t	ta	t	t,t	t,t	t	t	*,*	a	t	t,t	t,t	t	t	x
Pb210	x	t	t	t	t	t	t,t	t	*	g	t	t	t	t	t	t
Bi207	x	t	t	t	t	t	t,t	t	*	g	t,t	t	t	t	t	t,t
Bi208	x	t	t	t	t,t	t	t	t	*	g	t	t,t	t	t,t	t	t,t
Bi209	x	t	t	t	t	t,t	t	t,t	*	g,g	t	t	t,t	t,t	t,t	t
Bi210	x,t	t	t	t,t	t	t	t,t	t,t		g	t	t	t	t	t,t	t
Po209	x	t	t,t	t	t	t	t	t	*	g	t	t	t	t,t	t	t

A = ACTL evaluation to 20 MeV
E = ENDFIB-V evaluation to 20 MeV
G = estimate based on similar reaction
H = HEDL evaluation
L = LANL evaluation
T = THRESH calculation to 40 MeV
Ta = ACTL evdluation to 20 MeV, normalized THRESH calculation to 40 MeV
Te = ENDFIB-V evaluation to 20 MeV, normalized THRESH calculation to 40 MeV
Th = HEOL evaluation to 20 MeV, normalized THRESH calculation to 40 MeV
X = reaction not allowed or leads to isotope with unknown mass
Y = reaction leads to isomeric state with half-life less than 1 minute and which decays predominately through isomeric transition
* = no data

Li 6	n,2na(E)			
Li 7	n,2na(E)			
B 10	n,nd2a(E)	n,2np(E)	n,ta(E)	
C 12	n,n2a(E)			
N 14	n,2a(E)			
Fe54	n,2na(L)	n,3na(L)	n,pn(L)	n,2np(L)
Fe56	n,2na(L)	n,3na(L)	n,2np(L)	

CHAPTER 4

FUNDAMENTAL MECHANICAL BEHAVIOR

DETERMINATION OF THE HARDENING RESPONSE IN THREE SURROGATE MATERIALS USING BALL MICROHARDNESS TECHNIQUES

G.E. Lucas, K. Shinohara†, G.R. Odette (University of California, Santa Barbara)

1.0 Objectives

The objective of this effort was to determine the viability of using ball microhardness techniques to monitor a hardening response in three heat treatable alloys.

2.0 *Summary*

The constitutive relationship of three heat treatable alloys was investigated with ball microhardness techniques. The three alloys, 17-4 PH stainless steel, a Cu-Be alloy, and 13-11-3 Ti, were heat treated to produce a hardening response similar to that exhibited by irradiated material. True stress-true plastic strain curves were determined by both conventional tension tests and ball microhardness tests conducted at ambient temperature. The two data sets showed good agreement, indicating the validity of using ball microhardness techniques to determine the flow property changes in a given material subject to environmentally-induced modification.

3.0

Title: Damage Analysis and Fundamental Studies for Fusion Reactor Materials Development
Principal Investigators: G.R. Odette and G.E. Lucas
Affiliation: University of California, Santa Barbara

4.0 Relevant DAFS Program Plan Task/Subtask

Subtask E Mechanical Properties

5.0 Accomplishments and Status

5.1 Introduction

Development of small specimen test techniques is an integral part of the fusion reactor materials program, since neutron irradiation volume limitations, as well as other restrictions, necessitate the use of relatively small volume specimens. Accordingly, we have been engaged in the development of a number of small specimen techniques,[1-6] one *of* which is ball microhardness testing. While it has been demonstrated that this technique can be used to determine the approximate constitutive relationship for a range of materials, it was desirable to demonstrate that *changes* in properties could be determined using ball microhardness, since property changes are of fundamental interest in studying radiation damage. Consequently, the purpose of this study was to demonstrate that ball microhardness tests could be used to measure the constitutive behavior of several alloys, heat treated to effect changes in strength and ductility.

---

† Visiting Scientist, Department of Nuclear Engineering, Kyushu University

5.2 Materials

We performed ball microhardness tests on three alloys which had been used previously in an investigation of the relationship between indentation pile-up geometry and plastic flow homogeneity. These alloys were 17-4-PH stainless steel, Cu-2 Be (17200 Beryllium copper), and a 13 V-11 Cr-3 Al titanium alloy. Each of these alloys is age hardenable, and we investigated two conditions for each: a relatively hard and soft condition. The heat treatment for each is given in Table 1. Hence, the "hard" condition for each material was achieved by age hardening. The "soft" condition for Cu-2 Be was achieved by solution annealing, whereas for 17-4 PH stainless steel and 13-11-3 Ti it was achieved by overaging. These heat treatments were selected to optimize specimen preparation in addition to achieving a difference in strength level. To a certain extent, the age hardening response of the Cu-Be alloy could be considered as analogous to a radiation hardening response, whereas the overaging of the Ti alloy and the stainless steel gives rise to a response similar to that exhibited by materials during post-irradiation annealing.

5.3 Experimental Procedure

Three tensile specimens were fabricated and tested for each specimen. The specimens were 6.4 mm diameter x 50.8 mm long with a gage section 3.2 mm diameter x 25.4 mm long. Specimens of the 17-4 PH stainless steel and Cu-2 Be were fabricated prior to heat treatment. Specimens of the 13-11-3 Ti alloy were fabricated in the solution-annealed condition, and aging was performed subsequently. This was done to achieve optimum machinability during fabrication.

The fabricated, heat treated specimens were tested in uniaxial tension in an MTS 810 testing machine, using a calibrated clip gage extensometer to monitor gage section displacements. Tests were performed at ambient temperature at a constant displacement rate of .028 mm/s. True stress-strain curves were determined from the load displacement data.

Following tensile testing, the end sections of selected tensile specimens were sectioned off and mounted in phenolic resin metallographic mounts. The specimens were ground and mechanically polished through .05 μm Al_2O_3. Ball microhardness tests were then performed on each specimen using 0.25 mm, 0.76 mm and 1.52 mm diameter hardened steel balls and loads in the range 100 g to 10 kg. The resulting data were converted to true stress-strain data. Test equipment and procedures are described elsewhere.[5]

5.4 Results and Discussion

The true stress-strain curves determined from tensile tests are compared to ball microhardness data in Figs. 1-3. The small dashed lines represent linear regression fits to the microhardness data; and the values of the work hardening exponent, $n = d \log \sigma / d \log \varepsilon$, determined for both the tensile data and the ball microhardness data, are indicated on the figures. The microhardness data are in quite good agreement with the tensile data. They correctly predict the relative increase in flow stress between hard and soft conditions, and microhardness-derived predictions of the work hardening exponent are in reasonable agreement with values derived from tensile data, except for two cases: the hard condition of 17-4 PH stainless steel and the soft condition of 13-11-3 Ti alloy. In addition, it can be seen that in almost all cases the microhardness data tend to predict values of flow stress and work hardening exponents which are systematically high relative to the tensile data. This may be a result of using a value of $\Psi_{max} = P_m/\sigma = 2.8$ in our microhardness data correlation where P_m is the mean pressure at the indenter-specimen interface and σ_f is the flow stress of the material when the plastic zone below the indenter is fully developed. A value of 2.8 for Ψ_{max} has been adopted based on the work of Tabor[7] on a variety of metals, but it is well known that strain rate effects[8] and alloy variations can lead to small changes in Ψ_{max}. For instance, if an alternate value of $\Psi_{max} = 3.0$ were used for the materials investigated here it would decrease the value of the true stress for the data at $\varepsilon_p \gtrsim .05$, whereas the data below $\varepsilon_p \sim .05$ would be less affected. Hence, the microhardness data would fit the tensile data better, and values of n evaluted from the two data sets would be more similar. To fine tune the procedure it may be necessary in the future to calibrate the microhardness correlation, and particularly the value of Ψ_{max}, against known constitutive data prior to applying the correlation to evaluate changes in mechanical properties induced by heat treatments or irradiation.

5.5 Conclusions

We have performed both uniaxial tension and ball microhardness tests on three alloys heat treated to two conditions of relative hardness. The ball microhardness data were in reasonable agreement with the tensile

Table 1

Schedule of Heat Treatments

Material	Heat Treatment	
	"Soft"	"Hard"
17-4 PH Stainless Steel	Solution Anneal @ 1040°C, 1h; Water Quench; Age @ 650°C, 6h	Solution Anneal @ 1040°C, 1h; Water Quench; Age @ 480°C; 1h
Cu-2 Be	Solution Anneal @ 800°C, 0.5h; Water Quench	Solution Anneal @ 800°C, 0.5h; Water Quench; Age @ 330°C, 1h
13-11-3 Ti	Solution Anneal @ 845°C, 1h; Oil Quench; Age @ 540°C, 1h	Solution Anneal 845°C, 1h; Oil Quench; Age @ 260°C, 1h

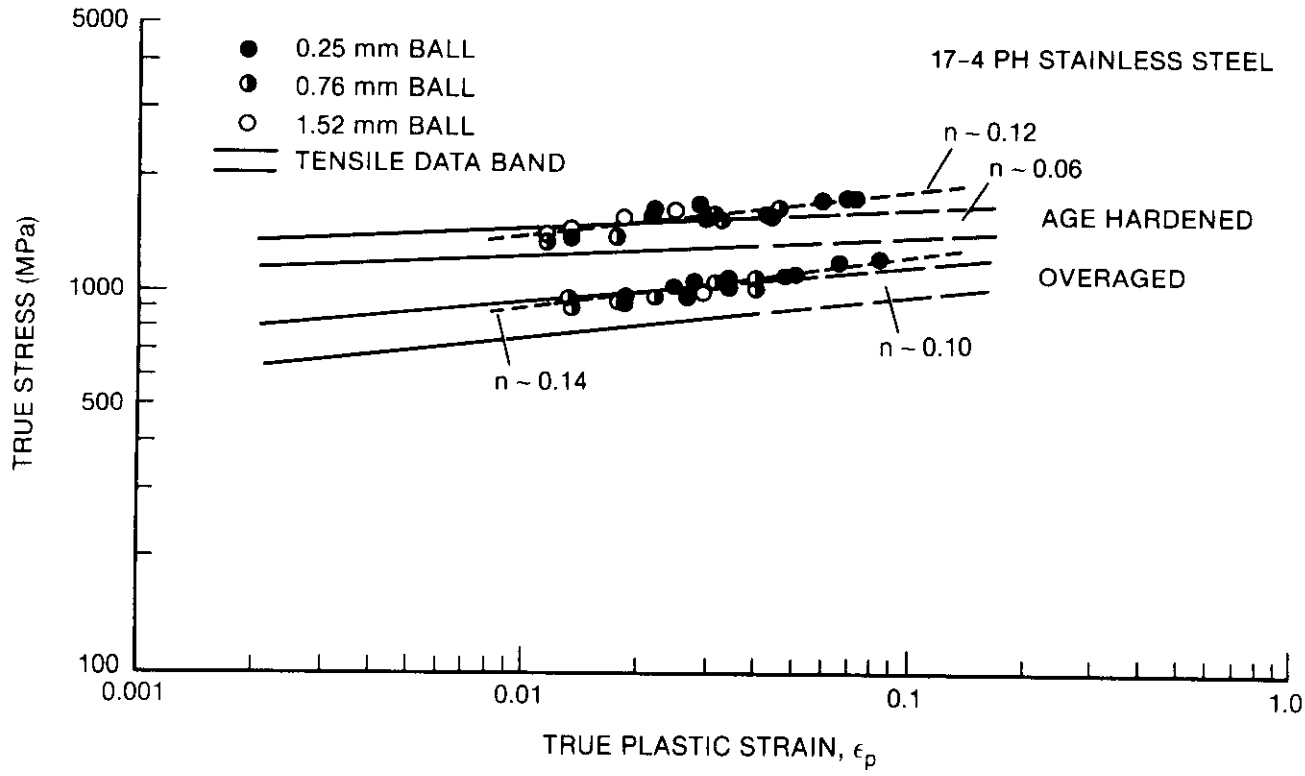

Fig. 1. Comparison of true-stress, true-plastic-strain data obtained from tension tests and ball microhardness tests for 17-4 PH stainless steel.

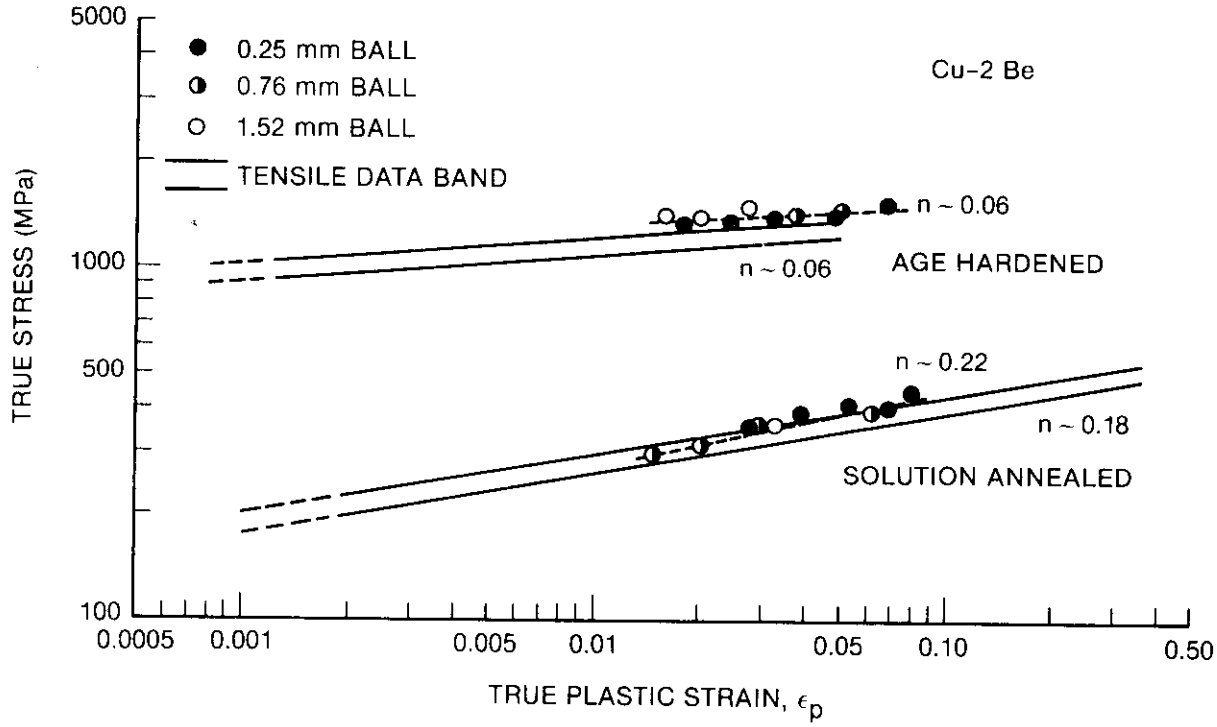

Fig. 2. Comparison of true-stress, true-plastic-strain data obtained from tension tests and ball microhardness tests for Cu-2 Be.

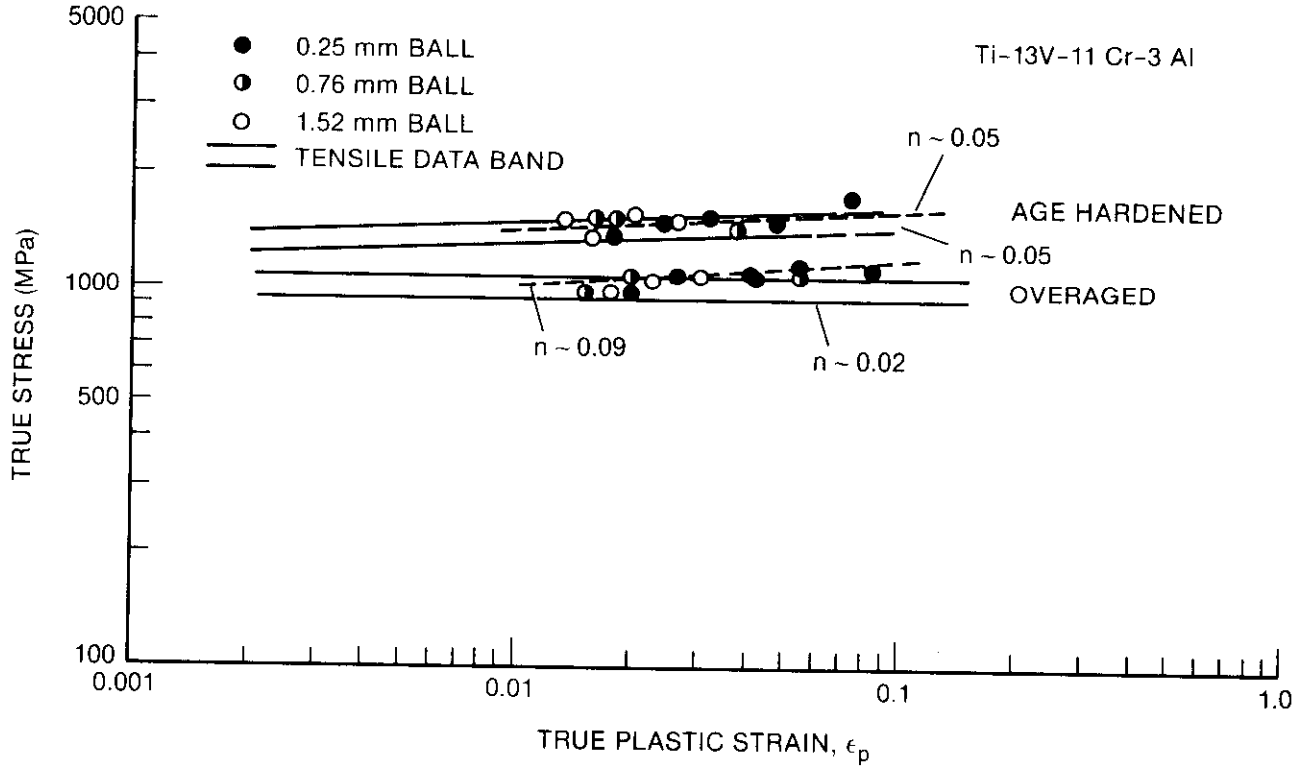

Fig. 3. Comparison of true-stress, true-plastic-strain data obtained from tension tests and ball microhardness tests for 13-11-3 Ti alloy.

data, indicating the viability of using the technique to monitor changes in the constitutive behavior of a material as a function of environmental history. However, the microhardness-based flow stress and work hardening exponents tended to be systematically high. This can be resolved by using a higher value of Ψ_{max} than is currently used in the correlation procedure, and it may be necessary in the future to determine the optimum value of Ψ_{max} for a particular material by a calibration procedure.

6.0 References

1. G.E. Lucas and N.F. Panayotou, J. Nucl. Mater., 103/104 (1981) 1527

2. G.E. Lucas and C. Pendleton, J. Nucl. Mater. 103/104, (1981) 1539

3. M. Dooley, G.E. Lucas, and J.W. Sheckherd, J. Nucl. Mater., 103/104 (1981) 1533.

4. G.E. Lucas, J. Nucl Mater., 117 (1983) 327

5. G.E. Lucas, J.W. Sheckherd, G.R. Odette, "Shear Punch and Microhardness Tests for Strength and Ductility Measurements," Proc. of Symp. on Use of Nonstandard Subsized Specimens for Irradiated Testing", ASTM, Albuquerque, NM, September 1983.

6. G.E. Lucas, G.R. Odette, J.W. Sheckherd, P. McConnell, and J. Perrin, "Subsized Bend and CVN Specimens For Irradiated Testing," Ibid.

7. D. Tabor, The Hardness of Metals, Clarendon Press, Oxford (1950).

PREDICTIONS OF FRACTURE TOUGHNESS IN IRRADIATED AISI 316 BASED ON A TENSILE-TOUGHNESS CORRELATION

M. L. Hamilton, F. A. Garner and W. J. S. Yang (Hanford Engineering Development Laboratory)

1.0 Objective

The object of this effort is to provide predictive correlations for fracture toughness of irradiated materials based on more easily obtained tensile data.

2.0

Since the microstructural origins of radiation-induced toughness degradation are presumed to be identical to those that cause changes in tensile properties, it appears possible to make predictions of residual fracture toughness based on changes in the tensile behavior and and the associated microstructural evolution of the steel. A model for tensile-toughness correlations is presented which appears to be valid for radiation-hardened stainless steels. Tensile data from both ducts and cladding tubes of 20% cold-worked AISI 316 irradiated in EBR-II are used to make the prediction that sufficient toughness is retained in this steel for both fast reactor and fusion reactor applications.

3.0 Program

Title: Irradiation Effects Analysis (AKJ)
Principal Investigator: D. G. Doran
Affiliation: Hanford Engineering Development Laboratory

4.0 Relevant OAFS Program Plan Task/Subtask

II.C.14 Models of Flow and Fracture Under Irradiation
II.C.16 Composite Correlation Models and Experiments

5.0 Status and Accomplishments

5.1 Introduction

Radiation-induced reductions in the fracture toughness of structural metals have been cited as a major potential limit on the lifetime of the first wall of a fusion reactor.[1,2] Both the fatigue crack growth rate and the mode of failure (leak vs. sudden crack propagation) will depend on the fracture toughness. Unfortunately, there is only a rather small amount of published data on the toughness of irradiated metals.

Since the microstructural origins of toughness degradation are presumed to be identical to those of tensile properties, there is hope that predictions of toughness reduction can be based on changes in the tensile behavior and the associated microstructural evolution of the steel. Current efforts in this activity are focused on cold-worked AISI 316 stainless steel, which is currently used in U.S. fast reactors and is also proposed as a candidate for use in first generation fusion devices.

There are a variety of problems to surmount in the development of a tensile-toughness correlation which would be applicable to a wide range of irradiation and test environments. First, one must select and validate a suitable model. Second, sufficient toughness and tensile data must be available, preferably on a single heat of material in order to avoid heat-to-heat variations in radiation-induced response. Finally, some estimate must be made of the possible differences in response that might arise due to dif-

ferences in neutron flux and spectrum between the environment from which the data were derived and that of the fusion device. Since most of the relevant data were derived from fast reactor irradiations, one of the primary spectral-related concerns is that of the helium/dpa ratio, which will be much larger in fusion devices.

For AISI 316 there is a very limited amount of toughness and tensile data derived from the same starting material, and the toughness data are only available for a narrow range of irradiation temperatures around 400°C. Although tensile data on the same or closely-related steels are available at other irradiation temperatures, they were derived largely from tests on thin-walled cylindrical tubes representative of that used in fast reactor fuel cladding. While strength measurements on tubes are generally quite consistent with measurements made on ldrqer flat tensile specimens, it is known that ductility values dre generally smaller for tubes.[3]

Recently, there have been a series of successful correlations between microstructure and tensile properties in 300 series stainless steels[3-7] and one correlation for irradiation at 400°C between tensile behavior and toughness.[8] Advances have also been made in our understanding of the influence of helium and other spectrum-related considerations on radiation-induced microstructure and associated dimensional changes. This paper attempts to extend this record of success and develop a fusion-relevant tensile-toughness correlation applicable to a wider range of irradiation temperature and neutron spectra.

5.2 The Choice of Model

Wolfer and Jones have provided an assessment of the models available to correlate the toughness and tensile properties of irradiated metals.[9] They showed that the model of Krafft[10] was more successful than was the model of Hahn and Rosenfield[11] in predicting reasonable values of fracture toughness for 20% cold-worked AISI 316 irradiated in mixed spectrum reactors. Huang and Wire also showed that the Hahn-Rosenfield model could not predict the toughness of 20% cold-worked AISI 316 irradiated in the EBR-II fast reactor hut that it could reproduce the behavior of unirradiated steel.[12,13]

Hamilton and coworkers successfully predicted the behavior of irradiated 20% cold-worked 316 observed by Huang using the model of Krafft[10] as modified by Schwalbe and Backfisch.[14] However, the *input* parameters were modified somewhat in that analysis. This twice-modified version of the Krafft model will also be employed in this paper.

The Krafft model considers fracture instability as occurring in small elemental fracture cells lying along the crack front. These cells act as coherent ductile ligaments which are the last connecting links at the crack front. Instability is visualized to occur when a critical strain develops over a specific distance ahead of the crack tip. This distance is referred to as the process zone size, and is the smallest material dimension necessary for a crack propagation element. The choice of the appropriate process zone size requires some knowledge of the nature of the fracture surface and the crack nucleation sites.

The modified Krafft correlation is given by

$$\sigma_y = \frac{\pi(1+n)d^* (\varepsilon_f E/\sigma}{} \qquad (1)$$

where: σ_y = yield strength
ε_f = true fracture strain
E = Young's modulus
u = Poisson's ratio
n = strain hardening exponent
d^* = size of the fracture process zone

If power-law strain-hardening is assumed,

$$\varepsilon/\varepsilon_0 = (\sigma/\sigma_0)^{\frac{1}{n}}, \qquad (2)$$

where ε_0 and σ_0 are two arbitrary reference values of the unaxial strain and stress, respectively. The strain-hardening exponent n can then be obtained from the relationship

$$n = \ln(\sigma_u/\sigma_y) \;/\; \ln(E\ \varepsilon_u/\sigma_y), \qquad (3)$$

where σ_u and ε_u are the true ultimate stress and true uniform strain. In the irradiated specimens considered in this study, n was found to be small, on the order of 0.03.

The values of d^* and ε_f were somewhat vaguely defined in previous studies, and there has been no definitive guidance for their selection. For irradiated austenitic stainless steels, the grain size and the total elongation, respectively, were chosen by Hamilton and coworkers.[8] The choice of these convenient and easy-to-measure parameters was defended in terms of both their success and because of the extensive radiation-induced hardening that occurs in this steel at temperatures in the range of 370-500°C. The radiation-induced microstructure occurs on a very fine scale within the grains, but the small voids and other microstructural components do not appear to act as crack nucleation sites. Larger precipitates at the grain boundaries could serve as such sites, however. The deformation is characterized by channeling of dislocation motion into narrow deformation zones that can span the entire grain. Distortion of irradiation-induced voids within these zones leids to local strain estimates of several hundred percent.[8] When these zones intersect grain boundaries, particularly near large boundary precipitates, crack nucleation is a potential consequence. Thus the process zone size d^* was chosen to be the averaqe grain diameter.

The presence of flow localization of this type apparently does not invalidate the use of a fracture model which assumes that deformation around the crack tip can be described by the macroscopic deformation law for plasticity. The reason why the Krafft model appears to work for highly irradiated metals is probably that the extent of the plastic zone (estimated to be ~2 mm) is much larger than the microscopic scale of flow localization. Thus the stress relaxation invoked by this model occurs over a dimension in which only the average strain is important.

5.3 The Toughness Data

Huang and Fish[14] performed tensile tests at 593°C on notched and unnotched specimens made from 20% cold-worked 316 ducts irradiated at 375-415°C in EBR-II to a fluence of 7.8 x 10^{22} n/cm^2 (E > 0.1 MeV). Based on a J-integral analysis of the load-displacement curves from two notched specimens irradiated at 375 or 415°C and tested at 593°C, they obtained fracture toughness values ranging from 57.2 to 67.7 MPa $\sqrt{m}$.

Huang and Wire[12] also made measurements on compact tension specimens fabricated from an EBR-II duct irradiated to fluences of 11.0 to 11.3 x 10^{22} n/cm^2 (E > 0.1 MeV) at temperatures ranging from 377-400°C. The test temperatures were 20, 232, 427, 538 and 649°C. These results have recently been revised slightly by Huang[13] and are shown in Figure 1.

Huang concluded that irradiation of 20% cold-worked AISI 316 at ~400°C leads to a reduction in toughness on the order of ~20 MPa fm that is relatively independent of test temperature. This reduction appears to saturate with neutron fluence and allows adequate remaining toughness for fast reactor applications.

5.4 Test of the Correlation

As described elsewhere[8] the correlation given in equation 1 was tested using tensile data derived from the same duct material as that used by Huang and coworkers to derive the toughness data. The excellent agreement between tensile-based predictions and measurements is shown in Figure 2.

While there are no toughness data at an irradiation temperature of 425°C on the duct material, there are tensile data. Figure 3 shows that this correlation predicts a sensitivity to irradiation temperature which is strongest for tensile tests conducted below the irradiation temperature. Since Huang concluded that the toughness was adequate for irradiation temperatures near 400°C, it should be more than adequate for higher irradiation temperatures. Additional data at other temperatures are necessary to confirm this conclusion, however.

5.5 Predictions Using Tube Data

A wider range of irradiation temperatures (370-650°C) has been explored in the tensile experiments conducted on irradiated cladding tubes.[3,15,16] As shown in Figure 4, tensile data developed from tubes show that cold-worked AISI 316 tends to harden at lower irradiation temperatures and soften at higher temperatures. This behavior has been explained in terms of the behavior of the microstructural components induced by radiation.[4,5] Note in Figure 4 that the yield strength in AISI 316 tends to saturate at relatively low fluence and not change with further irradiation. A similiar behavior is observed in the ductility. Note that with two exceptions the data do not extend beyond 5 x 10^{22} n cm^{-2} (E > 0.1 meV) or 25 displacements per atom (dpa) at most irradiation temperatures. Hamilton and coworkers showed that, with one exception, the tendency of the yield strength to saturate is maintained to fluences as high as 1.3 x 10^{23} n cm^{-2} (E > 0.1 MeV) or 65 dpa. This exception involves a subequent softening at temperatures below 400°C and very high neutron exposures and will be discussed later.

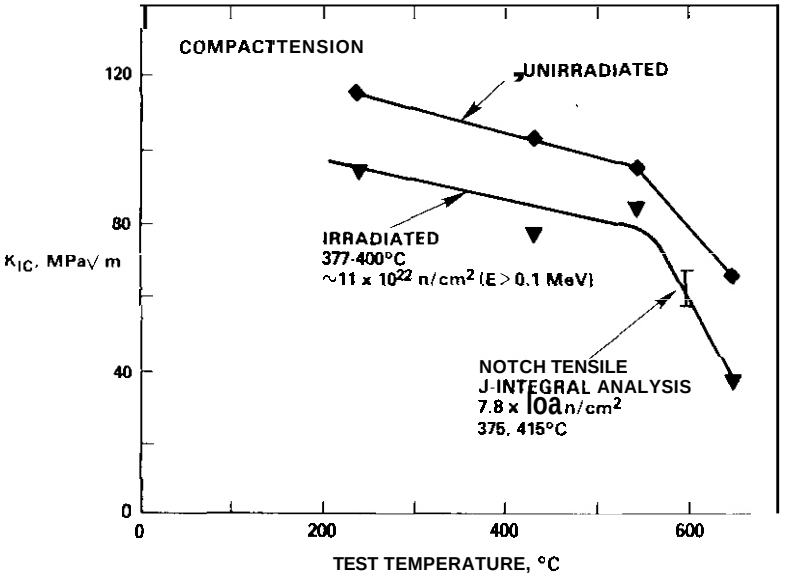

Figure 1: *Fracture Toughness* Data for 20% Cold-worked 316 Stainless Steel, by Huang and Coworkers.[12,14] The specimens were irradiated at temperatures and neutron fluences shown.

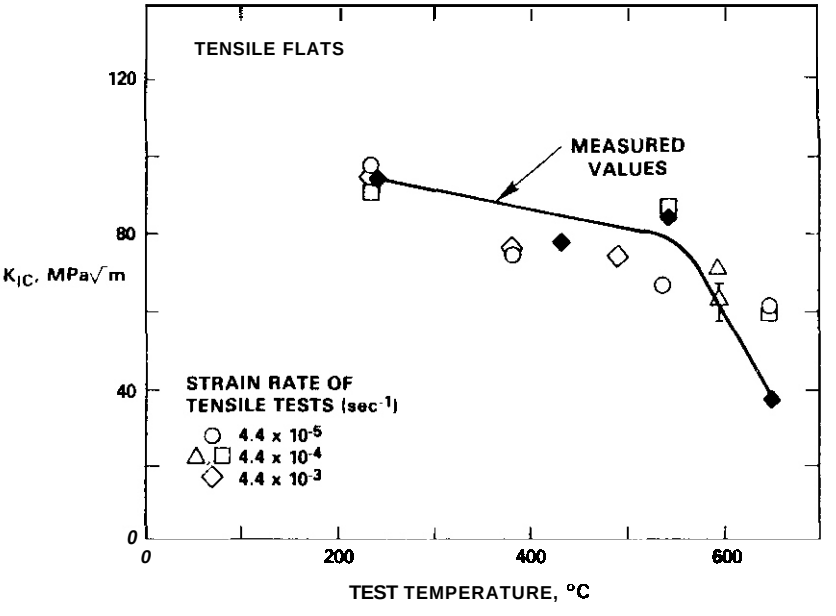

Fiqure 2. Comparison of Tensile-Based Predictions for an Irradiation Temperature of 379°C with Toughness Data (solid symbols) on EBR-II Ducts Irradiated at 375-415°C.[8]

Using the tensile data of reference 8 and a grain size (20 μm) appropriate for the tubes, Figure 5 shows a comparison between predictions of the modified Krafft Model and toughness data. A correction was required for the factor of two reduction observed in total ductility of tubes compared to tensile flats. Note first that the tube-based prediction at 404°C agrees well with the duct data generated at 377-400°C. This provides some additional confidence in the tensile-toughness correlation.

It also appears from the tube-based predictions that the toughness should increase with irradiation temperature as suggested earlier in Figure 4. Comparison of the data at 30-40 dpa with that at 60-65 dpa also support the earlier conclusion that both the toughness and tensile properties should saturate.

It now appears, however, that the saturation observed in both microstructure and tensile properties does not necessarily represent the equilibrium or terminal state, particularly for lower irradiation temperatures. Figures 6 and 7 show that at 370-405°C the yield strength beqins to fall and the ductility

starts to increase above 1.0×10^{23} n cm^{-2} (E > 0.1 MeV) or 50 dpa. It is obvious that this softening will have an impact on the fracture toughness. It is expected, however, that the toughness will increase only slightly or remain roughly the same. The tendency to increase should arise from the softening which returns the material to a state of hardness characteristic of a higher irradiation temperature. The increase is not expected to be large, since for small work-hardening coefficients, equation (1) reduces to

$$K_{IC} \sim (\sigma_y \varepsilon_f)^{1/2}. \qquad (4)$$

Thus opposing changes in yield strength and ductility tend to cancel each other.

The origin of the softening does not appear to be related to changes in void, dislocation or Frank loop microstructure. Microscopy examination shows that the hardening arising from these microstructural components remains essentially constant at higher fluence. The softening was found to be a consequence of the removal of molybdenum, chromium and silicon from the alloy matrix. These elments are slowly segregated in large grain boundary n-silicide precipitates. There is a concurrent dissolution of a fine dispersion of small carbide precipitates which formed early in the irradiation at sizes on the order of 2.0 nm. The late-term softening is therefore a consquence of reductions in both solute and precipitate hardening of the matrix in both solute-hardening and precipitate hardening of the matrix.

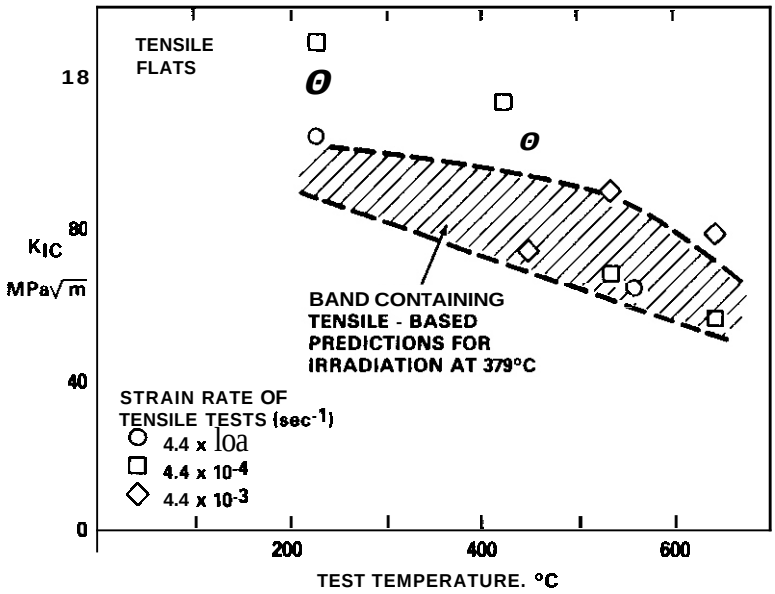

Figure 3. Comparison of Toughness Predictions for Irradiations on EBR-II Ducts Conducted at 379°C (Data Band) and 425°C (Data Points).[8]

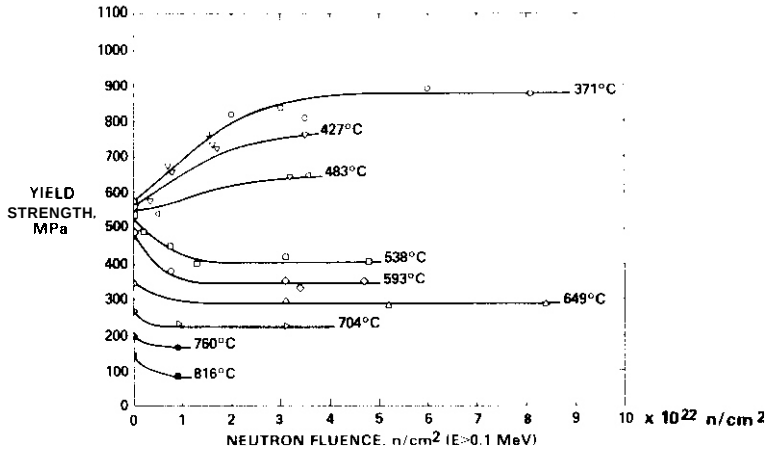

Figure 4. Irradiation-Induced Changes in Yield Strength of 20% Cold-worked AISI 316 Cladding Tubes Tested at the Irradiation Temperature.[15,16]

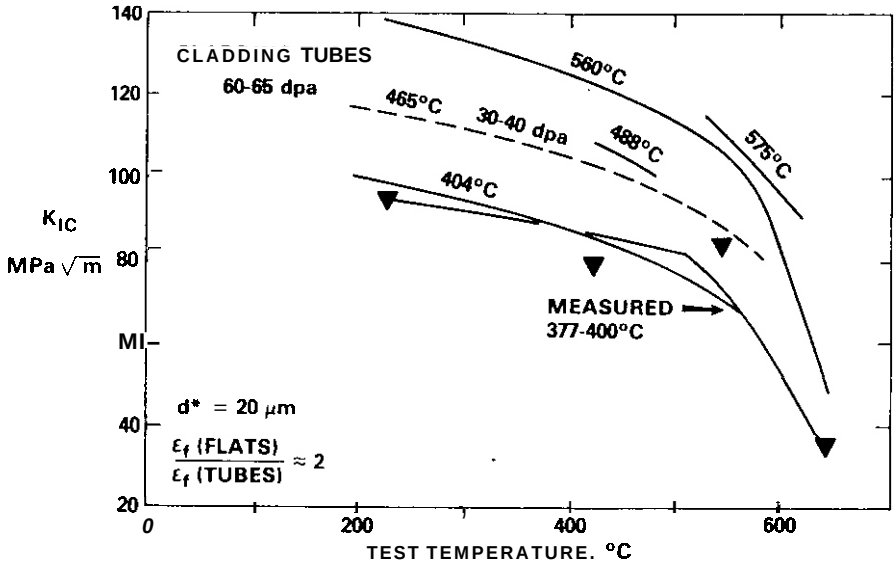

Figure 5. Predications of Touqhness of Irradiated AISI 316 using Tensile Data from Fuel Cladding. Solid lines denote predictions at 1.2 to 1.3 x 10^{23} n cm^{-2} (E > 0.1 MeV) or 60 to 65 dpa. The dotted line corresponds to a prediction at 6.0 to 8.0 x 10^{22} or 30 to 40 dpa.

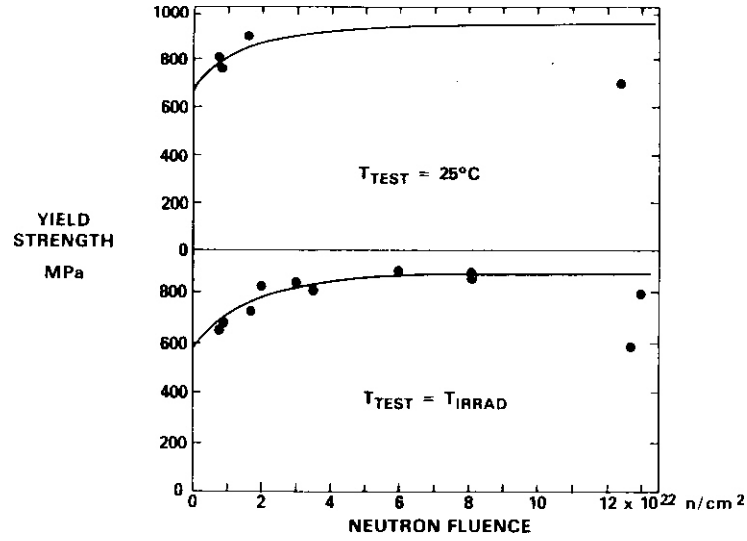

Figure 6. Softening Observed in 20% Cold-worked AISI 31b at 370-405°C and High Neutron Exposures in EBR-II.

5.6 Discussion

Based on the tensile-toughness correlation described in this paper it appears that 20% cold-worked AISI 316 will have sufficient toughness for fast reactor applications where the irradiation temperature lies in the range 380-575°C and the test temperature is below 575°C.

If we assume that the use of displacements per atom is an appropriate exposure parameter for both fission and fusion environments, we can expect that toughness losses will saturate in fusion reactor components before 25 dpa at most irradiation temperatures. The higher level of helium generation characteristic of fusion environments is not expected to cause large changes to toughness. Although helium tends to disperse the voidage on a finer scale in AISI 316[17] it has been shown that there is essentially no difference in tensile properties below 575°C for irradiations conducted in EBR-II or HFIR.[18] The latter reactor generates more helium than would be anticipated in fusion environments.

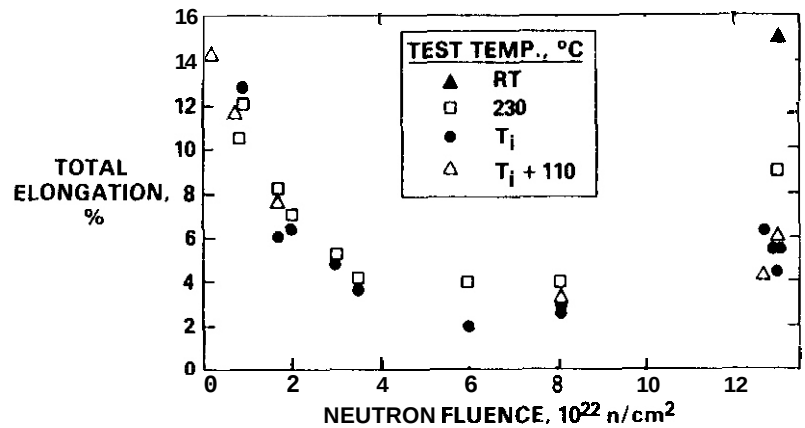

Figure 7. Total Elongation of 20% Cold-worked AISI 316 Irradiated at 370-405°C in EBR-II.

Another conclusion can be drawn from this study. It has been shown that the tensile properties of AISI 316 tend to saturate at equilibrium levels which are dependent on irradiation temperature but independent of the thermal-mechanical starting condition.[5] Thus we would predict that annealed AISI 316 will develop the same touqhness as that of cold-worked AISI 316.

5.7 Conclusions

A modified form of the Krafft model for fracture toughness has been used to predict the toughness of AISI 316 for irradiation temperatures between 380-575°C and test temperatures less than or equal to the irradiation temperature. The residual toughness is expected to saturate at relatively low exposure levels and to be sufficient for structural use in both fast reactor and fusion environments.

6.0 References

1. Watson, R.O., Peterson, R.R., and Wolfer, W. G., J. Nucl. Mater., Vol. 103 & 104, 1981, p. 97.

2. Watson, R. O., Peterson, R.R., and Wolfer, W. G., J. Pressure Vessel Tech., Vol. 105, 1983, p. 144.

3. Hamilton, M. L., Cannon, N. S., and Johnson, G. D., "Mechanical Properties of Highly-Irradiated 20% Cold-Worked Type 316 Stainless Steel," Effects of Radiation on Materials: Eleventh Conference, ASTM STP 782, H. R. Brager and J. S. Perrin, Eds., American Society for Testing and Materials, 1982, pp. 636-647.

4. Johnson, G. D., Garner, F. A., Brager, H. R., and Fish, R. L., "A Microstructural Interpretation of the Fluence and Temperature Dependence of the Mechanical Properties of Irradiated AISI 316," Effects Of Radiation on Materials: Tenth Conference, ASTM STP 725, David Kramer, H. R. Brager, and J. S. Perrin, Eds., American Society for Testing and Materials, 1981, pp. 393-412.

5. Garner, F. A., Hamilton, M. L., Panayotou, N. F., and Johnson, G. D., J. Nucl. Mater,, Vol. 103 & 104, 1981, p. 803.

6. Brager, H. R., Blackburn, L. D., and Greenslade, D. L., J. Nucl. Mater., Vol. 122 & 123, 1984, p. 332.

7. Simons, R. L. and Hulbert, L. A., "Correlation of Yield Strength With Irradiation-Induced Microstructure In AISI 316 Stainless Steel," these proceedings.

8. Hamilton, M. L., Garner, F. A., and Wolfer, W. G., "Correlation of Fracture Toughness With Tensile Properties for Irradiated 20% Cold-Worked 316 Stainless Steel," J. Nucl. Mater., Vol. 122-123, 1984, pp. 106-110.

9. Wolfer, W. G. and Jones, R. H., J. Nucl. Mater., Vol. 103 & 104, 1981, pp. 1305-1314.

10. Krafft, J. M., Appl. Matls. Res., Vol. 3, 1964, p. 86.

11. Hahn, G. T. and Rosenfield, A. R., in Applications Related Phenomena in Titanium Alloys, ASTM STP 437, American Society for Testing and Materials, 1968, p. 5.

12. Huang, F. H. and Wire, G. L., "Irradiation Effects on the Fracture Toughness of 20% Cold-Worked Type 316 Stainless Steel," in Proc. Int. Conf. on Dimensional Stability and Mechanical Behavior of Irradiated Metals and Alloys, British Nuclear Energy Society, April 1983, Brighton, England, Vol. 1, pp. 135-138.

13. Huang, F. H., "The Fracture Characterization of Highly-Irradiated Type 316 Stainless Steel, Inter. J. of Fracture, 25 (1984) 181-193.

14. Huang, F. H. and Fish, in ref. 3, p. 701.

15. Fish, R. L., Cannon, N. S., and Wire, G. L., "Tensile Property Correlations for Highly Irradiated 20 Percent Cold-Worked Type 316 Stainless Steel," Effects of Radiation on Structural Materials, ASTM STP 683, J. A. Sprague and D. Kramer Eds., American Society for Testing and Materials, 1979, pp. 450-465.

16. R. L. Fish and J. J. Holmes, J. Nucl. Mater., 46 (1973) 113.

17. Brager, H. R. and Garner, F. A., J. Nucl. Mater., 117 (1983) 159-176.

18. Rowcliffe, A. F. and Grossbeck, M. L., J. Nucl. Yatrr., 127 & 123 (1984) 181-190.

7.0 Future Work

No further work is anticipated.

8.0 Publication:

None.

THE INFLUENCE OF COMPOSITION ON MICROSTRUCTURAL EVOLUTION AND MECHANICAL PROPERTIES OF IRRADIATED Fe-Ni-Cr TERNARIES

H. R. Brager, F. A. Garner and M. L. Hamilton (Hanford Engineering Development Laboratory)

1.0 Objective

The object of this effort is to determine the origins of the sensitivity of radiation-induced property changes in irradiated metals to environmental and material variables.

2.0 *Summary*

Five simple Fe-Ni-Cr ternary alloys in the lnvar compositional region were irradiated as tensile specimens in EBR-II at 395, 450 and 550°C to 10.5-12.5 dpa. The density changes were measured by an immersion density technique. Specimens irradiated at 450°C were examined by electron microscopy and identical specimens were tensile tested at 450°C. Swelling exhibited a dependence on nickel and chromium content that was consistent with the results of earlier studies. The compositional dependence of swelling arises primarily from the dependence on nickel of both vacancy diffusivity and radiation-induced phase decomposition. There is also a small dependence of Frank loop and dislocation evolution on composition. Although there was excellent agreement between the measured strength and a prediction based on observed microstructure for an alloy containing 25% nickel, an increasing disparity developed between the two for alloys with higher nickel levels. This disparity is thought to be related to the hardening associated with the spinodal-like decomposition of the alloy matrix.

3.0 Program

Title: Irradiation Effects Analysis (AKJ)
Principal Investigator: O. G. Doran
Affiliation: Hanford Engineering Development Laboratory

4.0 Relevant OAFS Program Plan Task/Subtask

Subtask II.C.l Effects of Material Parameters on Microstructure

5.0 Accomplishments and Status

5.1 Introduction

Previous work suggests that, in the temperature range of 400-650°C, all simple Fe-Ni-Cr alloys will swell, after a transient regime, at ~1%/dpa during neutron irradiation in EBR-II.[1,2] The duration of the transient regime is rather insensitive to composition at the lower irradiation temperatures, but becomes quite sensitive at temperatures above a "break-away'' temperature. This break-away temperature was also found to be dependent on composition. The longest transient regimes were found to occur for Fe-35.5Ni-7.5Cr and at about 45% nickel for higher chromium levels.

The compositional region centered at Fe-35Ni and low chromium levels is often designated the Invar region, a reference to the very low or "invariable" coefficient of thermal expansion at relatively low temperatures (<150°C). Many other physical properties also exhibit a marked variation with nickel content in this region. These anomalies tend to disappear as the temperature is raised or as solutes such as

chromium are added.[3-5] The anomalous behavior also disappears during irradiation.[6,7] This study spans a range of each of these three variables.

It has also been shown that the alloy Fe-35.5Ni-7.5Cr exhibits micro-oscillations of composition after neutron irradiation at ~600°C. Regions of enhanced nickel and reduced chromium and iron were separated with a period of about 200 nm from regions of depleted nickel and enhanced chromium and iron.[7] A similar behavior, but with a period approaching 400 nm, was found in Fe-35.0Ni-7.0Cr ion-bombardea at 625°C.[8] This decomposition appears to be proceeding toward the development of near-stoichiometric zones of Fe_3Ni and FeNi. A similar behavior has been observed in Fe-Ni alloys during low temperature (<250°C) irradiation, but the FeNi phase is ordered.[6] Since a change in lattice parameter accompanies the decomposition, it has been inferred from density change data that micro-oscillations in composition probably develop over a fairly wide range of composition in the vicinity of 35% nickel.[1,7]

This tendency toward a spinodal-like decomposition is believed to compete with another composition-dependent phenomenon, the dependence of the vacancy diffusion coefficient on the nickel and chromium content, in determining the compositional dependence of the transient reqime of swelling.[9] To complete the model, however, the compositional dependence of the dislocation microstructure needs to he obtained.

Since the ternary compositional reqion around 35% nickel is of current interest for both fundamental and applied fusion materials studies, it was decided to explore the compositional sensitivity of both void and dislocation microstructure in a series of simple ternary alloys. Both microscopy and tensile measurements were used to assess the nature of the neutron-produced changes in microstructure and matrix comoosition.

5.2 Experimental Details

Five simple Fe-Ni-Cr ternaries were prepared in the annealed condition (954°C for 15 min. and air-cooled) in the form of flat tensile specimens. Five specimens of each alloy were irradiated in the AD-1 experiment in EBR-II at 395, 450 and 550°C to fluences of 2.1-2.5 x 10^{22} n cm^{-2} (E > 0.1 MeV) or 10.5-12.5 dpa. These alloys form a compositional crossroads with Fe-34.5Ni-15.1Cr at the center; the nickel content varies from 24.4 to 45.3 wt% and chromium from 7.5 to 21.7 wt%. The exposure level for this experiment was chosen to be less than but near the termination of the transient regime of swelling as determined from earlier experiments.[2]

While immersion density changes were measured on tensile specimens irradiated at the three temperatures, microscopy was performed only on the specimens irradiated at 450°C. It was felt that the microstructures at 395°C would be too dense to allow confident quantitative analysis and those at 550°C would not contain a sufficient microstructural record at this exposure, particularly for Frank loops.

The flat tensile specimens were 0.76 mm thick, with a gauge width and length of 1.52 and 20.3 mm, respectively. To date only the specimens irradiated at 450°C have been tested. All tensile tests were performed at 450°C at a strain rate of 4 x 10^{-4}/sec. A stabilization period of 15 minutes at the test temperature was allowed prior to each test. Yield strengths were calculated at 0.2% offset.

5.3 Results

The density change data presented in Table I are very consistent with the more extensive density change data obtained earlier from TEM disks irradiated in the AA-VII experiment.[2] In both experiments swelling tends to increase with increasing chromium and decreasing nickel content for nickel levels <45%. Swelling also tends to decline with increasing temperature for nickel levels above 25%.[2] Unlike solute-modified austenitics, the swelling of simple ternaries appears to be relatively insensitive to minor differences in fabrication and irradiation history.

As shown in Table I, some specimens at 450°C exhibited a slight densification even though significant voidage was found. The densification at both 450 and 550°C is thought to be a consequence of a contraction in lattice parameter associated with a radiation-induced decomposition of the matrix.[7,9] At 450°C the microstructure is still too dense, however, to differentiate the micro-oscillations dun to spinodal-like decomposition from that of the perturbations associated with various microstructural components. In addition it is suspected that the oscillation period at 450°C is comparable to the thickness of the foil

TABLE I
Immersion Density Results for the AD-1 Experiment

Alloy	Composition Wt.%	Swelling (%) 2.1* 395°C	2.5 450°C	2.5 550°C
F20	Fe-24.4Ni-14.9Cr	2.65	1.80	0.02
E22	Fe-34.5Ni-15.1Cr	0.63	0.54	-0.02
E23	Fe-45.3Ni-15.0Cr	0.77	0.17	-0.04
E37**	Fe-35.5Ni-7.5Cr	0.18	-0.005	0.13
		0.04	-0.060	-0.14
E25	Fe-35.1Ni-21.7Cr	0.81	0.58	-0.10

*Neutron fluence in units of 10^{22} n cm^{-2} (E > 0.1 MeV)
**Two identical specimens irradiated side-by-side.

(~50 nm) and the diameter of the volume sampled by the electron probe (~30 nm). Thus, we cannot at this point use energy dispersive x-ray techniques to conclusively establish the presence or absence of spinodal-like compositional oscillations in the specimens irradiated at 450°C.

, , ... determined by microscopy agrees fairly well with that determined by immersion density. As shown in Figure 1 and Table II the void density falls markedly with nickel content but exhibits only a shallow minimum at ~15% Cr in the Fe-35Ni-XCr series. The mean void size at all nickel levels and higher chromium levels is not very sensitive to composition. At the low chromium level of 7.5% both the void size and the density change exhibit a sharp decrease, however. The dislocation density does not vary strongly with composition, hut the dislocation density does appear to be increasing more sharply as the nickel level falls toward 25%. The largest Frank loop density was also found in the 25% nickel alloy. The lowest loop density was observed in the Fe-35Ni alloy series but the difference in loop densities among the various alloys is not very large. The mean loop sizes also do not vary substantially with composition (see Table II).

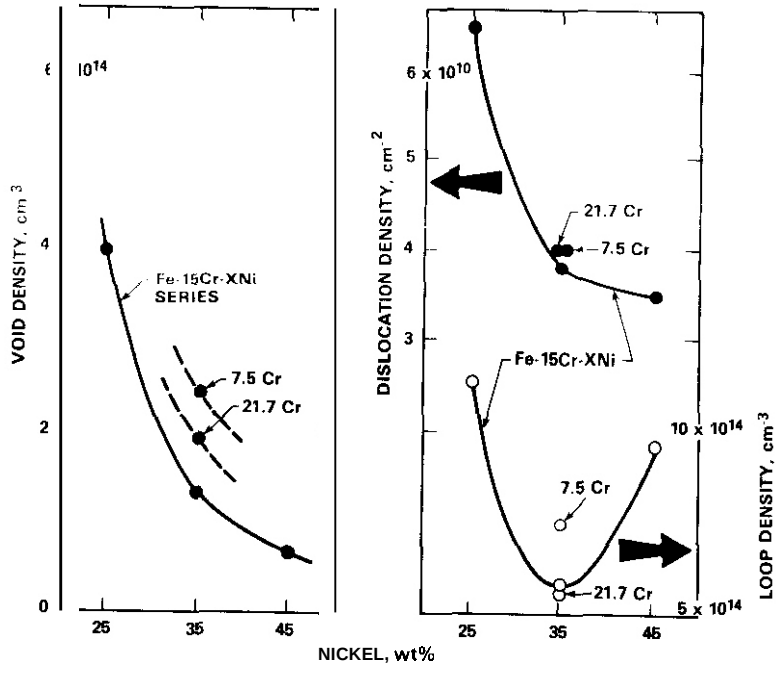

Figure 1: Compositional dependence of radiation-induced microstructural components in simple Fe-Ni-Cr alloys at 450°C and 12.5 dpa.

Table II

Microstructural Components Induced by Irradiation at 450°C and 2.5 x 10^{22} n/cm^2 (E > 0.1 MeV)

Alloy	VOID CHARACTERISTICS mean diam. nm	density cm-3	swelling %	DISLOCATIONS density cm^{-2}	FRANK LOOPS mean diam. nm	density cm^{-3}
Fe-24.5Ni-14.9Cr	35.0	3.9 x 10^{14}	0.8	6.4 x 10^{10}	30.0	1.14 x 10^{15}
Fe-34.5Ni-15.1Cr	42.5	1.3 x 10^{14}	0.6	3.8 x 10^{10}	25.0	5.2 x 10^{14}
Fe-45.3Ni-15.0Cr	40.0	6.5 x 10^{13}	0.2	3.5 x 10^{10}	33.0	9.6 x 10^{14}
Fe-35.5Ni-7.5Cr	25.0	2.4 x 10^{14}	0.2	4.0 x 10^{10}	30.5	7.5 x 10^{14}
Fe-35.1Ni-21.7Cr	40.5	1.9 x 10^{14}	0.6	4.0 x 10^{10}	38.5	5.7 x 10^{14}

Table III and Figure 2 present the results of the tensile tests. While chromium acts as a solution hardening agent for unirradiated Fe-35Ni-XCr alloys, there is little effect of nickel in the Fe-XNi-15Cr alloys. The increment of yield stress induced by radiation is relatively insensitive to composition at 294 ±17 MPa although it apppears to increase slightly with increasing nickel content. The ductility decreases subtantially with irradiation for all five alloys.

Table III

Tensile Uata for Ternary Alloys in the AD-1 Experiment

Alloy	Strength (MPa) 0.2% Yield	Ultimate	Elongation (%) Uniform	Total
Fe-24.5Ni-14.9Cr	96*	315	31.9	36.0
	373	373	0.3	4.2
Fe-34.5Ni-15.1Cr	90	375	35.8	38.5
	384	422	1.0	1.7
Fe-45.3Ni-15.0Cr	102	397	33.0	35.8
	413	486	8.3	11.4
Fe-35.5Ni-7.5Cr	62	303	27.7	30.6
	350	512	2.5	5.9
Fe-35.1Ni-21.7Cr	129	412	35.0	37.5
	418	473	7.5	9.8

*The first number in each column is the value for the unirradiated alloy, the second number is for the irradiated alloy.

5.4 Discussion

The microstructural data confirm the previously observed sensitivity of void nucleation to nickel content but they do not indicate a strong dependence of dislocation evolution on composition in the Invar region. Although the composition dependence of vacancy diffusivity would lead to a prediction of a stronger dependence of void density on nickel content,[9] the observed lesser dependence is thought to arise as a consequence of the anomalous tendency of high nickel alloys to decompose in a spinodal-like manner during irradiation.[7-9]

There is no indication of anomalous behavior in the strength data at 450°C for the unirradiated or irradiated Invar alloys until one attempts to correlate strength changes with microstructural changes. The calculation of strength changes employs the equation shown in Figure 3, which was previously used to successfully predict strength changes in neutron irradiated AISI 316 stainless steel.[10,11] Figure 3

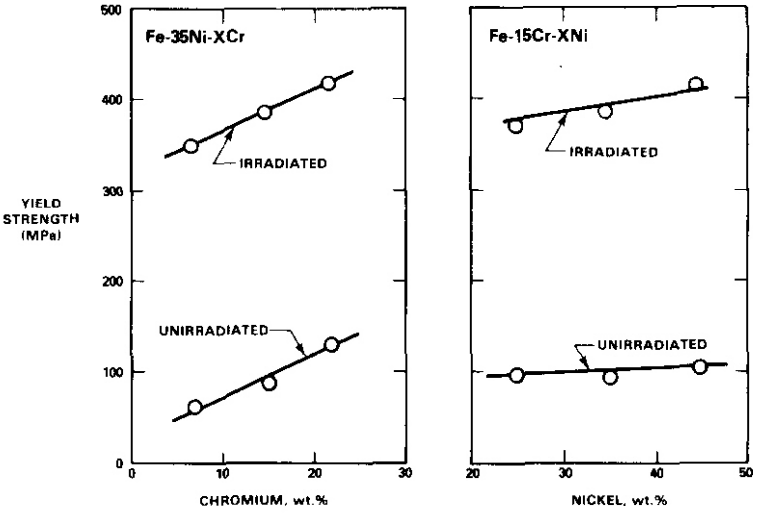

Figure 2: Compositional dependence of yield strength at 450°C observed in five simple Fe-Ni-Cr alloys for both the unirradiated and irradiated conditions.

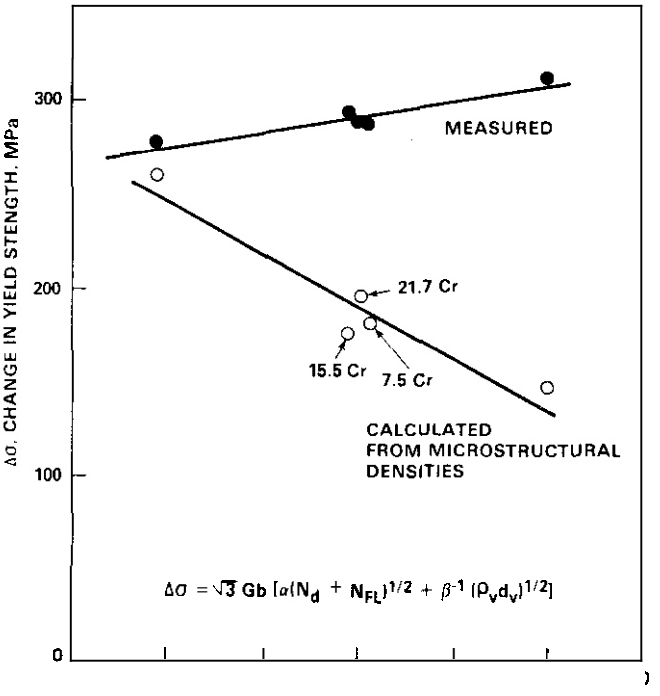

Figure 3: Disparity observed between measured and predicted radiation-induced changes in yield strength. G is the shear modulus, b the Burger's vector, α = 0.2, β = 1.0, N_d and N_{FL} are the line lengths of dislocations and Frank loops, ρ_V is the density of voids and d_V their mean diameter.

shows that excellent agreement with the experimental value was reached for the Fe-24.4Ni-14.9Cr alloy. As the nickel level increases, however, the difference between measured and predicted changes in strength also increases. While chromium has a relatively strong effect on the strength of unirradiated alloys, it has essentially no effect on the magnitude of the radiation-induced change in strength. This behavior is opposite to that of nickel, which has a negliqible influence on unirradiated strength.

The decrease in the predicted change in strenqth as the nickel content increases does not arise from a decrease in the shear modulus. The shear modulus of annealed Fe-15Cr-XNi alloys actually increases ~10%

over the range 25 < x < 45% at 450°C for unirradiated alloys.[3] The decrease is a consequence of the lower microstructural densities observed at higher nickel levels. In order to account for the increasing disparity between the measured and predicted strength at higher nickel levels one must either invoke a large irradiation-induced increase in shear modulus or look for other hardening sources. While the modulus of the fully annealed condition is somewhat sensitive to composition, an irradiation-induced increase of more than a factor of two would he required for Fe-45Ni-15Cr. This is highly unlikely. As for other hardening sources, there is no indication that discrete phases of any type form as small precipitates, consistent with previous observations. Therefore the origin of the additional hardening is postulated to arise from the spinodal-like decomposition that we believe to he present.

The postulated existence of spinodal-like micro-oscillations at 450°C is supported by several observations. First, there is the segregation-induced densification[7] that was observed even in specimens containing significant void volume. Second, the hardening contribution attributed to spinodaling increases with nickel content and is relatively insensitive to chromium. This behavior is consistent with the tendency above 25% Ni of increasing phase decomposition into Fe_3Ni and FeNi in Fe-Ni alloys irradiated at lower temperatures (<250°C)[6] and the fact that chromium appears to mirror the behavior of iron in the decomposition process.[7,8]

Hardening has been predicted to result from spinodal decomposition[12] and this prediction has been verified in several alloy systems.[13,14] The major component of hardening arises from the interaction of the strain field of a dislocation with the strain and internal stress fields associated with the spinodal. in addition, several other hardening mechanisms may operate in this alloy system. First, if the zones with composition near FeNi were ever partially ordered, they would offer additional resistance to the movement of dislocations and the associated disorder such movement would create.[15] Second, those regions that are depleted in nickel and enriched in chromium will have a substantially lower stacking fault energy.[16] This will lead to larger distances between partial dislocations and qreater resistance to both cross-slip and cutting of forest dislocations.

5.5 Conclusions

When simple Fe-Ni-Cr alloys in the Invar region are irradiated at 450°C, one observes a dependence of microstructural development on composition that is associated primarily with the compositional dependence of void nucleation and the tendency for phase decomposition to occur at increasinq nickel levels. The evolution of Frank loop and dislocation microstructures is also affected by composition but the differences, however, are not very large.

The predicted changes in yield strength arising from the radiation-induced microstructure and its dependence on composition diverge strongly from the observed changes in strength as the nickel Content increases above 25%. The level of chromium does not appear to affect the magnitude of the disparity. Based on radiation-induced spinodal-like micro-oscillations observed at higher temperatures and the associated lattice contractions observed at both lower and higher temperatures, it is deduced that micro-oscillations in composition also occur at 450°C hut on a scale near experimental resolution using energy dispersive x-ray analysis. In agreement with theoretical predictions, these oscillations appear to lead to additional resistance to dislocation motion that increases with nickel content.

6.0 References

1. F. A. Gamer, J. Nucl. Mater., 122 & 123 (1984) 459-471.

2. F. A. Garner and H. R. Brager, "Swellinq of Austenitic Fe-Ni-Cr Ternary Alloys During Fast Neutron Irradiation," HEOL-SA-3039, also in ASTM STP 870 (in press).

3. J. F. Bates, J. Nucl. Mater., 87 (1979) 409-415.

4. G. Hausch and H. Warlimont, Z. Metallkunde, 63 (1972) 547-552.

5. V. M. Kalinin and V. A. Kornyakov, Fiz. Met. Metalloved. 51, No. 5 (1981) 1110-1113.

6. A. Chamberod, J. Laugier and J. M. Pennison, J. Magnetism and Magnetic Materals, 10 (1979) 139-144.

7. H. R. Brager and F. A. Garner, "Microsegregation Observed in Fe-35.5Ni-7.5Cr irradiated in EBR-II," HEDL-SA-3027, also in ASTM STP 870 (in press).

8. H. R. Brager, F. A. Garner and T. Lauritzen, "Compositional Micro-oscillations in Ion-Bombarded Fe-35.0Ni-7.0Cr," DAFS Quarterly Progress Report DOE/ER-0046/19 (Nov. 1984) 56-61.

9. F. A. Garner, "A Model Describing the Dependence of Void Nucleation in Irradiated Fe-Ni-Cr alloys," ASTM STP 870 (in press.)

10. F. A. Garner, M. L. Hamilton, N. F. Panayotou and G. D. Johnson, J. Nucl. Mater., 103 & 104 (1981) 803-808.

11. H. R. Brager, L. O. Blackburn and O. L. Greenslade, J. Nucl. Mater., 122 & 123 (1984) 332-337.

12. J. W. Cahn, Acta Met., 11 (1963) 1275-1282.

13. A. Datta and W. A. Soffa, Acta Met., 24(1976) 987-1001.

14. L. H. Swartz, S. Mahajan and J. T. Plewes, Acta Met., 22 (1974) 601-609; also pp. 911-921.

15. D. L. Douglass, G. Thomas and W. R. Roser, Corrosion, 20 (1966) 15.

16. O. Dulieu and J. Nutting, Special Report 86, Iron and Steel Institute (1964) 140-145.

7.0 Future Work

Tensile tests will be initiated on specimens irradiated at 395 and 550°C. A theory nf radiation-induced spinodal decomposition will be developed.

8.0 Publications

This report will be published by the Journal of Nuclear Materials in the Proceedings of the First International Conference on Fusion Reactor Materials, Tokyo Japan (December 3-6, 1984).

CHAPTER 5

CORRELATION METHODOLOGY

DEPTH-DEPENDENT SWELLING IN 14-MeV ION-IRRADIATEU P7 ALLOY

R.L. Sindelar, S.J. Zinkle and G.L. Kulcinski (University of Wisconsin)

1.0 Objectives

To investigate the trends in swelling rates in ion-irradiated 316-type stainless steels in the hiyh dose regimes and compare the ion-irradiation results with intrinsic swelling rates characteristic of fast neutron irradiation results.

2.0 Sumniary

The P7 alloy, a low-impurity single-phase austenitic alloy containing major alloying elements in Quantities close to the AISI 316 SS classification, was irradiated with 14-PleV Ni ions. Samples were irradiated to four fluence levels with peak damage rates of 4×10^{-3} dpa/s (K = 0.8) at 650°C. Damage levels to 100 dpa were attained with TEM-determined void swelling in excess of 30%. Swelling rates were-determined and compared to the ≈ 1%/dpa post-transient fast neutron rate.

3.0 Program

Title: Radiation Effects to Reactor Materials
Principle Investigators: G.L. Kulcinski and R.A. Uodd
Affiliation: University of Wisconsin-Madison

4.0 Relevant UAFS Program TaskiSubtask

Subtask II.B.3.2: Experimental Characterization of Primary Damage State; Studies of Metals
Subtask II.C.1.2: Modeling and Analysis of Effects of Material Parameters on Microstructure

5.0 Accomplishments and Status

5.1 Experimental

The composition of the P7 alloy used in this study is given in Table 1.[1] The alloy is termed a "pure 316" due to its low level of carbon and residual elements. However, this alloy contains oxygen at matrix saturation levels. A recent study attributes the rapid takeoff in the irradiation swelling response of this alloy to the effect of oxygen on the surface energy of void nuclei when it is chemisorbed on their surfaces.[1]

Irradiations were performed at the University of Wisconsin Heavy-Ion Irradiation Facility using 14-MeV Ni^{3+} ions. Figure 1 shows the depth-dependent displacement damage for 14-MeV Ni ions on 316-type stainless steel targets. A displacement efficiency value of K = 0.8 was used in this study so as to compare the swelling rate results (%/dpa) to those of neutron-irradiated 316 SS. However, recent damage efficiency studies by several groups indicate that K = 0.3 may be a more accurate measure of ttie displacement efficiency for both fast neutron as well as high energy heavy-ion irradiations of fcc metals[2,3] and further investigation of this topic is warrented.

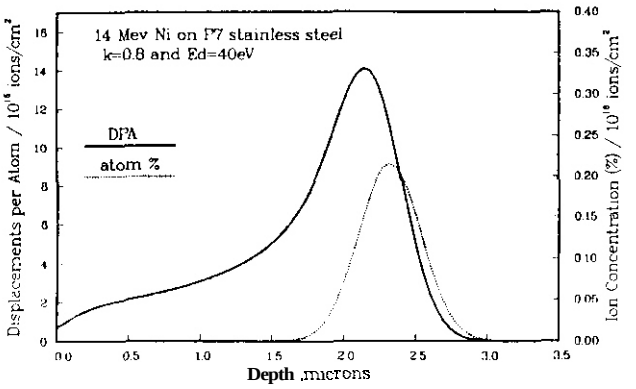

FIGURE 1. Damage (dpa) vs. distance from the irradiated surface calculated using the Brice code The damage efficiency (K) used is 0.8. E_d = 40 eV.

TABLE 1

COMPOSITION OF P7 ALLOY (wt.%)

Cr	Ni	Mo	Mn	Si	C
17	16.7	2.5	0.03	0.1	0.005
P	**S**	**Ti**	**O**	**W**	**Fe**
-	-	0.01	0.03	0.068	Gal.

TABLE 2

14-MeV Ni-ION ON P7 IRRADIATION PARAMETERS FOR
DISPLACEMENT EFFICIENCY K = 0.8, E_d = 40 eV, T_{irr} = 650°C

dpa at 1 μm	Peak dpa	Fluence (ions/cm^2)
2.3	10	0.8 x 10^{16}
10	40	3.3 x 10^{16}
17*	68*	5.6 x 10^{16}*
25	100	8.3 x 10^{16}

*Damage rate at 1 μm from surface is 1.6 x 10^{-3} dpais, at the peak it is 6.4 x 10^{-3} dpa/s; the other samples were irradiated at 0.8 x 10^{-3} dpais at 1μm and 3.2 x 10^{-3} dpa/s at the peak damage region.

The irradiation parameters used in this study are contained in Table 2. Post-irradiation specimens were cross-sectioned[14]) to allow TEll analysis over the entire damage range (see Figure 1).

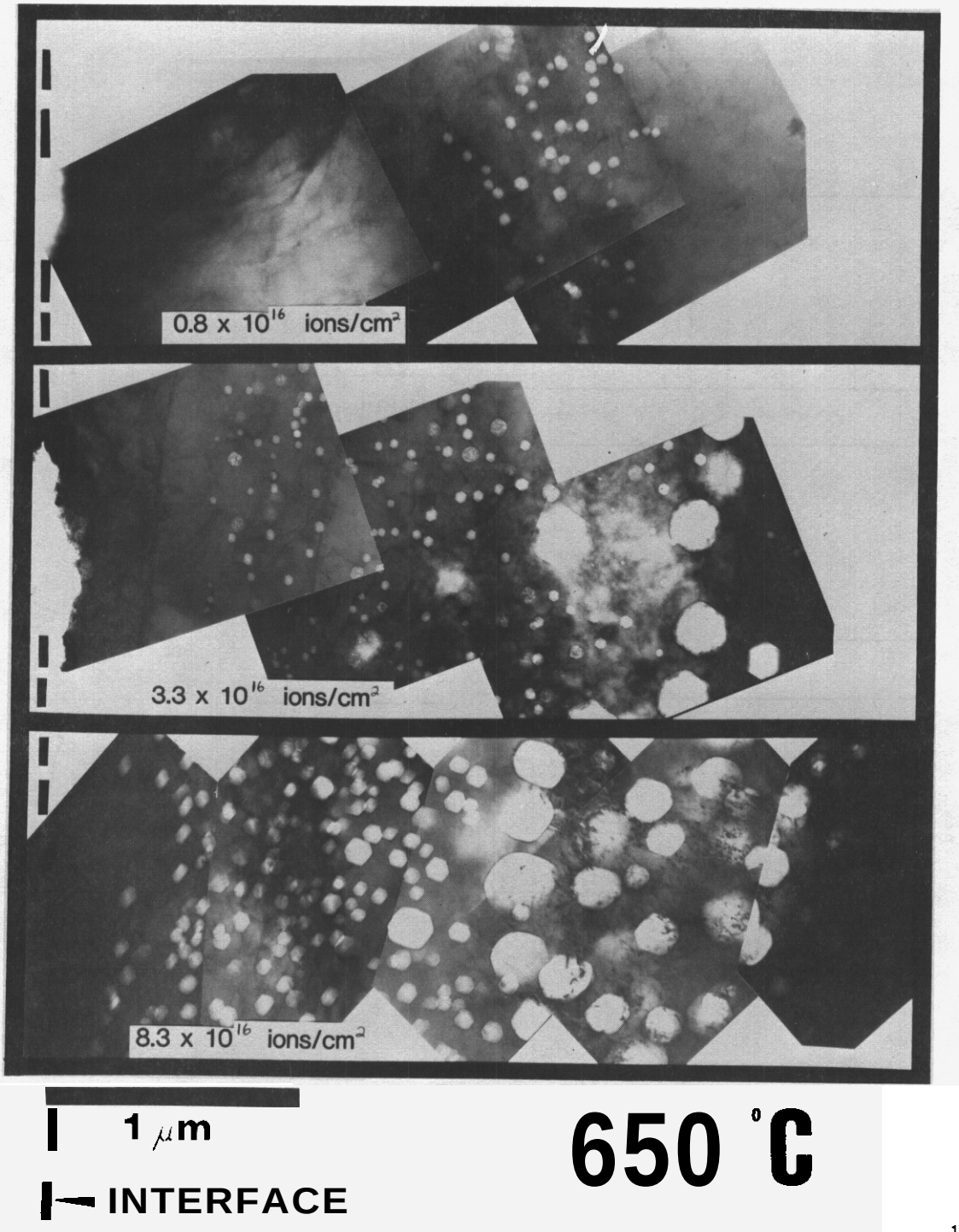

FIGURE 2. 14-MeV Ni ion-irradiated P7 to peak doses of 10, 40, 100 dpa for 0.8, 3.3 and 8.3 x 10^{16} ions/cm^{-2} respectively.

5.2 Results

Figure 2 shows the low contrast micrographs which highlight the void structure in the low, intermediate, and high fluence P7 samples. A mechanism describing the evolution of the void distributions in the low and intermediate fluence samples is given elsewhere.(1) The graphs in Figure 3 display the depth-dependent void parameters obtained from these samples.

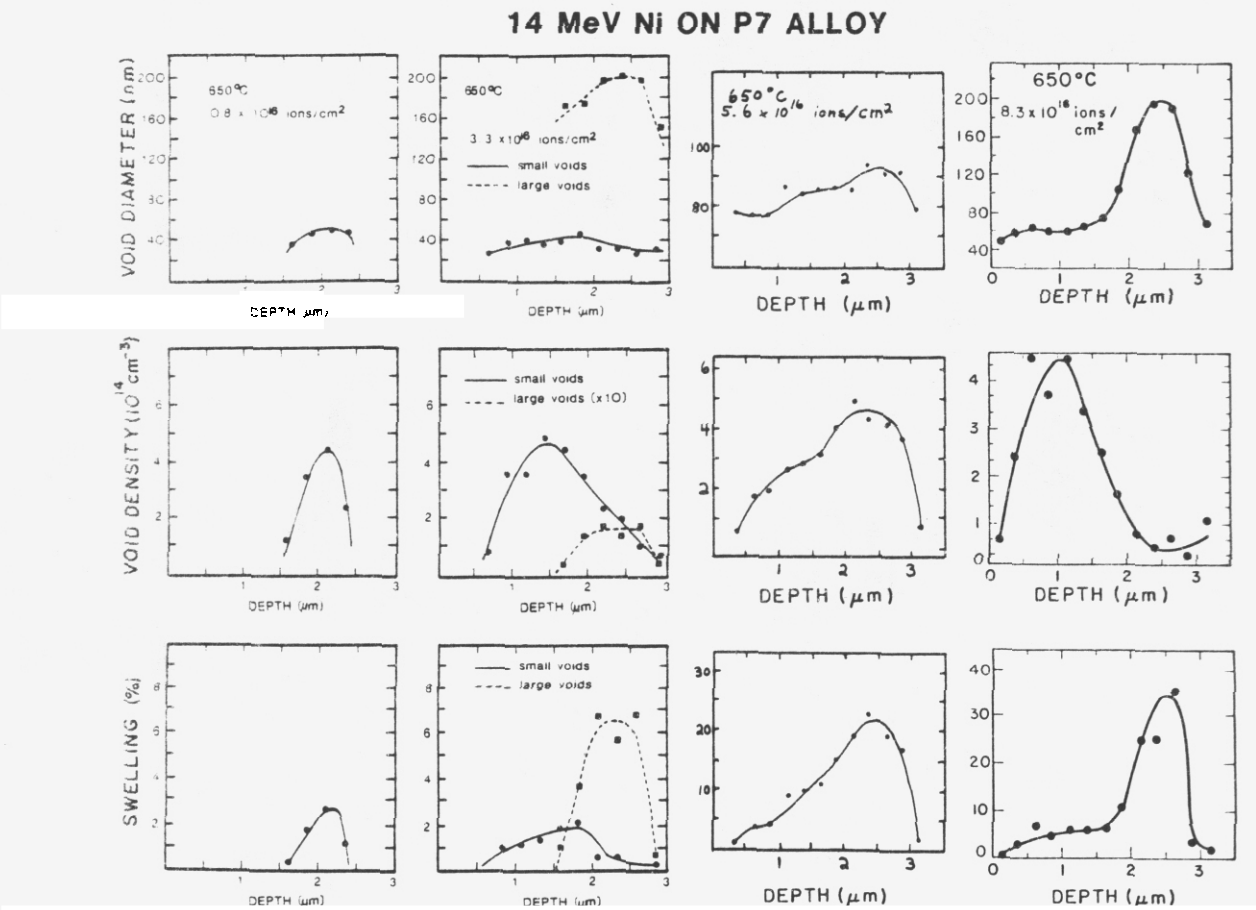

FIGURE 3. void parameters for the high fluence P7 sample.

Figure 4 displays the swelling vs. dpa results for 14-MeV Ni ion irradiated P7. The data were taken from tne 1 μm depth as well as the swelling peaks of Figure 3. The peak swelling value was assumed to occur at the peak. dispiacement damage level as indicated in Figure 1. This is chosen even though the physical location of the peak swelling (in relation to the front surface) occurs deeper than the 2.2 μm level associated with void-free material. It is seen that the swelling rate approaches 0.4%/dpa when using data from the 1 μm depth as well as data from the swelling peak.

5.3 Discussion

Previous irradiations of P7 with 5 MeV Ni ions[6] used step height techniques[7]) to determine irradiation-induced swelling in P7. Results of those studies showed that a 0.2-0.4%/dpa swelling rate occurs over a dose regime of 25 to 300 dpa for this alloy. Irradiations with 4 MeV ions[5,8,9] have shown a similar

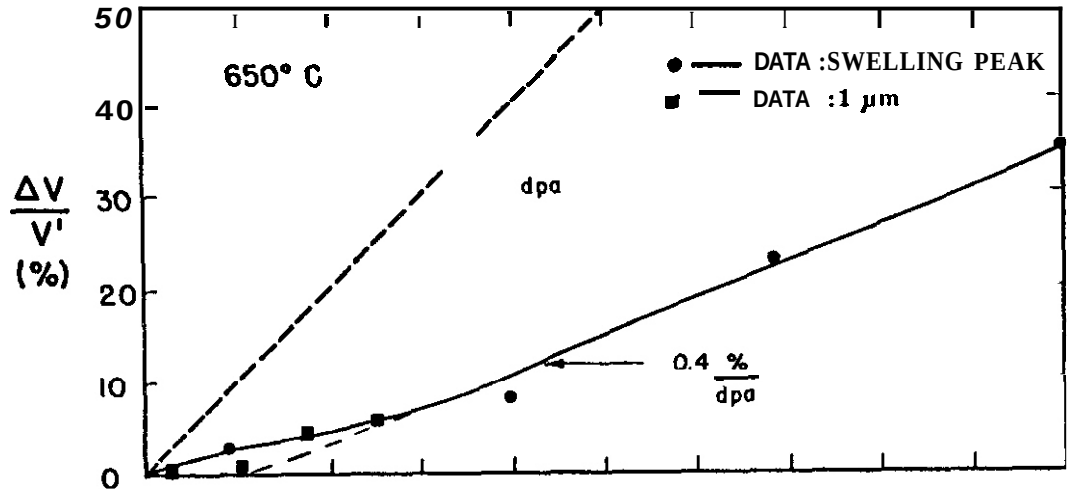

swelling response when the data is extracted from TEM specimens. These rates are a factor of 2 to 3 lower thdn the fast neutron swelling rates which Garner has shown to approach ≈ 1%/dpa.[10] This rate appears to be only a function of the crystal structure.[12] Recent studies show the post-transient fast neutron swelliny rate is insensitive to the original microstructure as well as irradiation parameters of temperature, gas content, etc.[10] In a direct coinparison between neutron and heavy-ion damage in P7, Farrell and Packan[11] observed peak swelling levels in ion-irradiated samples to be 1/3 that for neutron[11] irradiated samples which agrees with the results of this study.

Several possible mechanisms may account for the swelling-rate discrepancy of heavy-ion data when compared with fast neutron data. These mechanisms include: 1) foil surface effects on void swelling in ion-irradiation experiments, 2) injected interstitial effects from the bombarding ion species, 3) damage efficiency differences in ion-induced defect production and fast neutron-induced defect production at high temperatures, 4) decreased damage energy deposition at the peak swelling depth in ion-irradiation experiments (void straggling effects), 5) diffusional spreading of point defects away from the peak swelling depth, 6) anisotropic stresses along the ion range and, 7) damage rate effects on swelling rate.

HVEM studies by Garner and Thomas[13] have shown that a void-free zone ≈ 0.6 μm exists at 650°C in 316 SS. Therefore, data was extracted at depths > 1 μm in this study to preclude surface effects.

A recent study[14] has shown that the effects of injected interstitials on the suppression of the cavity density is temperature dependent. It was determined that injected interstitial8 from ion irradiation onlv caused a large suppression in void density in P7 for irradiation temperatures at or below 500°C, but there were no suppression effects at 650°C.

Odette, et al.[15] have investigated the manner in which voids affect the range and the energy deposition of energetic charged particles in metals. The presence of voids in material under ion-irradiation acts to alter the deposited damage energy from the void-free value by several processes. First, simple mass density corrections show that the deposited energy peak will "shift" to greater depths from the surface of the target with increasing amounts of swelling. In addition, the damage energy at any given depth will decrease with swelling simply due to the absence of material in which to deposit the energy. These effects, however, do not change the dpd value at a given mass depth. The "shift" of the deposited energy peak effectively

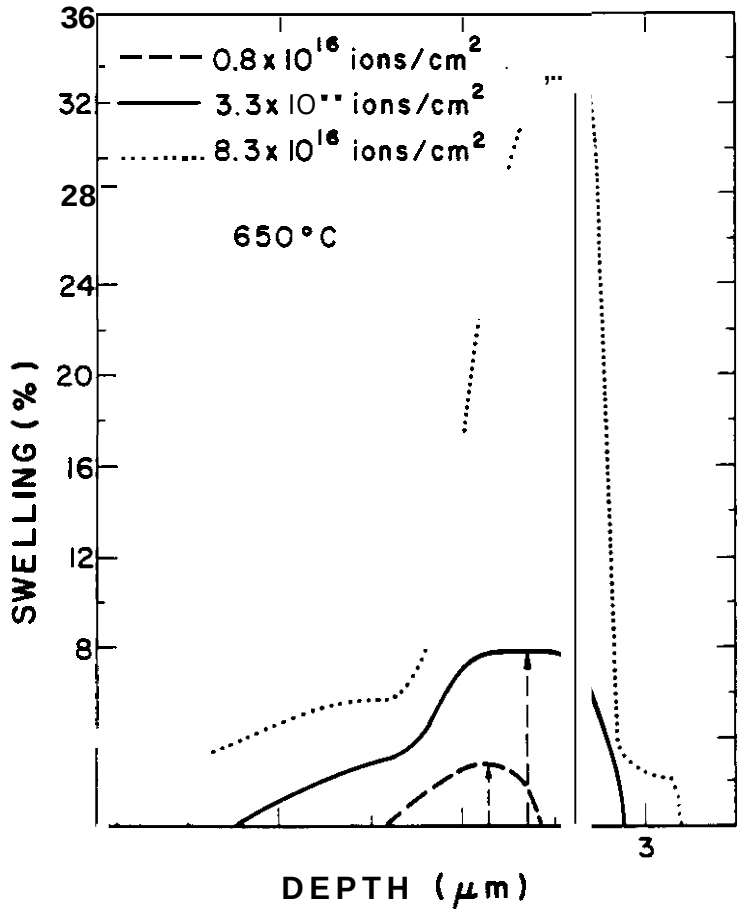

FIGURE 5. Uepth-dependent swelling P7 alloy as a function of ion fluence (see text).

shifts the swelling peak to greater depths from the surface with increasing fluence, as can be seen in Figure 5.

In addition tu mass density corrections, the interaction of the bombarding particles with voids creates a statistical fluctuation in the range of these particles which Odette terms "void-straggling". The void nicrostructure present in the high fluence samples in this study would be subject to "void-straggling" effects corrections. Simple calculations show that a 20% decrease in the peak damage level of the high-fluence sample due to "void-straggling" effects would be sufficient to cause the true swelling rate in this study to increase to ~ 1%/dpa. Further considerations of this point and the remaining points are currently underway.

5.4 Conclusions

Cross-section examination of 14 MeV Ni ion-irradiated P7 has yielded a swelling rate of 0.3-0.4%/dpa at both the 1μm and peak swelling depths. Both surface effects and injected interstitial effects are not considered to be responsible for the discrepancy with the 1%/dpa fast-neutron swelling rate.

6.0 Acknowledgements

The authors would like to thank D.L. Plumton and S.N. Farrens for their assistance in this project.

7.0 References

1. K.L. Sindelar, R.A. Uodd and G.L. Kulcinski, "A Comparison of Depth-Dependent Microstructures of Ion-irradiated 316-Type Stainless Steels", Presented at the 12th International Symposium on the Effects of Radiation on Materials, 18-20 June 1984, Williamsburq, VA. ASTM STP 870, F.A. Garner and J.S. Perrin, Eds.

2. J.H. Kinney et al., J. liucl. ilat. 122 & 123 (1984) 1028-1032

3. R.S. Averback, R. Benedek and K.L. Merkle, J. Nucl. Mat. 69 & 70 (1978) 786-789

4. R.L. Sindelar, G.L. Kulcinski and R.A. Dodd, J. Nucl. Mat. 122 & 123 (1984) 246-251.

5. N.H. Packan and K. Farrell, "Radiation-Induced Swelling in an Austenitic Alloy: Observations and interpretation of the Effects of Helium, in Nucl. Technology/Fusion, Vol. 3, May 1383.

6. W.G. Johnston, et al., "The Effect of Metallurgical Variables on Void Swelling", General Electric Report 76 CRD010, January 1976.

7. W.G. Johnston, J.H. Kosolowski and A.M. Turkalo, "A Direct Measurement of Gross Swelling in Nickel-Ion-Bombarded Stainless Steel," J. Nucl. Mat. 46 (1973) 273-280.

8. N.H. Packan and K. Farrell, J. Nucl. Mat. 85 & 86 (1979) 677-681.

3. K. Farrell and N.H. Packan, 3. Nucl. Mat. 85 & 86 (1979) 683-687.

10. F.A. Garner, J. Nucl. Mat. 122 & 123 (1984) 459-471.

11. K. Farrell and N.H. Packan, ASTM STP 732, H.R. Brager and J.S. Perrin, eds., 1982, pp. 953-362

12. J.J. Sniegowski and W.G. Wolfer, "On the Physical Basis for the Swelling Resistance of Ferritic Steels", Presented at the Topical Conference on Ferritic Alloys for Use in Nuclear Energy Technologies, Snowbird, UT, 19-23 June 1983.

13. F.A. Garner and L.E. Thomas, ASTM STP 529 (1973) 303-325

14. B. Badger Jr.. et al., "Experimental Investigation of the Effect of Injected Interstitials on Void Formation", presented at the 12th International Symposium on the Effects of Radiation on Materials, 18-20 June 1984, Williamsburg, VA. ASTM STP 870, F.A. Garner and J.S. Perrin, Eds.

15. G.R. Odette, D.M. Schwartz and A.J. Ardell, Rad. Effects 22 (1974) 217-223

THE ROLE OF PHOSPHORUS IN THE SWELLING AND CREEP OF IRRADIATED AUSTENITIC ALLOYS

F. A. Garner and H. R. Brager (Hanford Engineering Development Laboratory)

1.0 Objective

The object of this effort is to determine the mechanisms by which changes in dimensions and mechanical properties occur in metals during neutron irradiation.

2.0 Summary

Phosphorus is much more effective than other solutes in suppressing swelling and irradiation creep of austenitic alloys because it increases the vibrational frequency and diffusivity of matrix solvent atoms and it also increases the equilibrium vacancy concentration by orders of magnitude. It accomplishes the latter by strongly reducing the vacancy formation energy. The combined effect of both mechanisms is to reduce the vacancy supersaturation during irradiation, leading to a temporary reduction in void nucleation rate and an extension of the transient regime of swelling. The component of irradiation creep that is proportional to swelling is also reduced.

3.0 Program

Title: Irradiation Effects Analysis (AKJ)
Principal Investigator: D. G. Doran
Affiliation: Hanford Enqineering Development Laboratory

4.0 Relevant OAFS Program Plan Task/Subtask

Subtask II.C.l Effects of Material Parameters on Microstructure

5.0 Accomplishments and Status

5.1 Introduction

Solutes such as carbon, silicon, nitrogen, titanium, phosphorus and others are known to influence the radiation-induced swelling and creep of austenitic alloys. On a per-atom basis, however, phosphorus is one of the most effective solutes in reducing creep and swelling, particularly at relatively low radiation exposure levels. Figure 1 demonstrates this point, showing that the irradiation creep strain in AISI 316 measured at 450°C and 23 dpa in a series of nominally identical pressurized tubes is more sensitive to phosphorus than several other common solutes.[1] The strains of companion unpressurized tubes indicate that the stress-free swelling levels associated with the creep data in the phosphorus alloy series are 0.68, 0.02 and 0.005%. Since phase changes in irradiated AISI 316 contribute volume strains on the order of $\pm 0.2\%$[2], it must be assumed that the latter two swelling levels are essentially zero. This indicates a total suppression of swelling at 73 dpa and 450°C in AISI 316 by phosphorus levels above 0.01 wt.%. A strong suppression effect of low levels (0.003-0.028 wt.%) of phosphorus has also been observed in 200 KeV C+ ion irradiation of AISI 316 at 625°C and 48 dpa.[3]

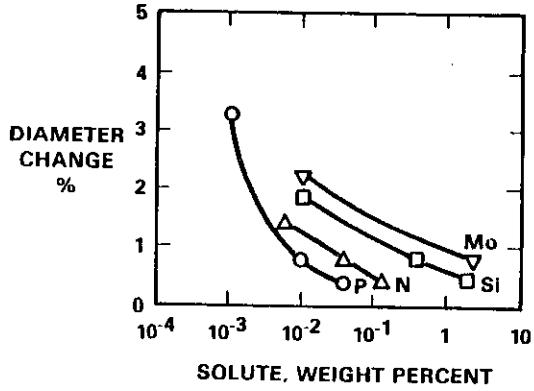

Figure 1. Effect of solute content on the irradiation creep of pressurized tubes of 20% CW AISI 316 irradiated in EBR-II.[1] The irradiation conditions were 450°C, 4.6 x 10^{22} n cm^{-2} (E > 0.1 MeV), 23 dpa and a hoop stress of 172 MPa.

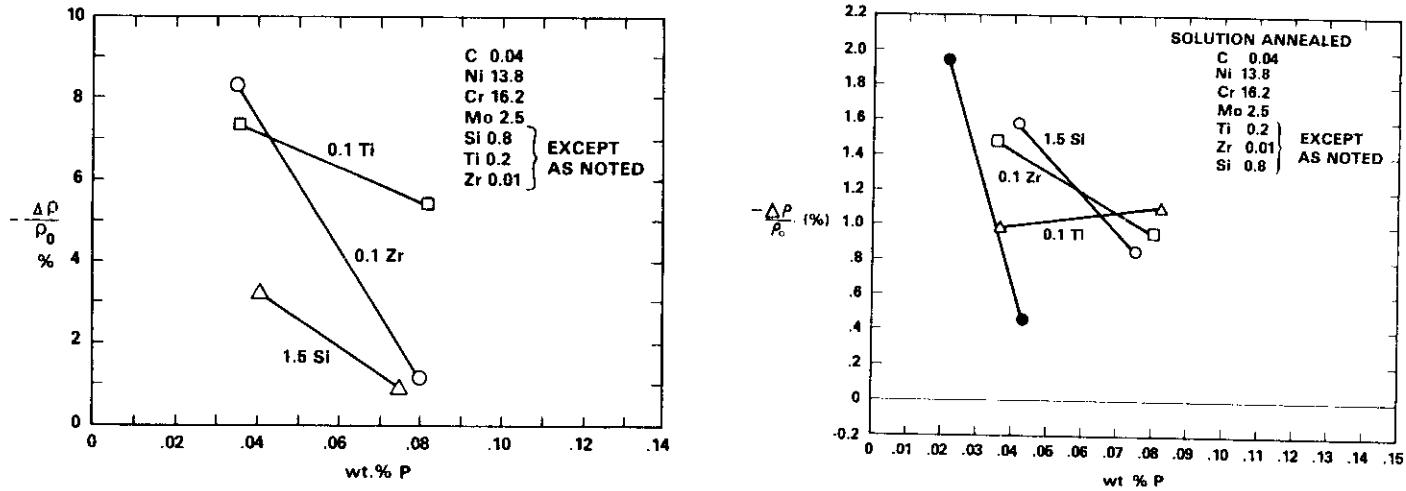

Figure 2. The influence of phosphorus additions on neutron-induced density changes of modified AISI 316 steels in the annealed condition.[5] The irradiation conditions in EBR-II were (a) 540°C, 10.0 x 10^{22} n cm^{-2} (E > 0.1 MeV) or 50 dpa and (b) 450°C, 7.6 x 10^{22} n cm^{-2} (E >0.1 MeV) or 38 dpa.

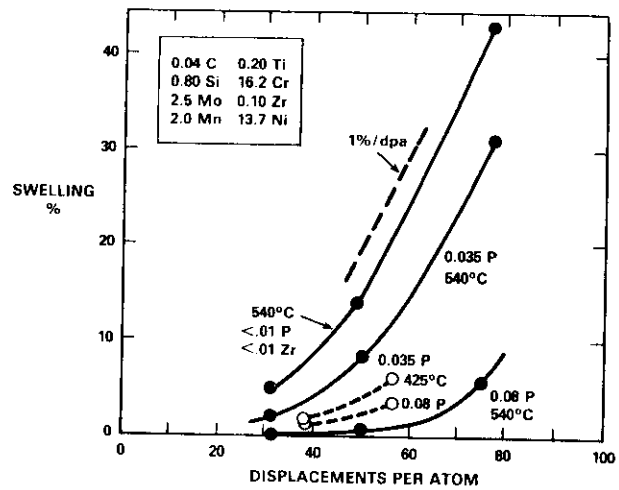

Figure 3. The effect of phosphorus additions and irradiation temperature on neutron-induced swelling of a modified AISI 316 stainless steel in the annealed condition. The 540°C curve at <0.01% P is for an alloy with a reduced level of Zr compared to that of the other curves.

At higher fluence levels the suppression is now known to be a relatively monotonic function of phosphorus content (Figure 2), although the degree of suppression is very sensitive to the concentrations of other solutes, as well as to other material and environmental variables such as irradiation temperature. As noted in other papers, however, the influence of phosphorus and other solutes in austenitic alloys is manifested only in the duration of the transient regime of swelling and not in the post-transient swelling rate[4,5]. This behavior is demonstrated in Figure 3. The purpose of this paper is to provide an explanation of the role of phosphorus in extending the transient regime of swelling.

5.2 Earlier Models

Previous explanations of the influence of phosphorus by Mansur and coworkers have focused on rate theory descriptions of the role of irradiation-induced phosphide precipitates in changing the sink strength of the microstructure.[6-8] An example of the concurrent suppression of swelling and the extensive formation of phosphide precipitates is shown in Figure 4. The rate theory interpretations were directed toward describing the relative swelling of alloys which varied significantly in both phosphorus (0.04-0.08%) and silicon (0.7-1.4%), with silicon's role discounted as being unimportant in the comparison. Since Mansur and coworkers considered silicon to act only as a trap for point defects, it was reasonable to assume that the trapping effect was fully saturated at these silicon levels. As shown in another paper, however, silicon has a potent and non-saturating effect on vacancy diffusivity.[9]

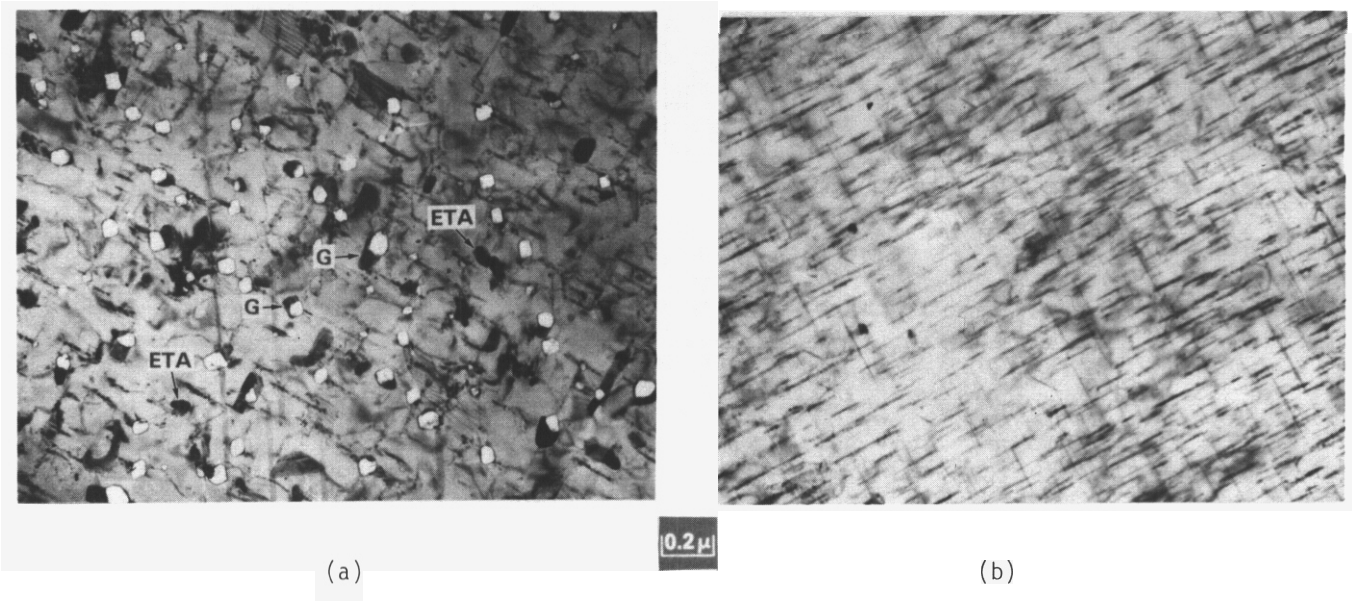

Figure 4. Influence of phosphorus on microstructural development in annealed AISI 316 in ERR-I1 showing (a) eta precipitates, some phosphides and void formation associated with G-phase particles at 0.04 wt.%P. (b) At 0.08% P no voids are visible and a fine network of phosphides has formed (540°C, 35 dpa). (Micrographs courtesy of W.J.S. Yang of Westinghouse-Hanford Co.)

It is now known that silicon's influence on extending the transient regime is relatively large[5,10] at the concentration levels studied by Mansur and coworkers, and therefore cannot be ignored in quantitative assessments of various mechanisms. This consideration does not detract from the validity of their proposed mechanisms, however, but does lessen confidence in the numerical assessments. Figures 1-3 and the data in reference 5 show that phosphorus additions indeed influence swelling strongly, even in the absence of variations in silicon content.

The phosphide precipitates have been identified as Fe_2P[11] and have been assumed to increase the sink strength and enhance point defect recombination at the particle-matrix interface, thereby reducing the cavity growth rate.[6] In a later paper, however, it was concluded that such precipitates cause only a small relative suppression of cavity growth via the several sink strength mechanisms considered.[7] Not only were the calculated precipitate sink strengths insufficient to account for the observed suppression of swelling, but there was a decrease rather than an increase observed in the dislocation density and its sink strength as a result of the high density of phosphide precipitates.[6] A more recent report

suggests that, since the particle-matrix interface serves as a nucleation site for a very fine dispersion of helium bubbles, the number of helium atoms per cavity is reduced and the time required to accumulate the critical number of gas atoms to initiate bias-driven growth is increased.[8] While these various precipitate-related mechanisms may be operating, there is a stronger role that is played by phosphorus. In effect, we should consider phosphides as merely another manifestation of phosphorus activity and not the sole causative agent in the suppression of swelling.

5.3 A proposed alternate diffusion-related mechanism

Garner and Wolfer[12] have shown, using the five frequency model of diffusion,[13] that the addition of small amounts of fast-diffusing elements to a metal can substantially increase the effective vacancy diffusion coefficient D_V^{eff} by increasing the vibrational frequency of the host solvent atoms. This leads to a very large reduction in the void nuleation rate, particularly at higher irradiation temperatures. One consequence of this reduction is an extension of the transient regime of swelling similar to that shown in Figure 3. Esmailzadeh and coworkers have extended this work, using published data for Ni-Si, Ni-Cr-Si and Fe-Ni-Cr-Si alloys, and demonstrated the large effect of silicon additions on D_V^{eff} and void nucleation.[9] Reference 1 and Figure 1 show, however, that phosphorus is much more effective than silicon in suppressing swelling and creep on a per-atom basis.

Is it also possible that the major effect of phosphorus lies in its ability to increase D_V^{eff}? A review of diffusion literature on phosphorus in γ-Fe and γ-Fe alloys indeed shows that phosphorus is a fast-diffusing element in iron-based austenitic alloys.[14] There are also data which support the concept of enhanced diffusion of the host solvent atoms in phosphorus-bearing alloys. The addition of 0.16 wt% phosphorus has been found to increase the diffusivity of nickel in Fe-10Ni and Fe-15Ni alloys hy almost an order of magnitude.[15] When one calculates D_V^{eff} and includes the diffusivity contribution Of phosphorus, the enhancement is larger than that exhibited by nickel alone. It has also been shown that the diffusion of chromium in Fe-16Cr-16Ni alloys increases substantially with small additions of phosphorus.[16]

According to a recent compilation of diffusion data, the diffusivity of phosphorus is not as well studied as that of silicon hut it appears that phosphorus does diffuse faster than silicon.[14] It is surprising, however, that on the basis of this mechanism alone, phosphorus should be so much more effective than silicon in increasing diffusion by a vacancy mechanism.

At this point it must be remembered that there are two mechanisms by which solute diffusion can be enhanced in a non-radiation environment. The first, which we have already considered, involves the increased vibrational frequency of atoms when fast-diffusing solutes are added. The second involves the possihility of an increase in the equilibrium vacancy concentration, allowing more opportunities for vacancy-atom exchanges. Positron annihilation measurements on Fe-18Cr-14Ni show that there indeed exists a strong phosphorus-vacancy interaction, resulting in a large decrease in the vacancy formation energy from 1.64 to 1.20 eV when small amounts (0.005-0.05 wt.%) of phosphorus are added.[17,18] Therefore, phosphorus additions decrease the supersaturation of vacancies present during irradiation and the nucleation of voids by two mechanisms. First, since the flux of radiation-produced vacancies $D_V^{eff}\ C_V$ is constant, the increase in D_V^{eff} reduces the concentration C_V of radiation-produced vacancies. Second, the equilibrium concentration of vacancies increases due to the large drop in vacancy formation energy. In effect, the supersaturation of vacancies is reduced from both ends, leading to a drastic reduction in void nucleation rates, as demonstrated in Figures 5 and 6. The nucleation theory, calculational methodology and diffusion data used to generate these figures are described elsewhere.[19] It should be noted that the large drop in void nucleation rates shown in Figure 6 for homogeneous nucleation will also occur for other nucleation conditions, such as higher helium levels and/or heterogeneous nucleation at precipitate-matrix interfaces.

Note that Figures 5 and 6 show that the influence of phosphorus increases with increasing temperature. This behavior is seen in the data in Figures 2 and 3, in which the effect at 540°C is much greater than that at 425 and 450°C. A similar effect of silicon has been reported elsewhere.[9,10]

The effect of phosphorus in increasing the equilibrium vacancy concentration manifests itself not only in reducing the nucleation of radiation-induced voids but also in the generation of voids in the absence of irradiation during quenching and aging experiments on phosphorus-containing alloys.[20-23] These quenching studies confirm that the equilibrium concentration of vacancies is increased by many orders of magnitude when small amounts of phosphorus are present.

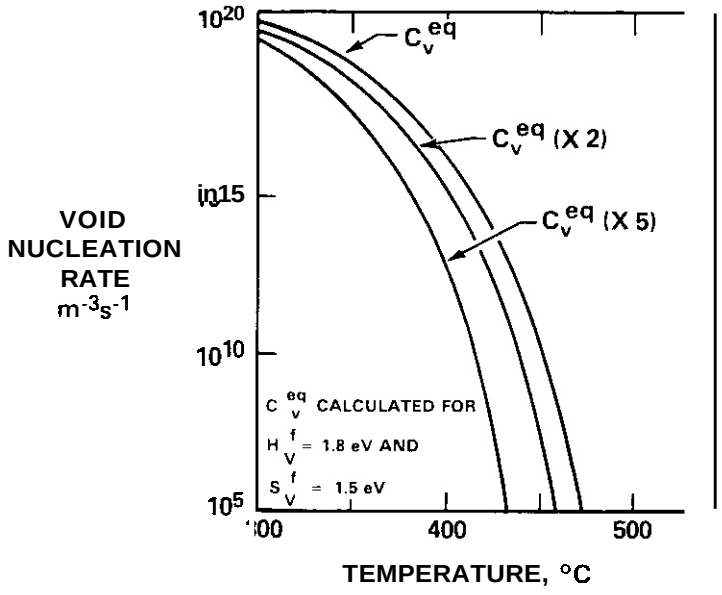

Figure 5: Illustration of the influence of the vacancy equilibrium concentration C_v^{eq} on the steady-state void nucleation rate in pure nickel at 1.0 x 10^{-6} dpa/sec. The sink strenoth assumed is 1.0 x 10^{14} m^{-2} and the bias factor ratio Z_i/Z_v is 1.5.

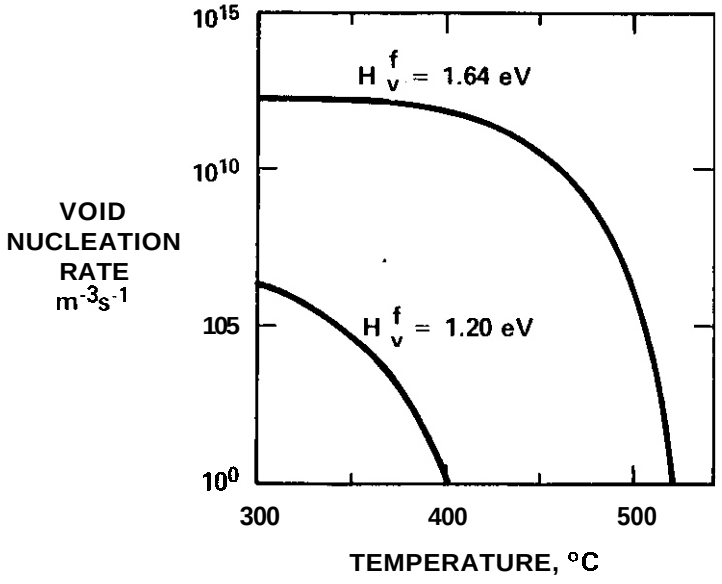

Figure 6: Calculated influence of the reduction in vacancy formation energy H_V^f on the steady-state void nucleation rate in Fe-15Cr-20Ni at 1.0 x 10^{-6} dpa/sec.

5.4 Discussion

While the mechanisms advanced by Mansur and coworkers[6-8] may be operating to reduce swelling, the measured influence of both silicon and phosphorus on the diffusional properties of vacancies was not included. If these were included in the calculations of ref. 8, they would overwhelm the influence of increased interfacial area. Ref. 8 also does not address the fact that the precipitate did not exist in the early stages of the irradiation where most void nuclei probably form.

However, the diffusion-based mechanism presented here is quite capable of extending the transient regime of swelling while the phosphorus is in solution. The phosphorus and other nucleation-suppressing elements such as silicon are inevitably removed from the alloy matrix by precipitation, however. This leads to a reduction in D_V^{eff}, an increase in both the vacancy supersaturation and void nucleation rate and the termination of the transient regime of swelling. Phosphide precipitates are very small in size and exist at such high densities that cascade-induced resolution probably keeps some fraction of the phosphorus continually in solution. This consideration may also contribute to the enhanced effectiveness of phosphorus on swelling relative to that of silicon and other solutes.

It is important to remember that the removal of phosphorus and other solutes from solution is a complex process involving the competition of a wide variety of phases. Each of these phases is sensitive to composition, alloy preparation and environmental variables in a different manner. This perhaps accounts for some of the differences in swelling observed in the various alloys in Figure 2. Figure 4 also illustrates another possible influence of phosphorus. Note that phosphides tend to form at high phosphorus levels instead of γ' and G-phase, both of which are rich in the nucleation-suppressing elements silicon and nickel.[9] The retardation of nickel silicide precipitates would thus tend to reduce void nucleation.[12]

Irradiation creep is now thought by some researchers to consist of two components, one independent of swelling and another proportional to the swelling rate[4,24]. Note in Figure 1 that ~0.4% creep strain is observed for specimens containing the highest level of P, N and Si. The 0.4% strain is thought by this author to represent the swelling-insensitive component. The increment of strain above 0.4% is thought to he the swelling-related component. Thus, when phosphorus suppresses swelling it also suppresses creep. For the experiment cited in Figure 1, the acceleration in creep is much more obvious than it is for swelling since the stress of 172 MPa is large and magnifies the creep strain relative to that of the swelling strain. At 450°C there is probably some slight enhancement of swelling with stress[25] that is not reflected in the stress-free swelling values quoted earlier for this experiment. Our lack of knowledge of the magnitude of the stress effect does not influence our conclusions on the effect of phosphorus.

5.5 Conclusion

Phosphorus has been shown to he much more effective *on* a per-atom basis than other solutes in suppression of swelling and irradiation creep in austenitic alloys. This suppression is temporary, however, and involves a reduction in the void nucleation rate and an extension of the transient regime of swelling. While in solution phosphorus increases the vibrational frequency and diffusivity of the host solvent atoms. More importantly, however, it reduces the vacancy formation energy substantially and thereby increases strongly the equilibrium concentration of vacancies. The combined effect of these two mechanisms is a drastic reduction in void nucleation rate. Even after precipitation of phosphides, it is proposed that cascade-induced resolution of the very small precipitates keeps a significant fraction of phosphorus in solution. Since the largest component of creep is proportional to the swelling rate, irradiation creep is also reduced by phosphorus additions.

6.0 References

1. J. F. Bates, R. W. Powell and E. R. Gilbert, in Effects of Radiation on Materials: Tenth Conference, ASTM STP 725, D. Kramer et al., Eds., 1981, 713-734.

2. F. A. Garner, W. V. Cummings, J. F. Bates and E. R. Gilbert, HEDL-TME 78-9, Hanford Engineering Development laboratory, June 1978.

3 M. Terasawa et al., in Proc. Conf. on Radiation Effects in Breeder Reactor Structural Materials, Scottsdale AZ, June 19-73, 1977, M. L. Bleiberg and J. W. Bennett Eds., TMS-AIME, 687-705.

4. F. A. Garner, J. Nucl. Mater., 122 & 123 (1984) 459-471.

5. F. A. Garner, H. R. Brager and R. J. Puigh, this report.

6. L. K. Mansur, M. R. Hayns and E. H. lee, in Phase Stability During Irradiation, J. R. Holland et al, Eds., TMS-AIME, Oct. 5-9, 1980, 359-382.

7. A. D. Brailsford and L. K. Mansur, J. Nucl. Mater., 103 & 104 (1981) 1403-1408.

8. E. H. Lee, L. K. Mansur and A. F. Rowcliffe, J. Nucl. Mater., 122 & 123 (1984) 299-304.

9. 8. Esmailzadeh, A. S. Kumar and F. A. Garner, this report.

10. F. A. Garner and W. G. Wolfer, J. Nucl. Mater., 122 & 123 (1984) 201-206.

11. E. H. Lee, P. J. Maziasz and A. F. Rowcliffe, in ref. 6, 191-218.

12. F. A. Garner and W. G. Wolfer, J. Nucl. Mater., 102 (1981) 143-150.

13. N. L. Peterson, Solid State Physics, 22 (1968) 409.

14. H. Oikawa, Tech. Reports, Tohoku Univ., 47, No.2 (1982) 215, also 48, No. 1 (1983) 7.

15. C. Narayan and J. I. Goldstein, Met. Trans., 14A (1983) 2437-2439.

16. G. R. Kegg, J. M. Silcock and D. R. F. West, Met. Sci., 8 (1974) 337-343.

17. A. Azarian and K. Kheloufi, J. Nucl. Mater., 97 (1981) 25-26.

18. A. Azarian, Doctoral Thesis, University of Paris, 1974.

19. B. Esmailzadeh and A. S. Kumar, "Influence of Composition on Steady-State Void Nucleation in Irradiated Alloys, ASTM STP 870 (in press.)

70. A. F. Rowcliffe and R. B. Nicholson, Acta Met., 20 (1972) 143.

21. A. F. Rowcliffe and 8. L. Eyre, J. Phys. F, 1 (1971) 771-777.

22. L. Roulanger, Scripta Met., 14 (1980) 67-69.

23. A. Azarian, M. Da Cunha Belo and J. Leteutre, Scripta Met., 9 (1975) 185-192.

24. K. Ehrlich, J. Nucl. Mater., 100 (1981) 149.

25. F. A. Garner, E. R. Gilbert and D. L. Porter, "Stress-Enhanced Swelling of Metals During Irradiation," ASTM STP 775 (1981) 680-697.

7.0 Future Work

No further work on phosphorus is planned.

8.0 Publications

This paper will be published in the proceedings of the First International Conference on Fusion Reactor Materials (Tokyo, Japan, Dec. 3-6, 1984).

CROSS-SECTION TECHNIQUE FOR ION-IRRAOIATEO HT-9 FERRITIC STEEL

J.J. Kai, G.L. Kulcinski, and R.A. Dodd (University of Wisconsin)

1.0 Objective

The purpose of this work is to characterize the effects that total dose and dose rate have on the microstructural evolution in heavy ion irradiated HT-9 ferritic steel with and without helium preinjection.

2.0 Summary

A cross-section technique using iron plating on a HT-9 specimen has been developed for the first time on a heavy ion irradiated HT-Y sample.

3.0 Program

Title: Radiation Effects to Reactor Materials
Principle Investigators: G.L. Kulcinski and R.A. Dodd
Affiliation: University of Wisconsin

4.0 Relevant OAFS Program Task/Subtask

Subtask II.C.I.I: Phase Stability Mechanics
Subtask II.C.6.1: Effect of Damage Rate on Microstructural Evolution

5.u Accomplishments and Status

5.1 Introduction

Heavy-ion irradiation is a very useful technique in studying radiation damage of metals. The high displacement damage rates associated with heavy-ion irradiations allows high damage levels to be achieved in a reasonably short time.

Up to the present time, most heavy-ion irradiation studies have used conventional "back-thinning" techniques for preparing transmission electron inicroscopy (TEM) specimens to examine the irradiated region. A more powerful technique is the cross-section method which is recently reviewed by Zinkle and Sindelar.[1] The cross-section technique allows the entire heavy-ion damaged region and the unirradiated control region to be examined at once. This is very important since the damage rate and also the total damage level vary with depth for heavy-ion irradiation. Figure 1 shows the displacement per atom (dpa) and nickel ion deposition distributions in HT-9 versus depth curves which are calculated from the Brice code with displacement coefficient k = 0.8. The purpose of this note is to show that the techniques previously described[1] can be extended to the analysis of the ferritic steel, HT-9.

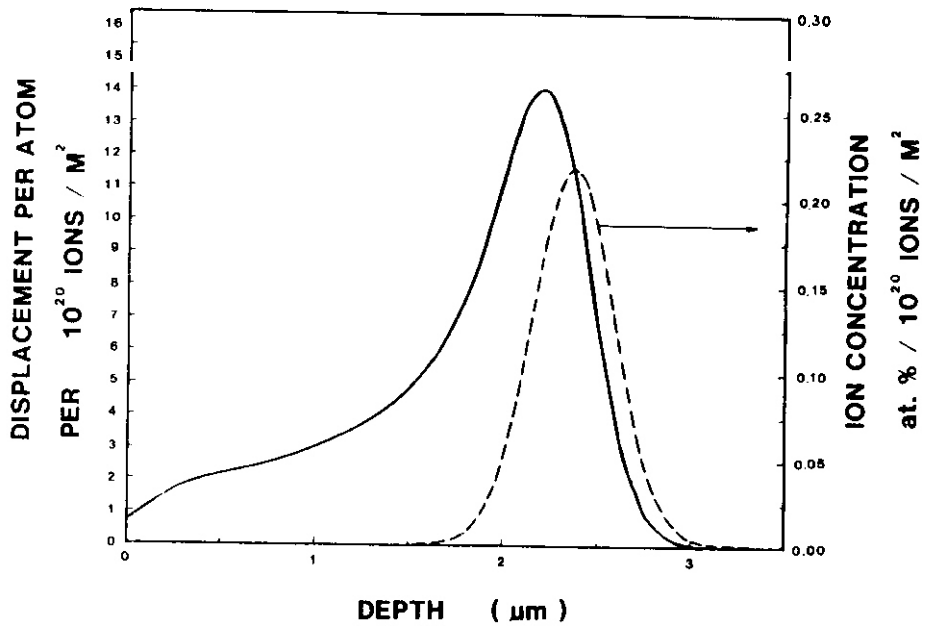

FIGURE 1. dpa and ion deposition vs. depth.

TABLE 1

THE CHEMICAL COMPOSITION OF THE HT-9 FERRITIC STEEL USED IN THIS STUDY[2]

Element	Fe	Cr	Mo	V	W	Mn	Ni	C	Si
wt.	balance	11.63	1.0	0.30	0.52	0.52	0.50	0.20	0.22

5.2 Experimental Procedures

The HT-9 ferritic steel used in this study is from GA and has heat treatment number 9607-R2. The chemical composition of this material is given in Table 1.[2] The as-received material vias successively cold rolled and heat treated[3] (1050°C, 1/2 hr + AC and 770°C, 2.5 hr + AC) to a thickness of 0.76 mm for this study. A foil size oi 10 mm x 5 mm x 0.76 mm was used for irradiation.

The general procedures of the cross-section method are the same as reviewed earlier.[1] The electroplating solution used ior iron plating consisted of 150 g ferrous chloride ($FeCl_2 \cdot 4H_2O$), 100 g calcium chloride ($CaCl_2$) and 800 ml distilled water. The plating is performed at 90°C and 60 mA. It usually takes about 15 hours to plate a 3 mm thickness. Before the plating is initiated, it is necessary to loosen and remove the oxide layer on the irradiated surface to ensure a successful plating. This step involves dipping in a

pickling solution (15 ml H_2SO_4, 2 g thiourea and 85 ml H_2O) for 4 minutes followed by a thorough water rinse and striking in the plating bath at 95°C and 60 mA for 10 seconds.

After electroplating, the specimen is mounted in epoxy. The epoxy block is then sliced by a diamond saw with the direction vertical to the irradiated surface of the specimen. A 3 mm disc is punched off from the irradiated portion of each slice. A commercial twin-jet polisher is used to polish the discs until perforation. The electropolishing solution used in this experiment consisted of 10% $HClO_4$ and 90% ethanol at the condition of -20°C and 40 mA.

The electropolishing rates of plated iron and the HT-9 steel are quite different. Therefore, a two-step polishing technique is used. The first step is to form an indentation region near the interface to induce the perforation to form at the proper position of the disc. This is accomplished by lacquering off almost all of the disc except a 50 μm wide strip along the interface in the HT-9 steel region, and then electropolishing for a period of time. The second step is a normal twin-jet polishing after dissolving off the protection lacquer by acetone. If the perforation does not take place along the interface, the specimen can be salvaged by using an ion mill to extend the thin area toward the interface. In general, there are at least 3 slices which can be cut from irradiated region, therefore, the successful probability of getting a good TEM specimen is better than 50%.

5.3 Results

Figure 2 shows a typical cross-section TEM picture of an iron plated unirradiated HT-9 specimen. Figure 3 shows a portion of the thin area which obtained from a HT-9 specimen irradiated with 14 MeV Ni ions at 500°C to a fluence of 3×10^{20} ions/m^2. In this specimen, the variation in dislocation density (both loops and segments) can be clearly seen through the end of damage range.

5.4 Summary

A routine experimental procedure has been developed in iron plated HT-9 steel which allows heavy-ion irradiated HT-9 specimens to be examined in cross-section. By using this cross-section technique, the total dose and dose rate effects of heavy ion irradiation on the microstructural evolution of the HT-9 ferritic steel can be easily addressed. Recent analysis has suggested that the microstructure will be altered due to the addition of injected interstitials during an ion-irradiation of materials.[4,5] The cross-section technique, combined with the 14 MeV heavy-ion irradiation, will be used to analyze the region free from surface effects and including excess interstitials to see if such a phenomenon does take place.

6.0 References

1. S.J. Zinkle and R.L. Sindelar in DAFS Quarterly Progress Report April-June 1984, DOE/ER-0046/18, pp. 133-141.

2. R.D. Stevenson, B.E. Thurgood, and S.N. Rosenwasser in ADIP Quarterly Progress Report June 30, 1980, DOE/ER-0045/3, pp. 192-200.

3. R.F. Bomagala, Sr., private communication, Material Science Division, Argonne National Laboratory.

4. D.L. Plumton and W.G. Wolfer, "Suppression of Void Nucleation by Injected Interstitials," to be published in J. of Nucl. Mat.

5. B. Badger, Jr., D.L. Plumton, S.J. Zinkle, R.L. Sindelar, G.L. Kulcinski, R.A. Dodd, and W.G. Wolfer, DAFS Quarterly Progress Report April-June 1984, DOE/ER-0046/18, pp. 107-121.

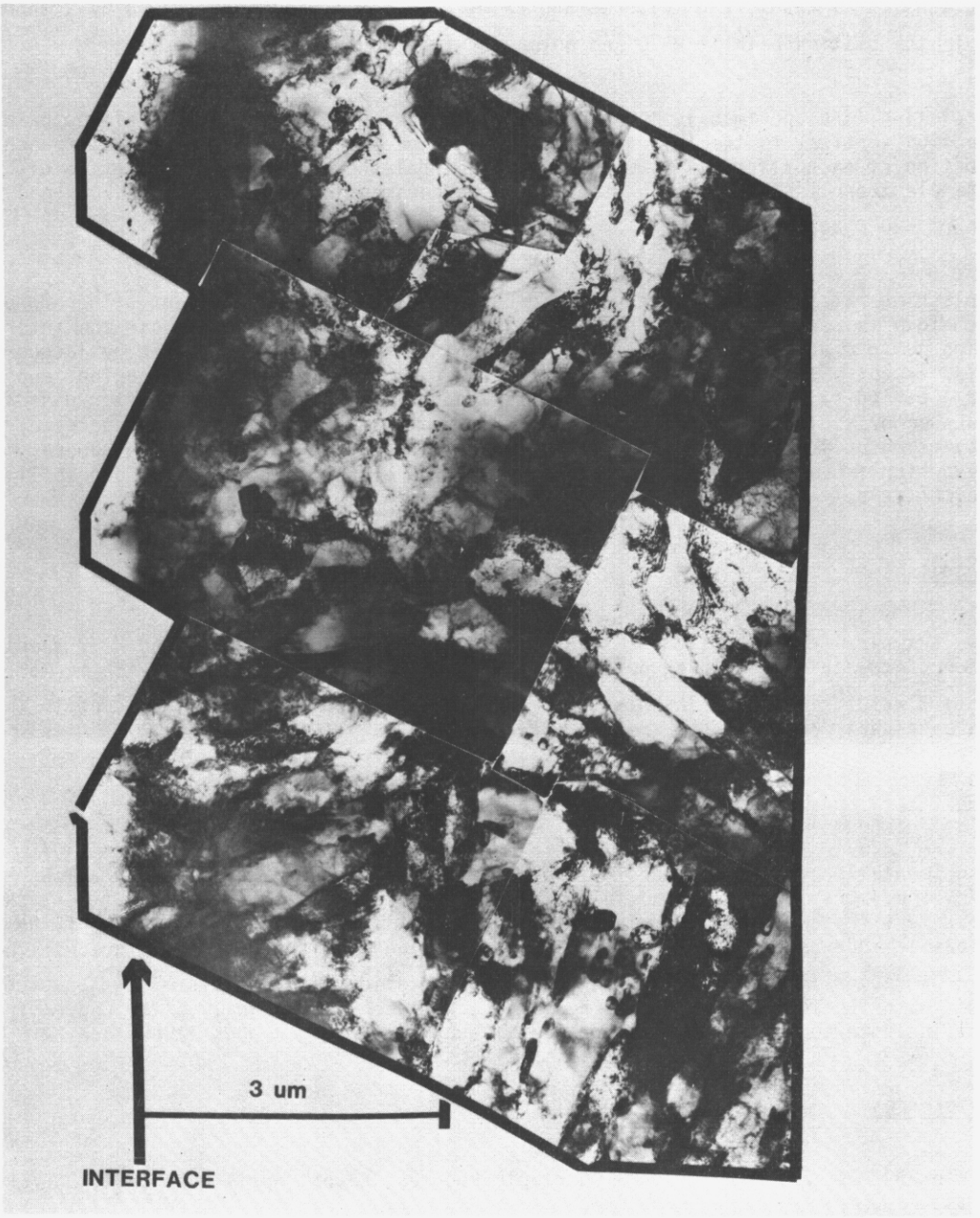

FIGURE 2. Cross-section of Fe-plated unirradiated HT-9 ferritic steel.

7.0 Future Work

Heavy-ion irradiation and subsequent analysis of the HT-9 ferritic steel with and without helium preinjection is in progress. The analysis will be proceeded in a JEOL 200 CX II TEMSCAN microscope and a Tracor Northern TN2000 EDS system will be used to assist in precipitate analysis.

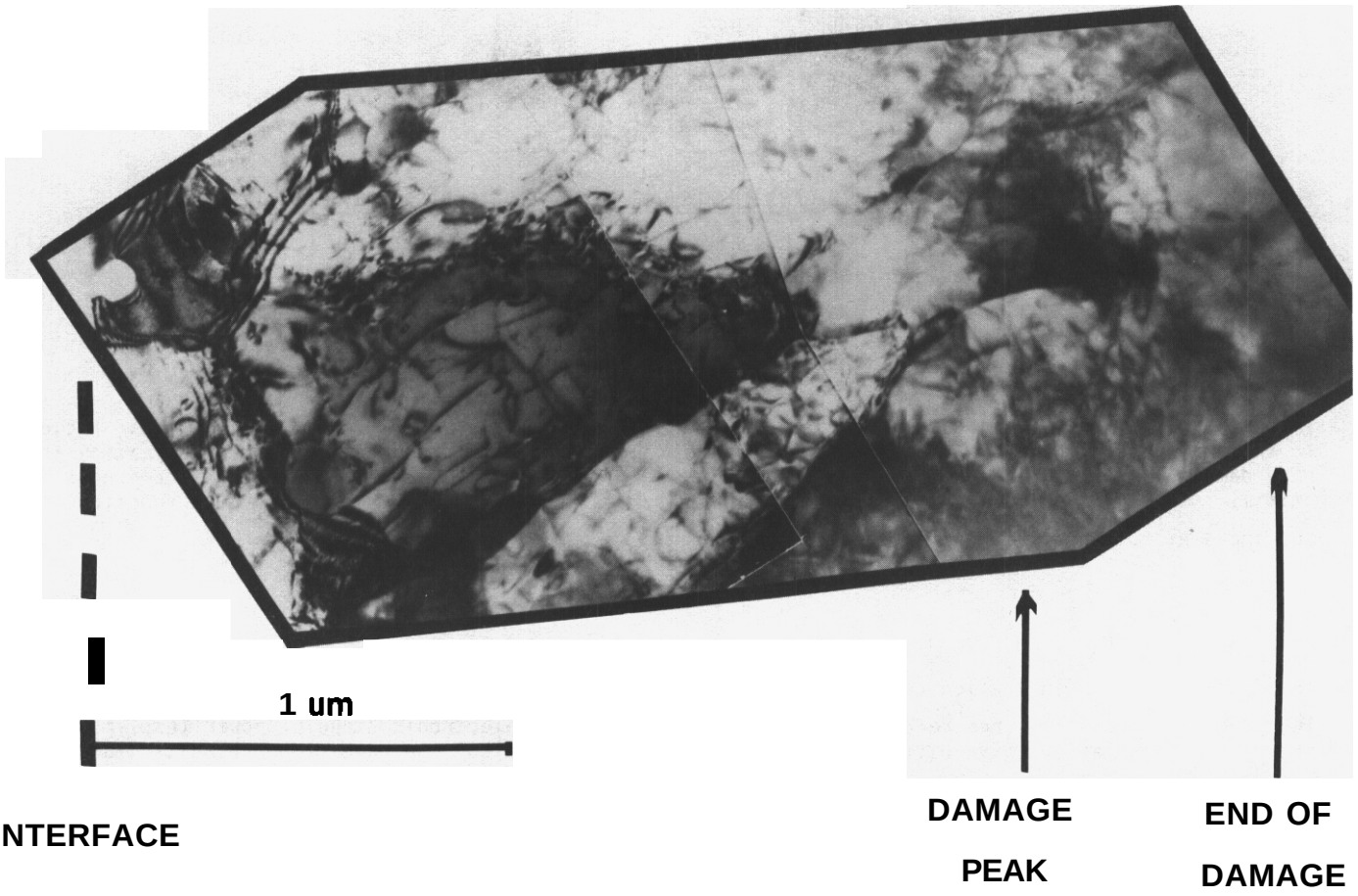

FIGUKE 3. **Cross-section** of HT-9 **ferritic steel irradiated with** 14 MeV **N ions to a calculated peak damage level** of 40 **dpa at** 500°C.

THE MAGNITUDE AND DISTKIBUTION OF THE EXCESS INTERSTITIAL FRACTION DURING HEAVY ION IRRADIATION

D.L. Plumton and G.L. Kulcinski (University of Wisconsin)

1.0 Objective

In heavy ion irradiation studies. the injected self-ion has recently been shown to suppress void nucleation in the ion deposition region. Previous theoretical calculations using steady state void nucleation theory have denonstrated that the predicted void number density is sensitive to small changes in the excess interstitial fraction, ϵ_i. In this paper the magnitude and distribution of ϵ_i is examined as a function of depth and incident ion energy for Ni irradiation of Ni.

2.0 Summary

The magnitude of ϵ_i in the ion deposition region increases as the incident ion energy decreases. This increase is especially large below 4 MeV. The use of different electronic stopping power (esp) models in the damage calculations gave differences in ϵ_i of ~ 20% where the LSS esp gave higher results than the Brice esp. For low energy (< 5 MeV) ion irradiations there exists no part of the ion range free from the presence of excess interstitials while for the high energy (14 MeV) case the region less than 1.2 μm in depth appears to have a negligible ϵ_i value.

3.0 Programs

Title: Radiation Damage Studies
Principle Investigator: G.L. Kulcinski and R.A. Oodd
Affiliation: University of Wisconsin-Madison

4.0 Relevant DAFS Program Task/Subtask

II.B.2.3
Subtask C. Correlation Methodology

5.0 Accomplishment and Status

5.1 Introduction

The injected ions in a heavy ion irradiation damage Study can affect the damage microstructure after they are deposited in the matrix. The injected ions come to rest in the solid as an interstitial without a vacancy partner. These excess interstitials have been shown to cause suppression of void nucleation and swelling in the ion deposition region. Brailsford and Mansur[1] first predicted that the injected ions would reduce the void swelling rate. This theoretical prediction has been expanded upon by Mansur[2,3] and also experimentally verified by Lee et al.[4] Plumton and Wolfer[5] have theoretically shown large reductions in void nucleation due to the excess interstitials. This reduction in the void number density in the peak damage region has been observed experimentally.[6,7] For example, Figure 1 is a through range micrograph**) of a Ni specimen irradiated at 450°C by 14 MeV Ni ions which illustrates the large suppression in

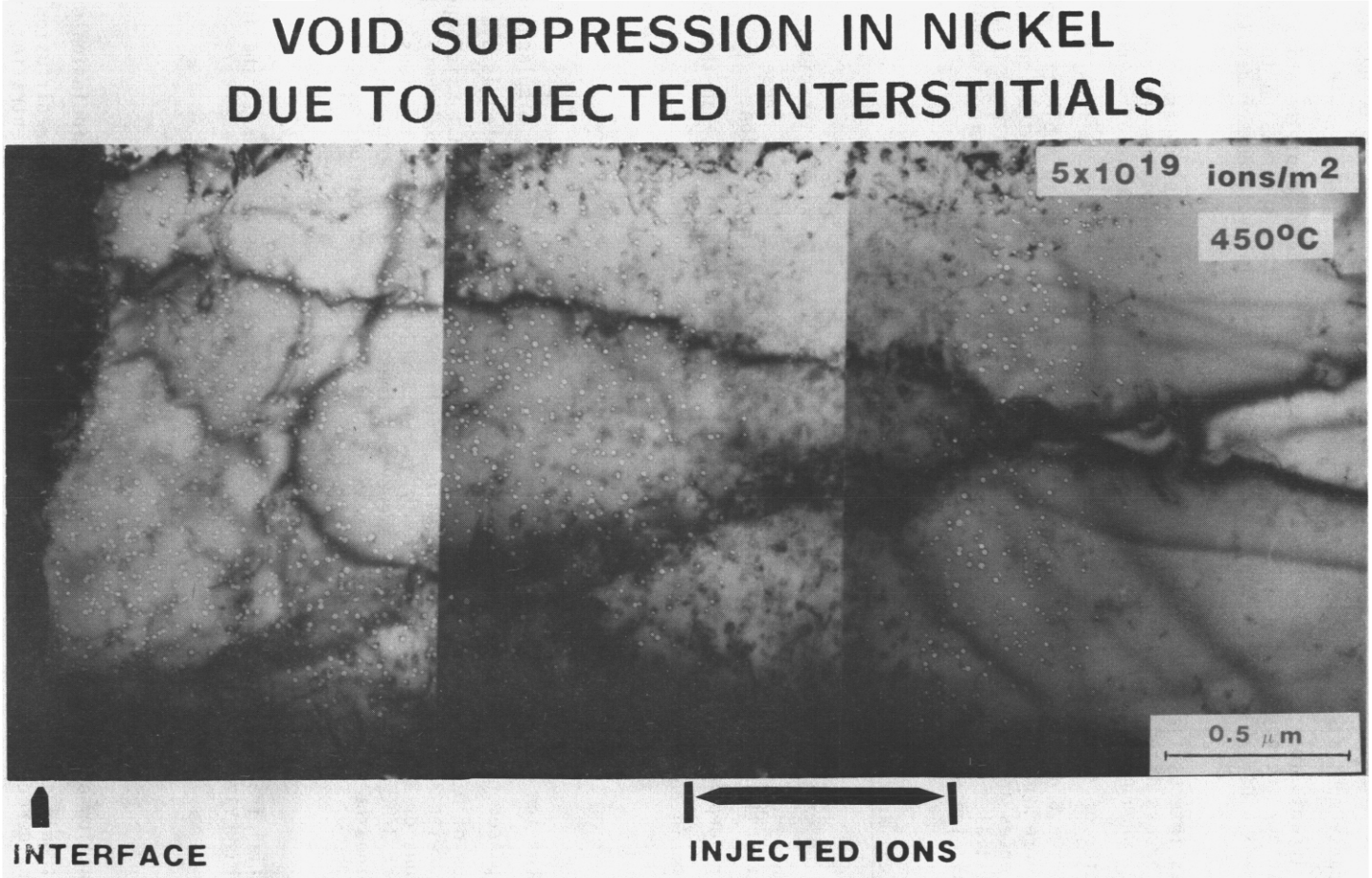

FIGURE 1. Depth-dependent void microstructure of nickel irradiated with 14 MeV Ni ions to a peak damage level of 5 dpa (K = 0.8) at 450°C. Note the absence of voids in the implanted ion region.

void density possible in the ion deposition region. A review of the experimental evidence on the suppression effect of the injected interstitials has recently been presented by Garner.[8] The suppression increases whenever recombination is the dominant point defect loss mechanism and occurs at low temperatures and/or when the vacancy mobility is reduced by impurity trapping. Kuinar and Garner[9] recently modeled the helium in dual ion irradiations as an additional excess interstitial because of the ability of helium in the matrix to trap a vacancy thereby freeing up an interstitial. This extra suppression to their void nucleation results suggests a possible explanation for previous experimental void number density anomalies.

The number of excess interstitials is a small fraction of the total number of damage produced interstitials (< 1%) so that the excess interstitials only become a significant portion of the interstitials reaching voids or void nuclei when most of the interstitials are recombining with vacancies. Previously it has been noted[5] that a factor of two difference in the excess interstitial fraction, ε_i (5×10^{-4} - 1×10^{-3}), can result in more than two orders of magnitude difference in the calculated void nucleation rate. That the inclusion of a few more hundredths of a percent to the total interstitial concentration can result in orders of magnitude differences in the nucleation rate indicates a highly nonlinear system. Calculating an accurate excess interstitial fraction is a necessity before good theoretical predictions on void nucleation and swelling during heavy ion irradiation can be obtained.

5.2 Theoretical Procedure

The damage rate or the excess interstitial fraction associated with a heavy ion irradiation can be calculated with damage codes such as the BRICE code[10] and the HERAD code.[11] From these codes one obtains an ion deposition distribution function, $f(x)$, and a displacement energy distribution, $S_D(x)$. Both of these are a function of the depth, x, along the ion range. The displacement rate, I_D, can then be calculated by using a modified Kinchin and Pease model[12] where

$$I_D(x) = \frac{\phi K S_D(x)}{2 \rho E_D} \quad . \tag{1}$$

Here ϕ is the incident ion flux, ρ is the atomic density and E_D is the effective displacement energy. To obtain accurate displacement values the displacement efficiency, K, should be taken as 0.3 in contrast to the traditional value of 0.8. A recent review by Kinney et al.[13] indicates that K is dependent on the incident ion energy, with K decreasing for increasing recoil energy. For high energy ($\gtrsim$ 1 MeV) neutron or heavy ion irradiations of FCC metals the efficiency is $\simeq$ 0.3 which reduces most previously cited damage values by a factor of 318. However, self-consistency requires the use of K = 0.8 since the low temperature work done to determine the fraction of defects escaping in-cascade recombination, E_{ff}, has already assumed K = 0.8.

The excess interstitial fraction has been taken[5] as the ratio of deposited ions to the interstitials produced by damage that survive in-cascade recombination. Therefore ε_i is

$$\varepsilon_i(x) = \frac{f(x)\phi}{E_{ff} \rho I_D(x)} \tag{2}$$

where E_{ff} is the fraction of defects that escape in-cascade recombination. The inclusion of E_{ff} into the formalism means that only those interstitials going to sinks or recombining after diffusion away from the cascade site are considered. This is a large reduction to the interstitial concentration since E_{ff} can be as low as 0.15[14] for FCC metals. The functional dependence of Eq. (2) can be seen through the use of Eq. (1). This gives ε_i as,

$$\varepsilon_i(x) = \frac{2 E_D}{K E_{ff}} \frac{f(x)}{S_D(x)} \tag{3}$$

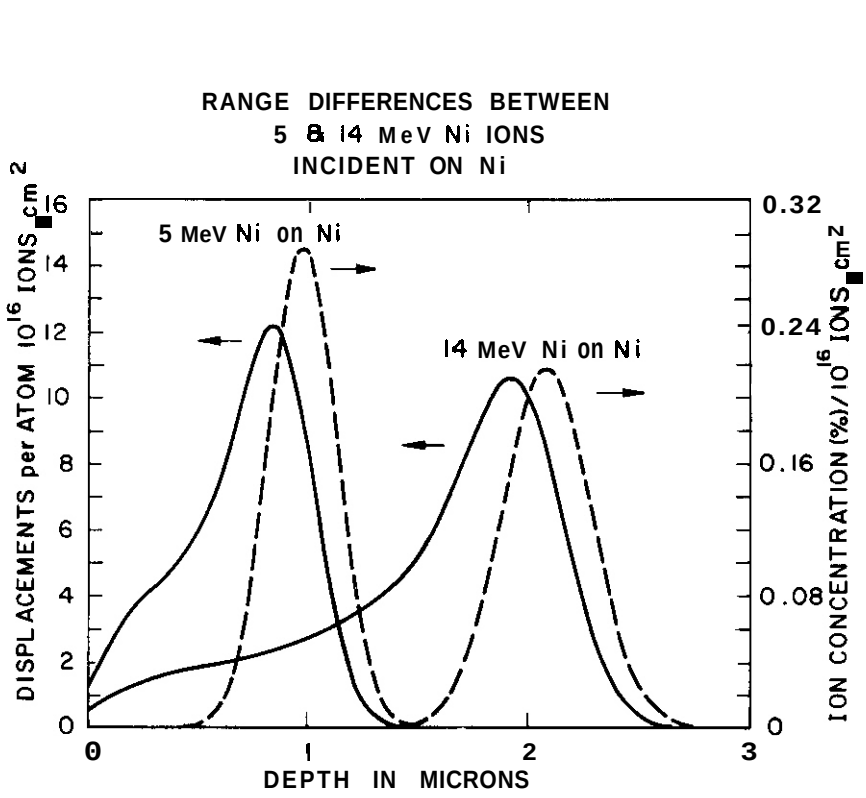

FIGURE 2. Displacement damage and implanted ion concentration (atomic %) versus depth for 5 and 14 MeV Ni on Ni where the BRICE code calculation used the LSS esp, E_D = 40 eV and K = 0.8.

The UKICE code and Eqs. (1) and (3) have been used to examine the interrelationship between ϵ_i and I_D for various incident ion energies for Ni on Ni. The distribution of $\epsilon_i(x)$ as a function of depth is examined for decreasing ion eneryies. The values of ϵ_i versus incident ion energies are shown for various points along the ion range with the additional effect of two different electronic stopping power models, Brice[10] and LSS[15], included. Finally the two damage codes BRICE and HERAD are shown to affect the depth distribution of ϵ_i in significantly different ways. All damage code results are for a Ni on Ni heavy ion irradiation.

5.3 Results and Discussion

From Eq. (3) we observe competing trends. Both f(x) and $S_D(x)$ go through a maximum as the depth, x, is varied from the front surface to the end of the ion range. This can be observed in Figure 2 where the BRICE code has been used to calculate the displacement value, Eq. (1), versus depth for 5 and 14 MeV Ni on Ni (solid line Figure 2). Additionally it can be noted that as the incident ion energy is decreased, f(x) (dashed line Figure 2) can completely overlap the damage profile. Plumton et al.[16] showed that for low energy ions this increased overlap causes increasing void nucleation suppression even though the displacement rate (i.e., $S_D(x)$) has increased.

The depth distribution of $\epsilon_i(x)$ is shown in Figure 3 for several incident ion energies. For consistency the $\epsilon_i(x)$ values are plotted out to an end of range value coincident with a damage rate of $\sim 10^{-6}$ dpa/s. For 0.5 MeV irradiations ϵ_i is extremely large which will give a large void suppression effect under even mild point defect recombination conditions. Under the appropriate irradiation conditions an excess interstitial fraction as low as 10^{-4} can have significant results.[5] Therefore, for Ni ions with incident energy $\lesssim$ 5 there is no area free from the presence of the excess interstitials and free from the influence of the front surface. In contrast, for a 14 MeV ion irradiation, there exists a depth region from *0.4* μm to 1.2 μm where ϵ_i should have little effect.

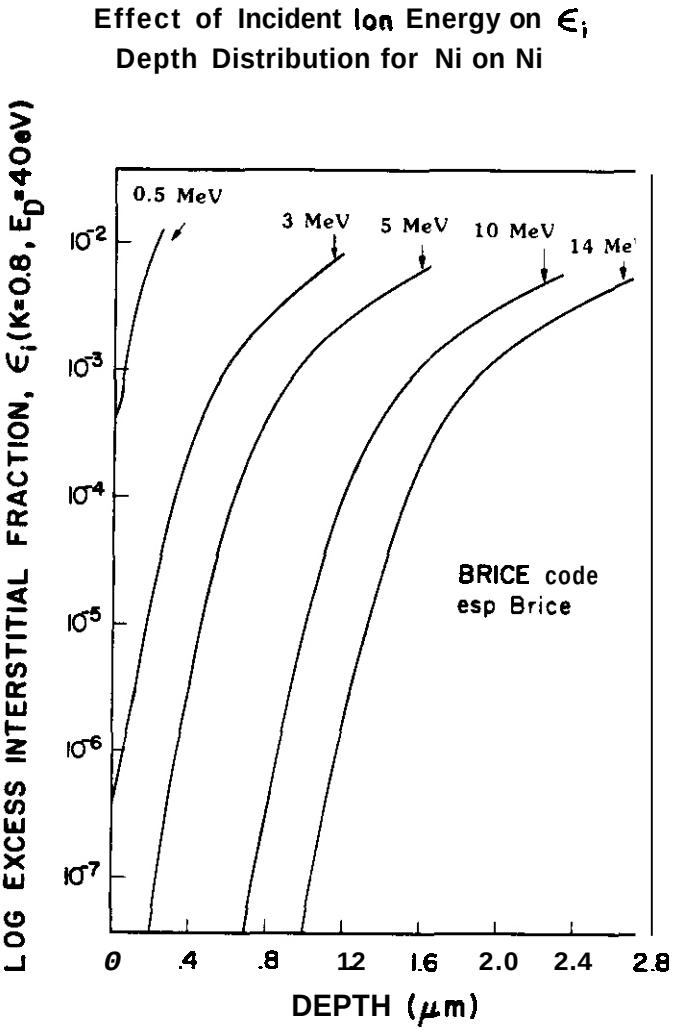

FIGURE 3. Log ϵ_i versus depth for Ni on Ni at several incident ion energies.

Examination of Figure 4, which compares ϵ_i as a function of depth between the two damage codes, BRICE and HERAD, shows a much larger ϵ_i value towards the front surface for the 14 MeV HERAD results as compared to the 14 MeV BRICE results. HERAD, which uses a more detailed physical modeling of the collision process coupled with the absence of any compromising assumptions regarding the solution of the transport equation, should result in a more accurate description of the ion deposition distribution function. The larger value of ϵ_i near the front surface for the HERAD results arises from a non-Gaussian shape for f(x) with a long tail towards the front surface. That a small value of f(x) should give such a large increase in $\epsilon_i(x)$ also results from the decreasing value of $S_D(x)$ towards the front surface. The magnitude of ϵ_i, 10^{-6}-10^{-4}, that the 14 MeV HERAD code gives for the $\lesssim$ 1.4 μm depth region is only significant under conditions where point defect loss is extensively dominated by recombination (i.e., low temperatures). Therefore, the two damage codes will only give significantly different void nucleation and/or swelling results when the temperature is low and/or the vacancy mobility is reduced through impurity trapping. The 5 MeV results, Figure 4, show again the trend of a larger value of $\epsilon_i(x)$ towards the front surface for HERAD compared to BRICE calculations. Comparison between the 5 and 14 MeV HERAD results at the 1 μm depth, which is a typical depth for transmission electron microscopy analysis, shows that ϵ_i (5 MeV) is mare than an order of magnitude larger than ϵ_i (14 MeV)

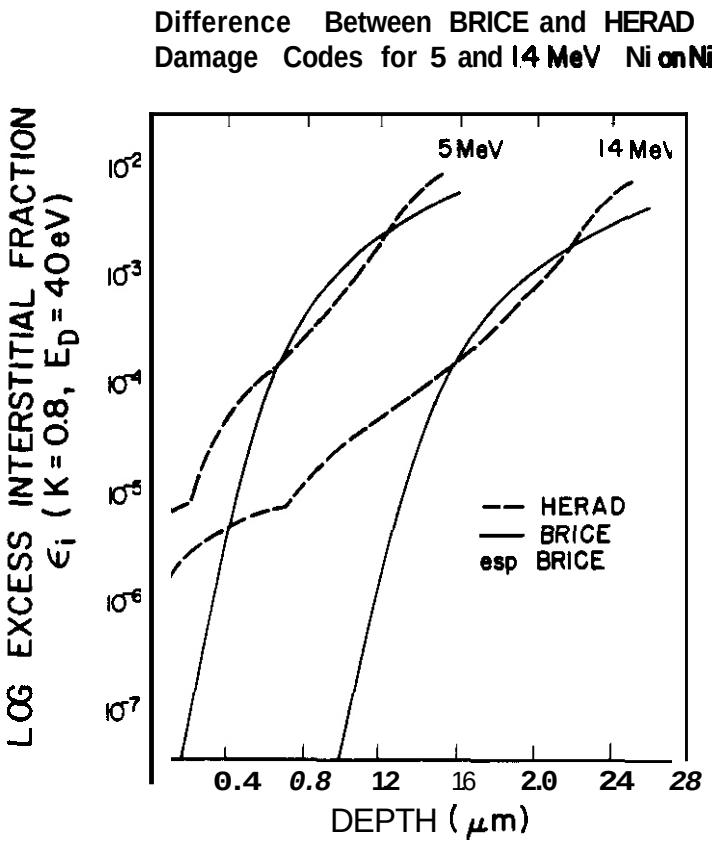

FIGURE 4. Log ϵ_i versus depth for 5 and 14 MeV Ni on Ni where the BRICE and HEKAD damage codes are compared.

This low but non-negligible value of $\epsilon_i(x)$ near the front surface might be responsible for some of the discrepancies observed between experimental results on nickel irradiated with 14 MeV Ni and the predictions of steady state void nucleation theory. Low temperature irradiations at 400°C[6] and 425°C[7] both showed that the void number density was suppressed for a depth of almost 2.5 μm. Void nucleation theory, using BRICE code data, predicted Only ~ 1 μm[5,7] of suppressed region. Part of the discrepancy may be attributed to the BRICE code's use of a Gaussian distribution function. This Gaussian distribution gives too small a value for ϵ_i near the front surface when compared to the more accurate HERAD results.

The two remaining figures show BRICE code results for the log of ϵ_i versus incident ion energy. Figure 5 shows ϵ_i versus incident ion energy for the ion deposition peak and the damage peak. In the deposition peak, we see a smooth increase in ϵ_i as the ion energy decreases. In the damage peak, the competing trends that f(x) and $S_D(x)$ impose on $\epsilon_i(x)$ cause a more complicated behavior. The dip in the ϵ_i values, at intermediate ion energies, occurs because $S_n(\sim)$ increases faster than f(x). In both peaks the LSS esp model gives higher ϵ_i values, ~ 20% greater than the Brice esp models. Finally, Figure 6 shows $\epsilon_i(x)$ versus ion energy for several damage rates in the ion deposition region. In all cases ϵ_i increases smoothly with decreasing ion energy. The 2 MeV ϵ_i value is about 50% larger than the 14 MeV ϵ_i value for the DRICE esp case, while the increase is ~ 70% for the LSS esp case. The LSS electronic stopping power models gives ϵ_i values 10-25% higher than the corresponding Brice esp model.

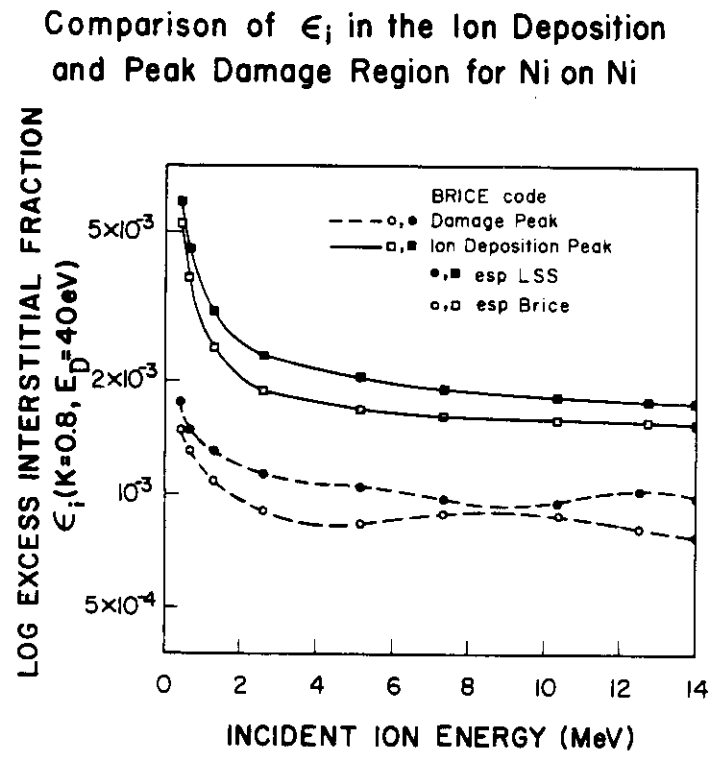

FIGURE 5. Log ϵ_i versus incident ion energy for Ni on Ni at the damage peak and at the ion deposition peak.

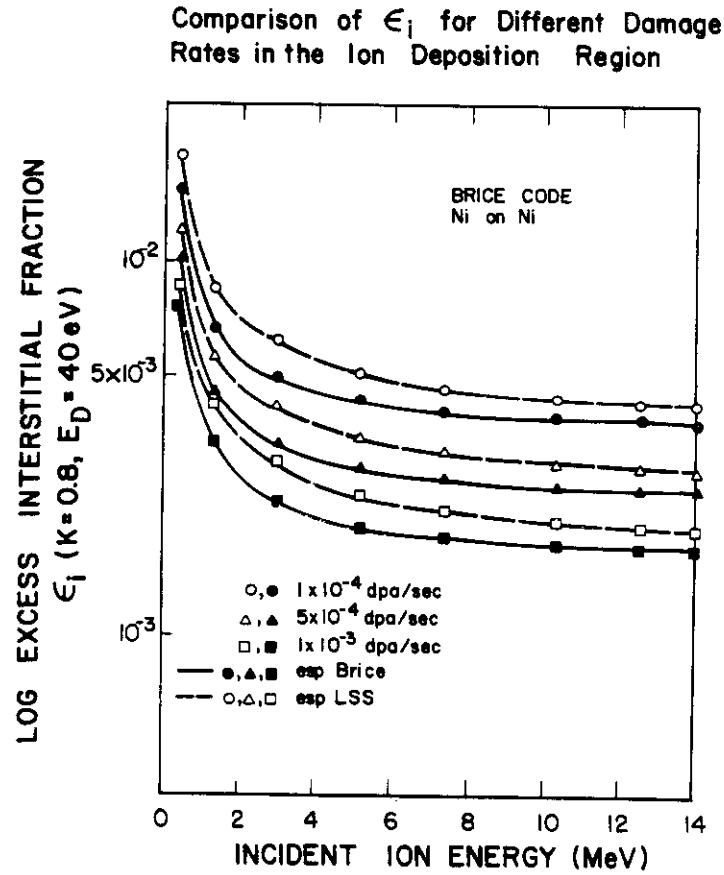

FIGURE 6. Log ϵ_i versus incident ion energy for Ni on Ni at various constant damage rates on the backside of the ion deposition profile.

5.4 Conclusions

1. The excess interstitial fraction in the ion deposition region decreases with increasing ion energy which favors the use of higher energy bombarding ions.

2. The use of the Brice electronic stopping power model gives a lower excess interstitial fraction than the LSS model in the damage and ion deposition peak.

3. For incident ion energies $\lesssim$ 5 MeV there exists no part of the ion range free from the presence of excess interstitials and is at the same time sufficiently far from the front surface to avoid surface phenomena.

6.0 Reterrnces

1. A.U. Brailsford and L.K. Mansur, J. Nucl. Mat. 71 (1977) 110.

2. L.K. Mansur, Nuclear Technology 40 (1978) 5.

3. K.U. Mansur and M.H. Yoo, J. Nucl. Mat. 85&86 (1979) 523.

4. E.H. Lee, L.K. Mansur and M.H. Yoo, J. Nucl. Mat. 85&86 (1979) 577.

5. D.L. Plumton and W.G. Wolfer, J. Nucl. Mat. 120 (1984) 245.

6. J.B. Whitley, Ph.D. Thesis, University of Wisconsin, 1978.

7. B. Baager, Jr., D.L. Plumton, S.J. Zinkle, R.L. Sindelar, G.L. Kulcinski, R.A. Uodd, and W.G. Wolfer, "Experimental Investigation of the Effect of Injected Interstitials on Void Formation," 12th Inter. Symp. *on* the Effects of Radiation on Materials, Williamsburg, VA, 18-20 June 1984.

8. F.A. Garner, J. Nucl. Mat. 117 (1983) 177

9. A. Kunar and F.A. Garner, "Dual Ion Irradiation: Impact of the Conflicting Roles of Helium on Void Nucleation," 12th Inter. Symp. on Effects of Radiation on Materials, Williamsburg, YA, 18-20 June 1984.

10. D.K. Brice, Report SAND-7500622, Sandia National Laboratories, July 1977.

11. H.M. Attaya, Ph.D. Thesis, University of Wisconsin, 1981.

12. I.M. Torrens and M.T. Robinson, Kadiation Induced Voids in Metals, J.W. Corbett and I.C. Ianniello eds., (1972) 739.

13. J.H. Kinney. M.W. Guinan and Z.A. Ilunir, J. Nucl. Mat. 122&123 (1984) 1028

14. U. Theis and H. Wollenberger, J. Nucl. Mat. 88 (1980) 121.

15. J. Linhard and M. Scharff, Phys. Rev. 124 (1961) 128.

16. D.L. Plumton, H. Attaya and W.G. Wolfer, J. Nucl. Mat. 122&123 (1984) 650.

CHAPTER 6

FUNDAMENTAL STUDIES OF SPECIAL PURPOSE MATERIALS

ION IRRADIATION OF COPPER AND COPPER ALLOYS TO 40 DPA AT 100-400°C

S.J. Zinkle and G.L. Kulcinski (University of Wisconsin)

1.0 Objectives

To examine the defect microstructure of copper following ion irradiation to high doses and to determine why certain copper alloys (and pure copper) are resistant to void swelling during charged particle irradiation.

2.0 Summary

Pure copper and several copper alloys were found to be resistant to void formation following ion irradiation to a calculated peak damage level of 40 dpa at 100-400°C. The absence of a significant void population is probably due to the low oxygen content in the foils, and also the absence of helium during the irradiation.

3.0 Program

Title: Radiation Effects to Reactor Materials
Principal Investigators: G.L. Kulcinski and R.A. Dodd
Affiliation: University of Wisconsin-Madison

4.0 Relevant OAFS Program Plan Task/Subtask

Subtask II.C.1.1: Phase Stability Mechanics
Subtask II.C.1.2: Modeling and Analysis of Effects of Materials Parameters on Microstructures

5.0 Accomplishments and Status

5.1 Introduction

There is currently a renewed interest in copper and its alloys for fusion reactor applications.[1] However, it may be stated that the irradiation behavior of copper is not very well characterized. More than 200 irradiation studies have been reported for copper and copper alloys, but the vast majority of these investigations have been limited to low damage levels and/or a limited temperature range.[2]) In particular, the void swelling behavior of copper has never been satisfactorily determined. There are thirteen known studies of copper or copper alloys at neutron irradiation conditions relevant for void formation.[2] Only two of these studies were performed at doses greater than 1 dpa, and they were each confined to a single irradiation temperature.[3,4] Low-fluence neutron results indicate that void formation occurs in copper for irradiation temperatures between 220 and 550°C (0.35-0.60 T_M).

High-dose electron and ion irradiation studies have generally found[2] that void formation occurs easily in copper for irradiation temperatures of 300-550°C. However. there have been several investigations of copper alloys where no voids were observed over this temperature range even after irradiation to 40 dpa.[5,6] The present report is intended to shed some light on the cause of this difference in void formation behavior.

TABLE 1

NOMINAL GAS CONTENT (PPM) OF FOILS USED IN THIS STUDY

	H	N	O
Copper	< 1.0	< 1.0	< 5.0
AMZIRC, AMAX-MZC	< 2	-	< 3

TABLE 2

IRRADIATION PARAMETERS FOR THE ION-IRRADIATED COPPER AND COPPER ALLOYS

Material	Irradiation Temperature	Calculated Damage (dpa) 1 μm	Peak (2 μm)
Cu, AMZIRC, MZC	100°C	10	40
Cu, AMZIRC, MZC	200°C	10	40
Cu, AMZIRC, MZC	300°C	10	40
Cu, AMZIRC, MZC	400°C	10	40
Cu (from Ref. 5)	400°C	2	9
Cu (from Ref. 5)	450°C	7	30
Cu (from Kef. 51	500°C	2	9

5.2 Experimental Procedure

Foils of MARZ grade copper and the copper alloys AMZIRC (Cu-0.15 at % Zr) and AMAX-MZC (Cu-0.8 at % Cr - 0.15 at % Zr - 0.04 at % Mg) in the solution annealed and aged condition[7] were selected for this irradiation study. The gas content of the manufacturer's Stock material for the pure copper and the copper alloys is given in Table 1. The pure copper foils were annealed at 800°C for 1.5 hours and cooled to room temperature in a hydrogen atmosphere prior to their preparation for irradiation.[5] Pre-irradiation treatment consisted of mechanical polishing followed by electropolishing for 5 seconds at an applied potential of 5 V in a solution of 33% HNO_3/67% CH_3OH cooled to -50°C. The foils were irradiated with 14-MeV Cu^{3+} ions using the University of Wisconsin tandem Van de Graaf accelerator.[8] The fluence for all samples was 3×10^{20} ions/m^2, with an average flux of 6×10^{16} ions/m^2-s. The BRICE code[9] was used to calculate the depth-dependent displacement damage. Table 2 lists the irradiation conditions for this study.

Following the irradiation, the samples were prepared for cross-section analysis.[10] The cross-section specimens were jet-electropolished in a solution of 33% HNO_3/67% CH_3OH cooled to -25°C at an applied voltage of 20 V, and were examined in a JEOL TEMSCAN-200CX electron microscope.

5.3 Results

The main finding of this investigation is that no substantial void formation was detected in pure copptr or the copper alloys for any of the irradiation conditions. A previous investigation at the University of Wisconsin[5] using the same lot of annealed copper foils and similar ion irradiation conditions found that there was no observable void formation at irradiation temperatures of 400, 450, or 500°C (see Table 2 for damage levels). In the present case, a sparse distribution of voids was observed in only one pure copper sample irradiated at 400°C. The average void diameter for this condition was 100 nm, with an estimated density of only $10^{17}/m^3$.

Irradiation of the copper and copper alloys at temperatures 100-300°C resulted in "black spot" damage and no void formation. A typical low-magnification cross-section micrograph for this irradiation temperature

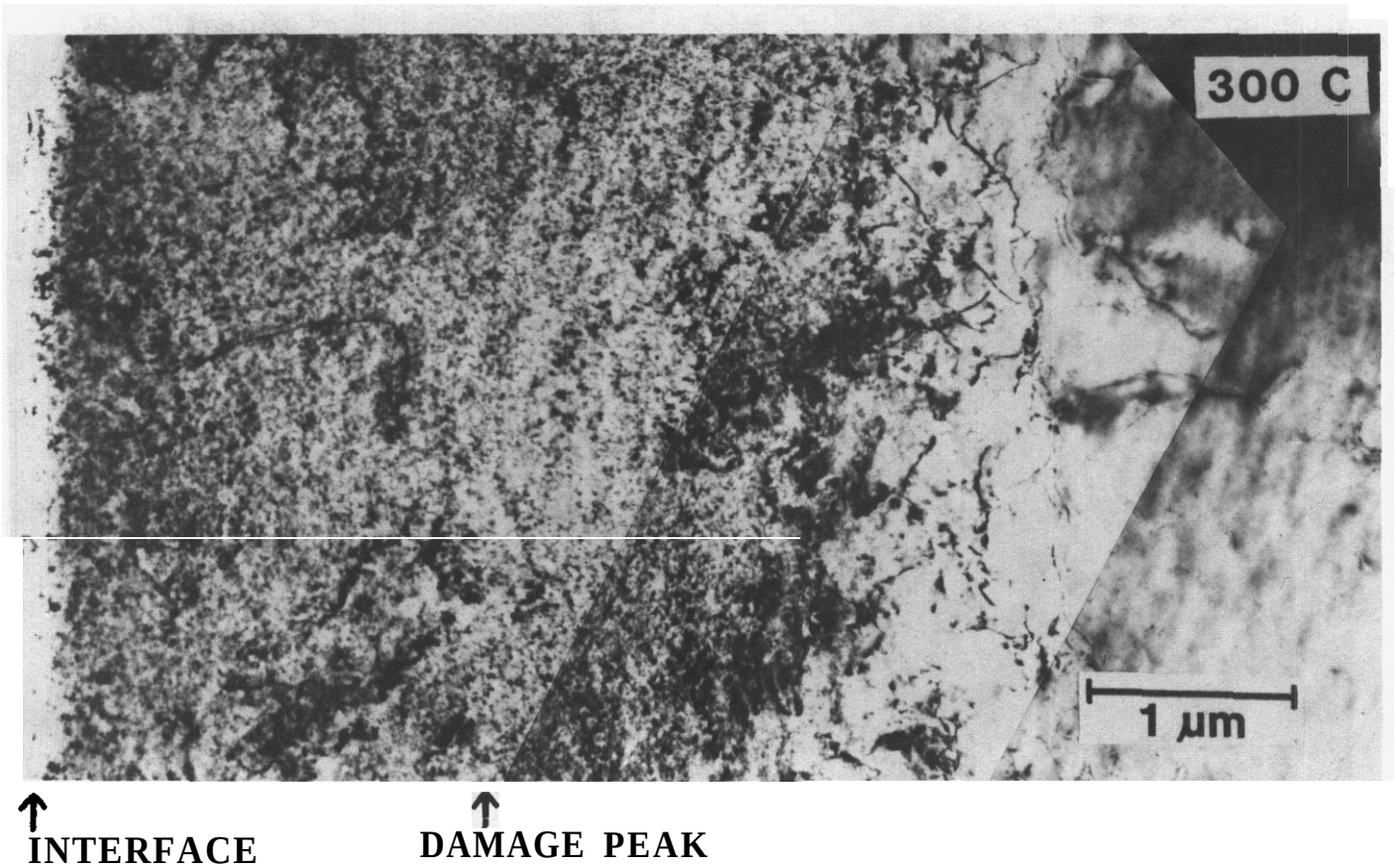

FIGURE I. Cross-section micrograph of copper irradiated with 14-MeV Cu ions to a calculated peak damage level of 40 dpa at 300°C.

regime is shown in Figure 1. Figure 2 shows the weak beam dark field microstructure of a representative damage region. The defect cluster density in the irradiated copper samples was roughly constant for irradiation temperatures of 100-200°C, and was lower for the sample irradiated at 300°C. Details of the cluster density and size distribution will be reported at a later date.

5.4 Discussion

The absence of appreciable void formation in the ion-irradiated copper and the AMZIRC and MZC copper alloys may initially be regarded as surprising in light of the numerous[2] experimental charged particle irradiation studies which have shown that void formation occurs easily in copper. However, theoretical calculations indicate that the most stable morphology of a vacancy cluster in copper is in a planar configuration, and not a void.[11,12] We have recently re-examined the relative energies of vacancy clusters in copper using the formalism of Refs. 11 and 13. The results of the calculation are shown in Figure 3. The surface energy and stacking fault energy data are from Cotterill[13] and Murr,[14] respectively. The energies of the loops and the stacking fault tetrahedron (SFT) were calculated according to Ref. 11, while the void energy was determined using equations given in Ref. 13. Figure 3 predicts that stacking fault tetrahedra are the most stable configuration for small vacancy clusters, and that perfect loops are the most energetically favorable morphology for very large vacancy clusters. Voids are predicted to be stable only over a very limited size range in pure copper. The use in the energy calculations of a larger surface energy value, such as given by Murr[14] (γ = 2.1 J/m^2 at 300°C), would cause the calculated void energy to be greater than the energies of all of the other vacancy cluster geometries over the entire size range considered in Figure 3.

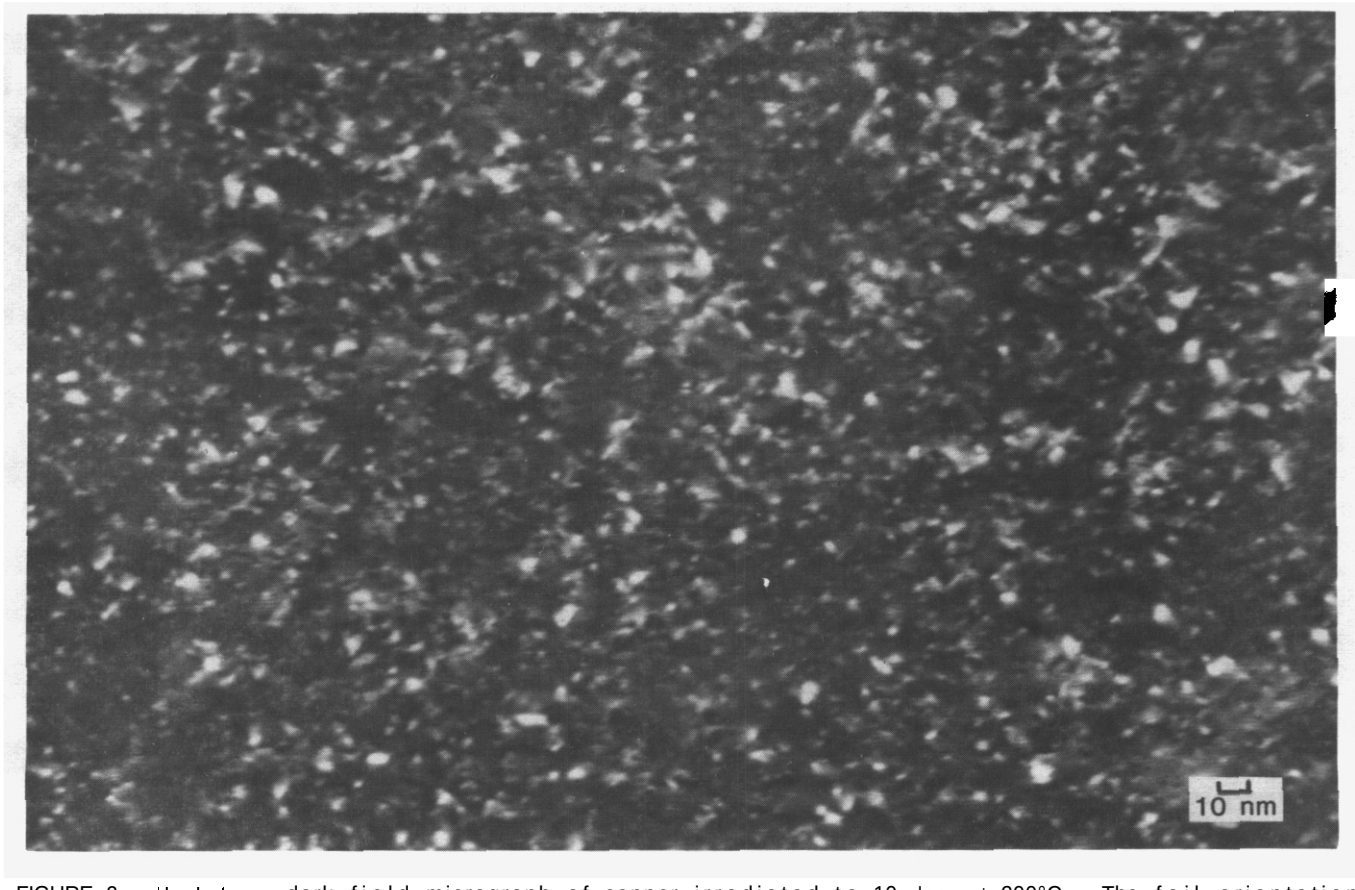

FIGURE 2. Weak beam dark field micrograph of copper irradiated to 10 dpa at 200°C. The foil orientation was close to B = (110) with (g,3g), g = 200.

Figure 4 gives the high-magnification microstructure of pure copper irradiated with Cu ions to 10 dpa at 200°C. Triangle-shaped stacking fault tetrahedra are visible along with other black spot defects that have no definite shape. Preliminary measurements have determined the mean SFT size to be 2.4 nm, with a number density of about $10^{23}/m^3$. SFT were also observed in the pure copper specimens irradidted at 100 and 300°C. Figure 5 shows enlarged black spot defects that are located in the near vicinity of dislocation lines. Since dislocation lines are known to be a preferential sink for interstitials, it appedrs likely that the enlarged black spot defects in Figure 5 may be small interstitial loops which have grown as a result of a favorable incident defect flux. The microstructural observations described above are in very good agreement with the experimental results of Yoshida et al.[15] on 14-MeV neutron irradiated copper

The observation of SFT in irradiated copper is supporting evidence that the elasticity equations used to construct Figure 3 are fundamentally correct. It may be argued that elasticity calculations are not valid at the very small vacancy defect sizes where void nucleation would occur.[13] However, molecular dynamics calculations, which are valid for small defect clusters, support the conclusion that the most stable vacancy cluster structure in pure copper is planar.[12] There have been several reported observations of SFT in irradiated copper and copper alloys (see, e.g., 15-18).

The presence of gas in copper may cause a shift in the energies of the various vacancy cluster configurations. In particular, oxygen is known to decrease the surface energy of pure copper,[19,20] which could make void formation energetically favorable over SFT. Glowinski and co-workers found that copper containing 48 ppm oxygen formed voids easily following electron[21] and ion[22-24] irradiation. Outgassing of the foils in a high-vacuum furnace reduced or completely eliminated void swelling, depending on the experimental

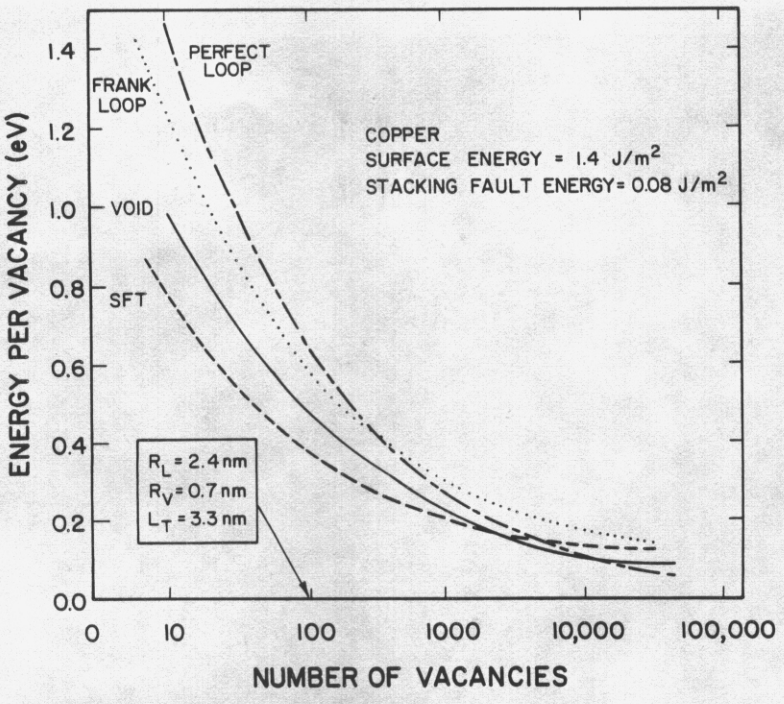

FIGURE 3. Calculated specific energies of vacancy clusters in copper.

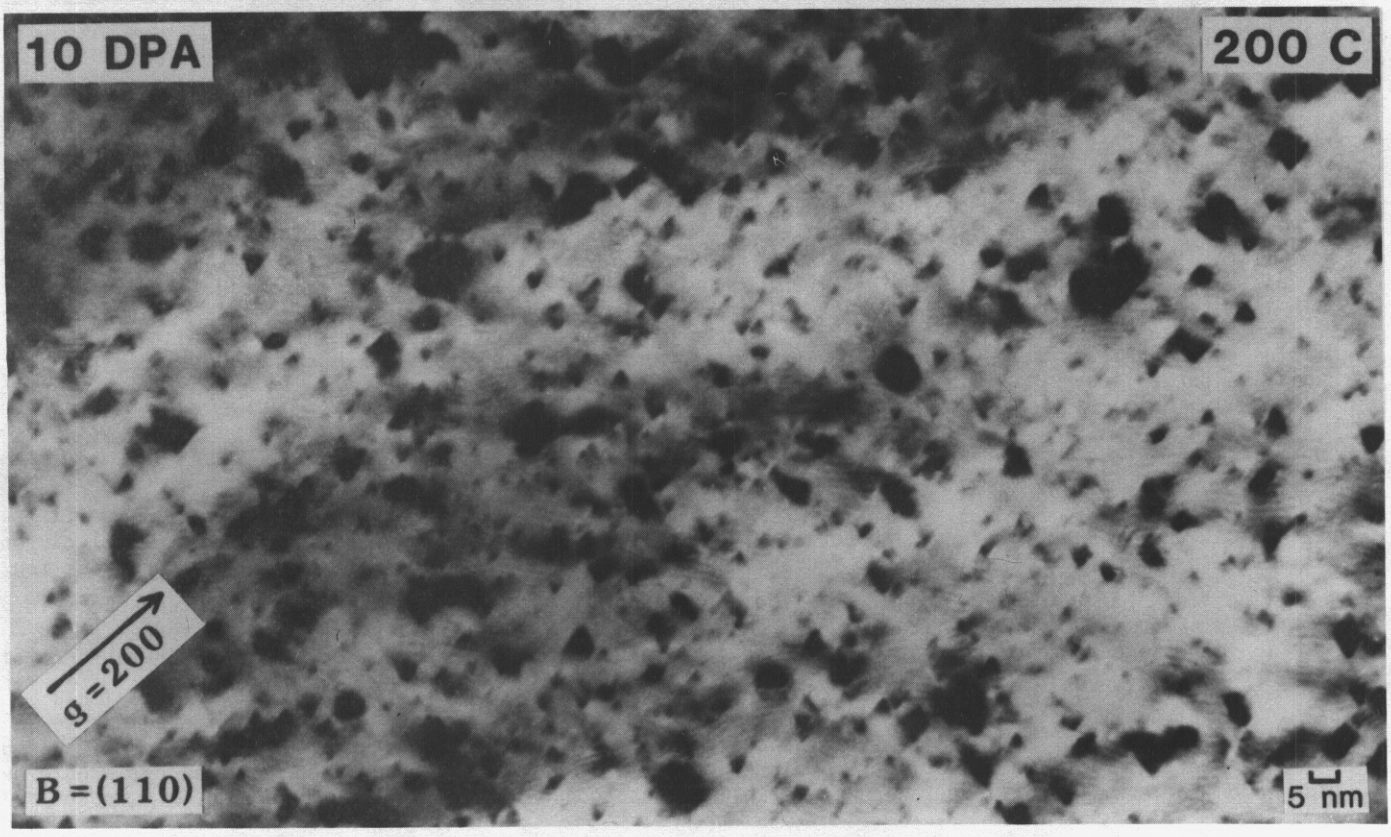

FIGURE 4. Stacking fault tetrahedra (SFT) in ion-irradiated copper.

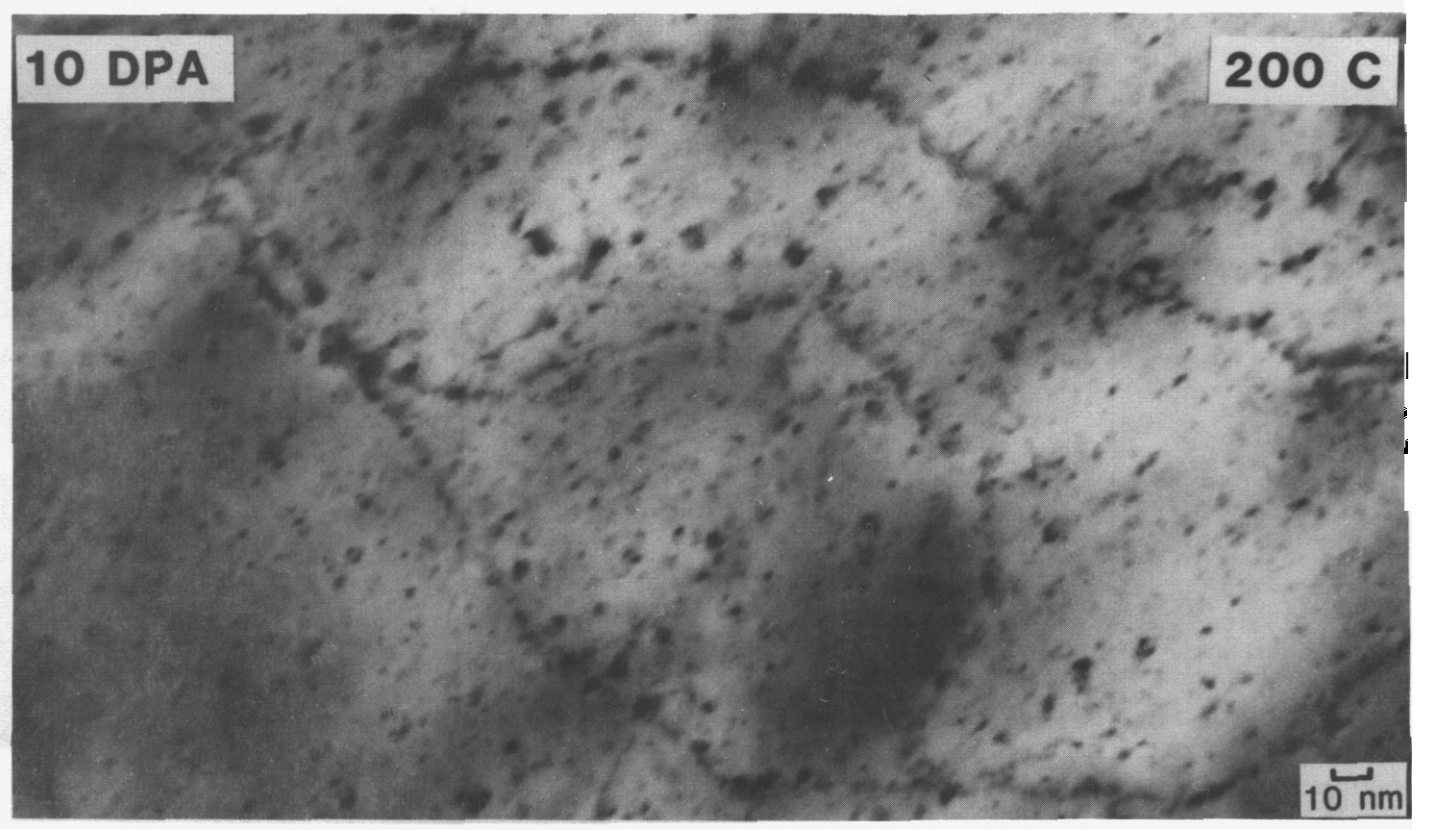

FIGURE 5. Enlarged defect clusters on dislocations in ion-irradiated copper.

conditions. The presence of helium during irradiation may stabilize Small void nuclei and prevent their collapse into loops or SFT. McLaurin observed that high-purity aluminum irradiated with 9-MeV Al ions did not form voids, whereas introduction of as little as 0.1 appm He resulted in copious void formation.[25]

It appears that the bulk of the more than twenty previous charged particle irradiation studies of pure copper and copper alloys that have reported void formation may need to be re-evaluated with regard to their initial gas content. Differences in initial gas concentration may have a strong influence on the types of radiation damage defects that occur during irradiation and could conceivably mask the effects of other irradiation parameters.

5.5 Conclusions

Ion irradiation at 100-400°C of pure copper and two copper alloys which contained very low levels of oxygen resulted in the formation of black spots and SFT, but no voids except in one case (400°C). A previous ion irradiation study[5] of the same lot of annealed pure copper determined that there was no observable void formation at 450 or 500°C. Therefore, we have determined that there *is* no appreciable void formation in single ion irradiated pure copper over the temperature range of 100-500°C ($0.28\text{-}0.59T_M$). In the absence of gas. it appears that stacking fault tetrahedra are the most stable form of vacancy clusters. However a small amount of gas (possibly < 10 appm) may modify the energetics of vacancy cluster configurations so as to cause void formation. Most of the previous charged particle irradiation studies on copper are clouded by the presence of an unknown amount of gas. Future irradiation studies on copper and copper alloys should be performed on foils with a well-known and preferably low gas concentration.

6.0 Acknowledgements

This work was performed under appointment to a Magnetic Fusion Energy Technology Fellowship and with funds supplied by the Department of Energy.

7.0 References

1. F.W. Wiffen and R.E. Gold (Eds.), Copper and Copper Alloys for Fusion Reactor Applications, DOE-OFE Workshop Proceedings (Oak Ridge National Laboratory, CONF-830466, June 1984).

2. S.J. Zinkle and R.W. Knoll, A Literature Review of Radiation Damage Data for Copper and Copper Alloys, University of Wisconsin Fusion Technology Institute Report UWFDM-578, June 1984 (94 pp.. 210 refs.).

3. A. Wolfenden, Rad. Effects 15 (19721 255-8.

4. H.R. Brager, H.L. Heinisch and F.A. Garner, "Effects of Neutron Irradiation at 450°C and 16 dpa on the Properties of Various Commercial Copper Alloys, 1st Intern. Conf. on Fusion Reactor Materials, Tokyo, December 1984.

5. R.W. Knoll, "Effects of Heavy Ion Irradiation on the Phase Stability of Several Copper-Base Alloys", Ph.D. Thesis. Nuclear Engineering Department, University of Wisconsin-Madison (1981), UWFDM-436; also see "Precipitation in Cu-3.4 at % Be Solid Solution During Heavy Ion Irradiation, Parts I and II", accepted for publication in J. Nucl. Mater., November 1984.

6. S.J. Zinkle, R.A. Dodd and G.L. Kulcinski, "Comparison of Thermal and Irradiated Behavior of High Strength, High-Conductivity Copper Alloys", 12th Intern. Symp. on the Effects of Radiation on Materials, June 1984, Williamsburg VA, F.A. Garner and J.S. Perrin, Eds. ASTM 870.

7. S.J. Zinkle, D.H. Plantz, A.E. Bair, R.A. Dodd and G.L. Kulcinski, "Correlation of the Yield Strength and Microhardness of High-Strength, High-Conductivity Copper Alloys", 1st Intern. Conf. on Fusion Reactor Materials, Tokyo, December 1984. Also see DAFS Report DOE/ER-0046/18 (August 1984) p. 143.

8. H.V. Smith and R.G. Lott, Nucl. Instr. Methods 143 (1977) 125-132.

9. D.K. Brice. Sandia National Laboratory Report SAND 75-0622, July 1977, Albuquerque. NM.

10. S.J. Zinkle and R.L. Sindelar, "Preparation of Ion-Irradiated Foils for Cross-section Analysis", DAFS Quarterly Progress Report DOE/ER-0046/18 (August 1984) 133-141.

11. J.A. Sigler and D. Kuhlmann-Wilsdorf, in The Nature of Small Defect Clusters, Vol. 1 (Consultants Symp.), M.J. Makin, Ed., Harwell Report AERE R5269, July 1966, pp. 125-143.

12. N.V. Doan, in Point Defects and Defect Interactions in Metals, J-I Takamura, M. Doyama and M. Kiritani, Eds. (Univ. of Tokyo Press, 1982) p. 722.

13. K.J.C. Cotterill, in The Nature of Small Defect Clusters. Vol. 1 (Consultants Symp.), M.J. Makin, Ed.. Harwell Report AERE R5269, July 1966, pp. 144-172.

14. L.E. Murr, Interfacial Phenomena in Metals and Alloys, Addison-Wesley, (1975).

15. N. Yoshida et al., J. Nucl. Mater. 122/123 (1984) 664-8.

16. A.Y. Stathopoulos et al., Phil Mag. 144 (1981) 309-322 (ion)

17. C.A. English, J. Nucl. Mater. 108/109 (1982) 104-123 (neutron).

18. H. Fujita, T. Sakata and H. Fukuyo, Jap. J. Appl. Physics 21 (1981) L235-6 (electron).

19. W.G. Wolfer, J. Nucl. Mater 122/123 (1984) 367-378.

20. M.F. Felson and P. Regnier, Scripta Met. 11 (1977) 133-6.

21. L.D. Glowinski, J. Nucl. Mater. 61 (1976) 8-21.

22. L.D. Glowinski, C. Fiche and M. Lott, J. Nucl. Mater. 47 (1973) 295-310.

23. L.D. Glowinski and C. Fiche, J. Nucl. Mater. 61 (1976) 22-28.

24. L.D. Glowinski and C. Fiche, J. Nucl. Mater. 61 (1976) 29-40.

25. S.K. McLaurin, "Radiation Damage from Heavy Ion Bombardment in High Purity Aluminum", Ph.D. Thesis, University of Wisconsin-Madison, January 1984. Also see S.K. McLaurin et al., J. Nucl. Mater. 117 (1983) 208.

8.0 Future Work

Annealed pure copper foils have been injected with 30-50 appm H or He and then irradiated with 14-MeV Cu ions over the temperature range of 100-500°C. The results of this investigation will be reported in future quarterly progress reports.

9.0 Publications

None

PHYSICAL PROPERTIES OF HIGH-STRENGTH, HIGH-CONUUCTIVITY COPPER ALLOYS

S.J. Zinkle, D.H. Plantz, R.A. Oodd, and G.L. Kulcinski (University of Wisconsin) and
A.E. Bair (Washington State University)

1.0 Objectives

To investigate the physical properties of two high-strength, high-conductivity copper alloys as a function of heat treatment and to establish a correlation between microhardness and yield strenuth. In conjuction with microstructural studies, this will allow for an estimation to be made of the effects of irradiation on the properties of these alloys.

2.0 Summary

Vickers microhardness, electrical resistivity, and miniature tensile specimen measurements were made on AMZIRC and AMAX-MZC copper alloys in the cold-worked plus aged and annealed conditions. It was determined that a large portion of the strength of these alloys is due to their cold-worked nature, and this strength is lost when recrystallization occurs. The recrystallization temperature of both alloys is about 475°C for a 1 hour anneal, and is estimated to be about 320°C for a 20 year anneal. A linear correlation between microhardness and yield strength was observed for AMZIRC and AMAX-MZC, namely σ_y (MPa) ≈ 3.0 VHN. The electrical conductivity of both alloys increased to a value near 100% IACS following thermal annealing at intermediate temperatures.

3.0 Program

Title: Radiation Effects to Reactor Materials
Principal Investigators: G.L. Kulcinski and R.A. Oodd
Affiliation: University of Wisconsin-Madison

4.0 Relevant DAFS Program Plan Task/Subtask

Subtask II.C.l.l Phase Stability Mechanics
Subtask II.C.l.l Modeling and Analysis of Effects of Materials Parameters on Microstructures

5.0 Accomplishments and Status

5.1 Introduction

One of the key material parameters that is used to characterize potential fusion reactor materials is the yield strength. Unfortunately, there are many instances where it is impractical to irradiate conventional tensile specimens to obtain this information. The irradiation volume is often of limited size, and it is therefore desirable to be able to extract mechanical property information from nonstandard, subsized specimens.[1] One procedure for estimating the yield strength of irradiated metals is to make use of available correlations between microhardness measurements and tensile data. (*) The use of nondestructive microhardness testing also allows the irradiated specimen to be subsequently analyzed using other experimental techniques, e.g. transmission electron microscopy (TEM).[3] There are presently no known microhardness yield strength correlations for high-strength, high conductivity copper alloys. In a continuation

of previous work[4-6], this investigation establishes a correlation between strength and hardness tor two of these copper alloys. Electrical resistivity measurements are included as part of the investigation of the alloys' physical properties.

5.2 Experimental Procedure

Two commercial hiyh-strength, high-conductivity copper alloys were selected tor an investigation of their mechanical properties. AMZIRC (Cu-0.15 Zr) and AMAX-MZC (Cu-0.04 big-0.15 Zr-0.8 Cr) are heat treatable materials that have yield strengths of 400-500 MPa and electrical conductivities of 80-90% ICCS (International Annealed Copper Standard).[**] Foils of 250 μm thickness were obtained from AMAX Copper, Inc. in both the cold-worked plus aged (CWA) condition and in the solution annealed plus aged (SAA) condition. The CWA heat treatment consisted of a solution anneal, followed by 90% cold-rolling and then aging for 30 minutes at 375°C tor the AMZIRC alloy and 400°C for the MZC alloy. Some of these foils were sutseouently solution annealed at 950°C for 100 hours and quenched in water (SA condition). The SAA heat treatment consisted of a solution anneal at 930°C for 45 minutes followed by aging for one hour at 450°C for AMZIRC and 500°C for MZC.

Specimens of the alloys in the CWA condition with dimensions of 0.5 by 5 cm were annealed tor tines ranging from 0.25 to 100 hours.[5] Electrical resistivity[4] and Vickers microhardness[5] measurements were made at room temperature on the as-received and the CWA plus annealed specimens using techniques that were previously described. Additional resistivity measurements were made on specimens in the CWA and SAA condition at 77 K and 4.2 K.

Miniature tensile specimens were punched from the as-received and annealed toils and deburred using procedures that are described in detail elsewhere.[8] The nominal dimensions of the gage section were 5.1 by I.U by 0.25 mm. The actual cross-sectional area tar each tensile specimen was determined by measuring the width and thickness of the gage section at five different locations and averaging the results. A minimum of two tensile specimens were tested in the longitudinal direction for each of the annealing conditions in this study using a precision horizontal test trame with a free-running crosshead speed of 2.5 μm/s. Data tor each tensile test were collected at room temperature in both a digital and analog manner. The 0.2 percent offset yield strength (σ_Y) and ultimate tensile strength (UTS) were calculated using a computer based digital data acquisition program. The strength parameters of selected specimens were also calculated by graphical techniques using the analog data. The results were in good agreement with the computer-generated values.

5.3 Results

Table 1 lists the measured room temperature mechanical properties of AMZIRC and AMAX-MZC in the SA, SAA and CWA condition. Within the scatter of the data, there was no difference in the mechanical properties as measured in the transverse and longitudinal directions. The AMZIRC alloy develops high strength only after cold work plus aging, and shows minimal precipitation hardening. AMAX-MZC exhibits appreciable precipitation hardening, but once again most of its strength in the CWA condition can be attributed to cold work effects.

The microhardness numbers of AMZIRC and MZC specimens which were initially in the CWA condition are shown in Figs. 1 and 2 as a function of anneal conditions. The arrows indicate the microhardness numbers for the alloys in the solution annealed condition, These figures have been updated from previously published results[5] to include the 100 hr data. The recrystallization temperature (i.e., the temperature where the microhardness decreases rapidly) depends on the annealing time and is about 475°C for both AMZIRC and AMAX-MZC for a one hour anneal. It has been empirically established that the recrystallization rate of metals follows an Arrhenius relationship.[9] The annealing data may therefore be plotted as a single curve by making use of the Larson-Miller parameter,[10] as shown in Fig. 3 for both alloys. Table 2 summarizes the extrapolated time-dependent recrystallization temperatures obtained from this analysis. The curves predict a recrystallization temperature of 320°C for both AMZIRC and MZC for a 20 year anneal, which is the maximum design lifetime of a copper alloy device in a fusion reactor.[***]

TABLE 1

MEASURED MECHANICAL PROPERTIES OF AMZIRC AND AMAX-MZC at 22°C

Alloy	Heat Treatment	Micro-hardness	Yield Strength (0.2% Offset)	Tensile Strength	Elongation in 5.1 mm
AMZIRC	SA	50 HV	110 MPa	150 MPa	21%
	SAA	51 HV	140 MPa	220 MPa	21%
	CWA	146 HV	440 MPa	500 MPa	9%
MZC	SA	46 HV	90 MPa	120 MPa	14%
	SAA	78 HV	220 MPa	260 MPa	23%
	CWA	168 HV	490 MPa	540 MPa	9%

SA = solution annealed; SAA: solution annealed, then aged; CWA: 90% cold-worked, then aged

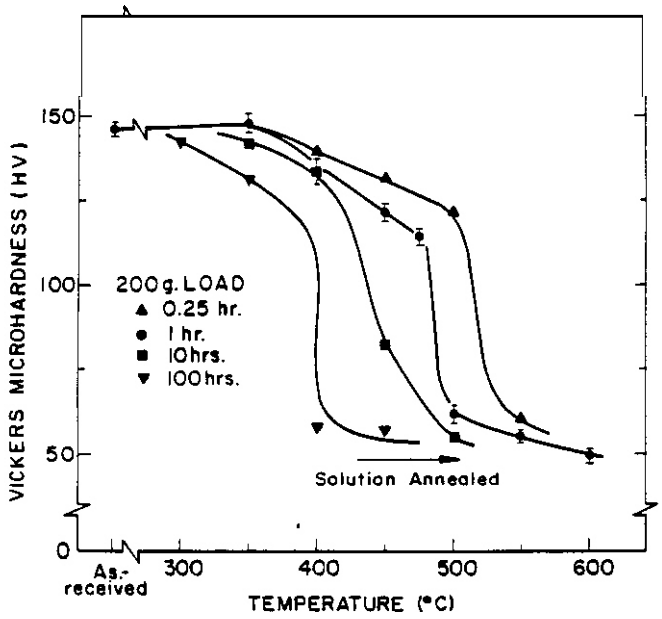

FIGURE 1. Vickers microhardness of cold-worked plus aged (CWA) AMZIRC as a function of annealing time and temperature.

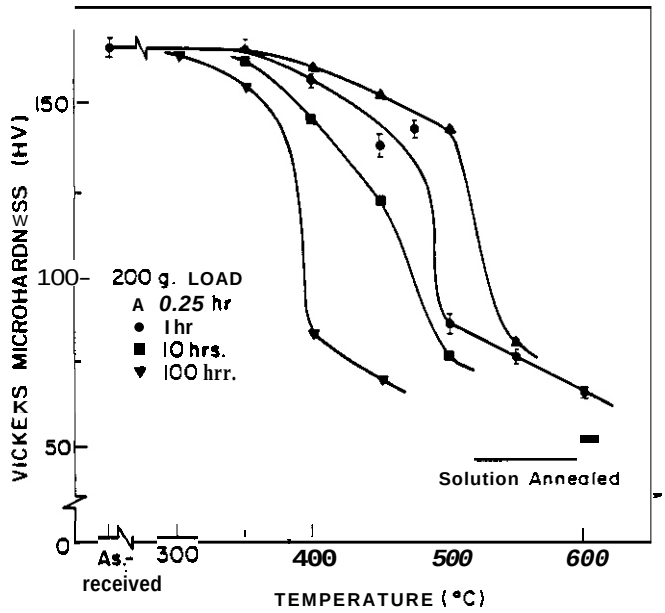

FIGURE 2. Vickers microhardness of cold-worked plus aged (CWA) AMAX-MZC as a function of annealing time and temperature.

TABLE 2

PREDICTED RECRYSTALLIZATION TEFIPERATURE (T_R) OF AMZIRC AND AMAX-MZC

Anneal Time	1 Month	1 Year	10 Years
T_R	380°C	350°C	330°C

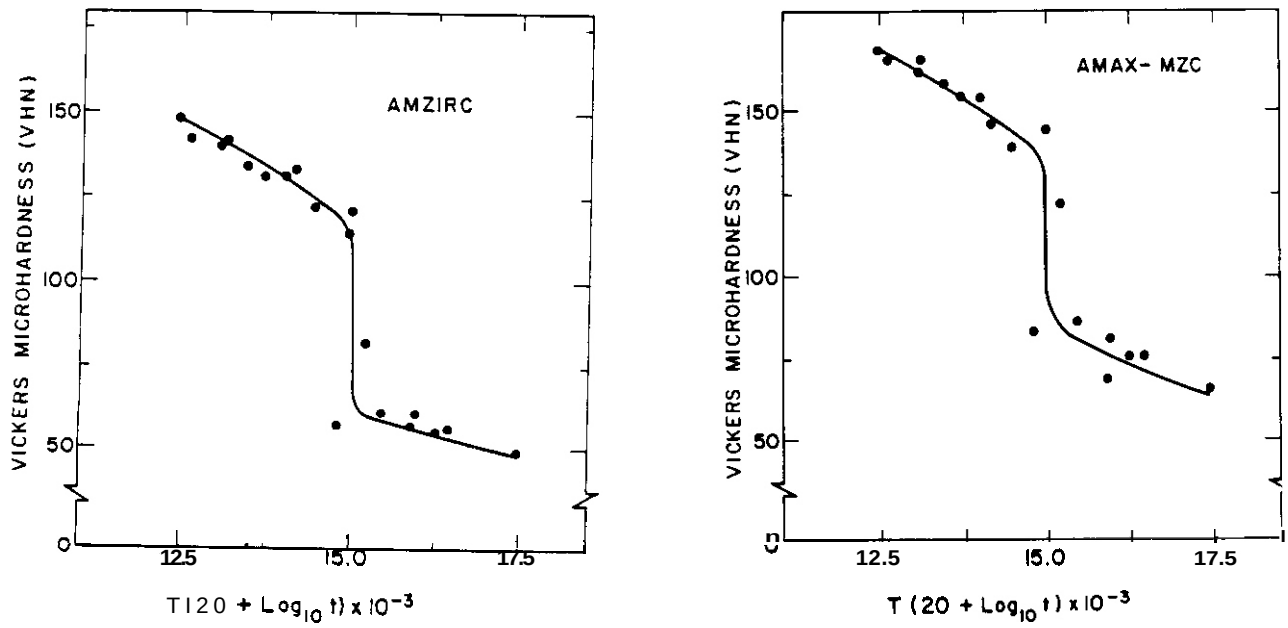

FIGUFE 3. Vickers microhardness of CWA AMZIRC (left) and AMAX-MZC (right) plotted as a function of the Larson-Miller parameter. The curve contains all of the data shown in Figures 1 and 2.

Comparison of the measured Vickers microhardness number and yield strength of cold worked plus aged AMZIRC and AMAX-MZC specimens in their as-received and dnnealed states leads to a linear relationship. The yield strength-microhardness correlation plots for AMZIRC and AMAX-MZC are given in Figs. 4 and 5. Data for the alloys in the SA and SAA conditions are also included in these plots. A direct, linear correlation between Vickers microhardness (VHN) and yield strength (σ_Y) exists over the entire range of conditions investigated. The correlation equations that described the least squares fit to the data are, for AMZIRC

$$a_Y(MPA) = 3.03\ VHN - 38 \qquad (1)$$

and for AMAX-MZC,

$$\sigma_y = 3.00\ VHN - 17\ . \qquad (2)$$

The fact that the correlation plots have a small nonzero intercept is believed to indicate that the correlations are not applicable for very low strength alloys (< 100 MPa yield strength). However, it should be noted that this strength level is less than the solution annealed yield strengths of the alloys.

TABLE 3

MEASURED ELECTRICAL PROPERTIES OF AMZIRC AND AMAX-MZC

Alloy	Heat Treatment	Resistivity ($n\Omega$-m) 295 K	77 K	4.2 K	RRR = ρ 295/ρ 4.2	Conductivity (22°C)
AMZIRC	SAA	23.5 ± 0.2	8.3 ± 0.2	5.9 ± 0.1	4.0	76% IACS*
	CWA	22.9 ± 0.8	6.5 ± 0.6	4.0 ± 0.3	5.7	77% IACS
MZC	SAA	33.2 ± 0.6	18.7 ± 0.9	18.3 ± 0.9	1.5	54% IACS
	CWA	29.4 ± 0.6	14.4 ± 0.8	13.5 ± 0.8	2.2	58% IACS

SAA = Solution annealed plus aged, CWA = cold worked plus aged.
*IACS = International Annealed Copper Standard

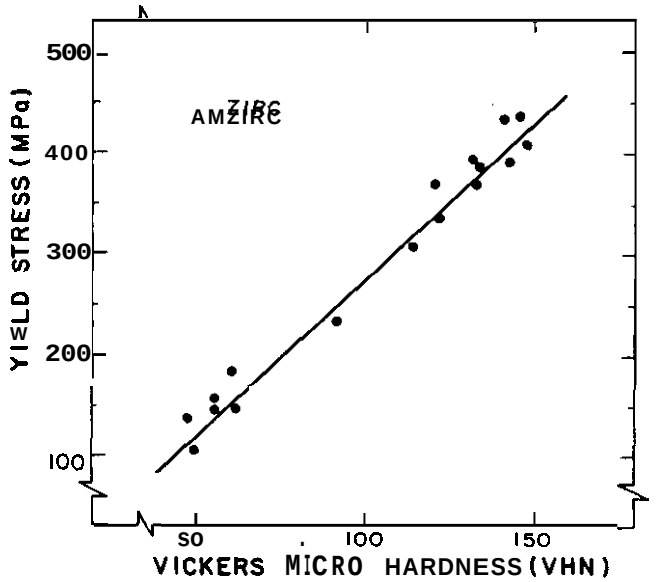

FIGURE 4. Yield strength - microhardness correlation plot for CWA and annealed AMZIRC.

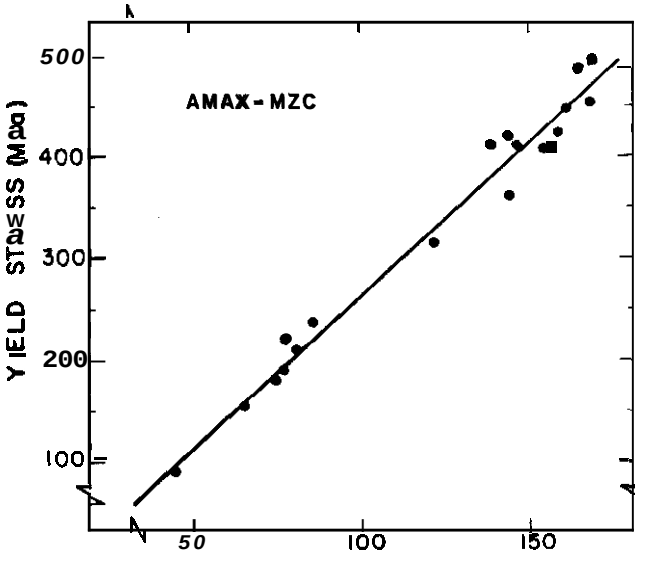

FIGURE 5. Yield strength - microhardness correlation plot for CWA and annealed AMAX-MZC.

The measured electrical properties of AMZIRC and AMAX-MZC in the SAA and CWA conditions are listed in Table 3. A comparison of these conditions for both alloys shows that cold-working prior to aging has a negligible effect on the electrical conductivity at room temperature. The room temperature conductivity of AMZIRC is about 40% larger than that of AMAX-MZC for both heat treatment conditions.

Figure 6 compares the room temperature electrical conductivity of the two as-received alloys as a function of temperature for a 1 hour anneal. The conductivities of both alloys increased steadily for anneal temperatures less than 550°C. The maximum electrical conductivities were about 100% IACS and 95% IACS for AMZIRC and AMAX-MZC, respectively. Thermal annealing at temperatures above 550°C caused the conductivity to decrease from the maximum value. This effect has been previously observed in Cu-Zr and Cu-Cr-Zr alloys,[12,13] and is probably due to solute reentering solution from the precipitates.

TABLE 4

GRAIN SIZE AND MINIMUM THICKNESS TO GRAIN SIZE RATIO (T/D) FOR MINIATURE TENSILE SPECIMENS

	Solution Annealed		Solution Annealed Pluc Aged		Cold-worked plus Aged: Annealed 1 hr, 600°C		Cold-worked plus Aged: No Anneal	
	AMZIRC	MZC	AMZIRC	MZC	AMZIRC	MZC	AMZIRC	MZC
Grain size (μm)	300	270	60	26	12	9	<1	<1
t/d	1	1	4	10	20	28	>250	>250

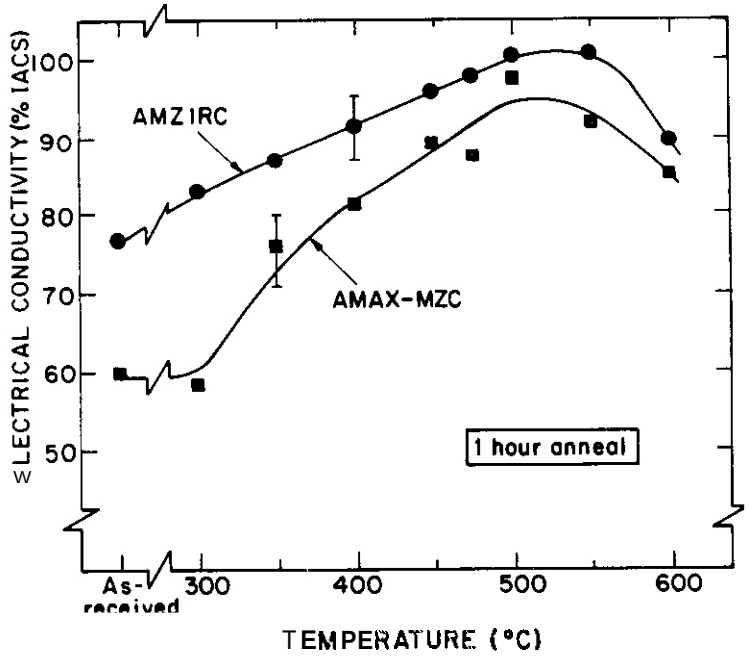

FIGURE 6. Electrical conductivity at 22°C of as-received copper alloys following a 1 hour thermal anneal.

5.4 Discussion

The average grain size and minimum thickness to grain size ratio (t/d) are given in Table 4 for the tensile specimens examined in this study. The number of grains across the smallest dimension of the tensile specimen was greater than twenty for all specimens except for the solution annealed and solution annealed plus aged alloys. A common rule-of-thumb is that at least ten grains across the smallest cross-sectional dimension of a tensile specimen are required to obtain bulk behavior.[8] Researchers have found that there is no grain size effect on the measured yield or tensile strength for miniature tensile specimens of austenitic or ferritic steel as long as $t/d > 3\text{-}5$.[8,14] Therefore, the miniature tensile specimen results should be representative of the bulk strength except possibly for AMZIRC in the SA and SAA conditions and MZC in the SA condition.

A slight peculiarity was noticed in the elongation data of AMZIRC and MZC in the SA and SAA conditions (Table 1). The measured elongation to fracture was greater for the aged alloys compared to the solution annealed condition, as was the strength of both alloys. Ductility generally decreases when strength increases, but there are many exceptions to this rule.[15] The observed increase in ductility is probably due to grain size effects. Ductility is known to increase with decreasing grain size,[15] and the SAA alloys have a much smaller grain size than the SA alloys (Table 2) due to different solution annealing treatments.

One valid criticism of the experimental procedure followed in this investigation is that all tensile specimens were punched from foils after they had been annealed. It is uncertain whether edge deformation due to punching has a significant effect on the measured mechanical properties of annealed miniature tensile specimens.

It is surprising that the correlation plot of yield strength and Vickers microhardness number is linear over the entire range of possible thermomechanical conditions for AMZIRC and MZC. We have previously shown[5] that the microstructures of the two alloys changed dramatically following the various annealing schedules. The slope of the correlation plot should depend on the work-hardening coefficient,[16,17] which increased significantly after annealing of the cold-worked plus aged alloys. The slope of the correlation plot was the same for both the precipitation-hardenable alloy (AMAX-MZC) and the alloy which does not exhibit appreciable precipitation hardening effects (AMZIRC). The derived correlation for these high-strength. high-conductivity copper alloys, $\sigma_y \sim 3.0$ VHN, is identical to the relation found for the strength increase in copper and copper alloys due to radiation hardening.[18] Similar correlation results have been reported for nonirradiated copper and other metals.[16,19]

Evaluation of the data presented in Figures 1-6 reveals that a variety of combinations of strength and electrical conductivity are possible for AMZIRC and AMAX-MZC. It is evident that AMZIRC is generally superior to AMAX-MZC in terms of maximum achievable conductivity. On the other hand, ANAX-MZC is capable of a larger yield strength value than AMZIRC at a given operating temperature. The best combination of high strength and conductivity is obtained by aging the alloys at conditions slightly below that required for recrystallization. The resultant optimum yield strength and electrical conductivity values are (350 MPa, 90% IACS) for AIIZIRC and (400 MPa, 85% IACS) for AMAX-MZC.

5.5 Conclusions

The recrystallization rate of cold-worked plus aged AMZIRC and AMAX-MZC copper alloys following short term thermal annealing apparently obeys an Arrhenius relationship. The recrystallization temperature for a 1 hour anneal is about 475°C for both alloys. The estimated recrystallization temperature for AMZIRC and AMAX-MZC for a 20 year anneal is about 320°C in the absence of stress or irradiation effects.

A linear correlation between yield strength and Vickers microhardness exists over a wide range of thermomechanical conditions for AMZIRC and AMAX-MZC. The relationship for both alloys is given by σ_Y(MPa) ≃ 3.0 VHN.

The electrical conductivity of AMZIRC and AMAX-MZC is controlled mainly by the character of their alloying elements, i.e. the relative partitioning of solute between precipitates and solid solution.

6.0 Acknowledgements

The authors gratefully acknowledge the assistance of N.F. Panayotou during the course of this investigation. We would like to thank A.R. Graviano of AMAX Copper, Inc. for supplying the copper foils and H.L. Heinisch for performing the digital data analysis of the tensile specimens. Some of this work (S.J.Z.) was performed under appointment to the Magnetic Fusion Energy Technology Fellowship Program and (A.E.B.) with funds supplied by the U.S. Department of Energy under contract DE-1AM06-76-RLO2225 (NORCUS Fellowship Program).

7.0 References

1. Symp. on Use of Nonstandard Subsized Specimens for Irradiated Testing, Albuquerque, NM, Sept. 1983; proceedings to be published by ASTM.

2. G.E. Lucas and N.F. Panayotou, J. Nucl. Mater. 103/104 (1981) 1527. See also N.F. Panayotou, J. Nucl. Mater. 108/109 (1982) 456.

3. H.R. Brager, et al., J. Nucl. Mater. 1031104 (1981) 955.

4. S.J. Zinkle, S.N. Farrens, G.L. Kulcinski and R.A. Dodd, DAFS Quarterly Progress Report DOEIER-0046115 (Nov. 1983) p. 127.

5. S.J. Zinkle, D.H. Plantz, R.A. Dodd and G.L. Kulcinski, DAFS quarterly Progress Report DOEIER-0046117 (May 1984) p. 110.

6. S.J. Zinkle, D.H. Plantz, G.L. Kulcinski and R.A. Dodd, DAFS Quarterly Progress Report DOE/ER-0046/18 (Aug. 1984) p. 143.

7. Interim Publications on AMZIRC and ANAX-MZC Copper Alloys, AMAX Copper, Inc., New York, New York (1982).

8. N.F. Panayotou, "Design and Use of Nonstandard Tensile Specimens for irradiated Materials Testing", in ref. 1.

9. R.E. Reed-Hill, Physical Metallurgy Principles, 2nd Ed. (Brooks/Cole, 1973) 286.

10. E.A. Wilson, "Worked Examples in the Kinetics and Thermodynamics of Phase Transformations", Inst. Metallurgists Monograph No. 7 (Chameleon Press Ltd., London).

11. F.W. Wiffen and R.E. Gold, Eds, "Copper and Copper Alloys for Fusion Reactor Applications", DOE-OFE Workshop Proceedings, (Oak Ridge National Laboratory, CONF-830466, June 1984).

12. T. Maruta, J. Japan Copper and Brass Res. Assn. 2, No. 1, (1983) 89-96.

13. T. Hagai, Z. Henmi, T. Sakamoto and S. Koda, Trans. JIM 14 (6) Nov. 1973, 462-9

14. N. Igata et al., "The Specimen Thickness Effects on the Strength Properties of Austenitic Stainless Steels" and D.G. Rickerby, "Comparison of Mechanical Properties in Thin Specimens of Stainless Steel with Bulk Material Behavior", in Ref. 1.

15. G.E. Dieter in Ductility, ASM Seminar, October, 1967, H.W. Paxton, Ed. (American Soc. Metals, Metals Park, Ohio, 1968) 19-24.

16. J.R. Cahoon, W.H. Broughton and A.R. Kutzak, Metall. Trans. 2 (1971) 1979

17. J.G. Tweedale, Mechanical Properties of Metals (Elsevier, 1964) 166.

18. S.J. Zinkle and G.L. Kulcinski, "Low-Load Microhardness Changes in 14 MeV Neutron Irradiated Copper Alloys", in Ref. 1.

15. J.J. Gilman in "The Science of Hardness Testing and its Research Applications", J.H. Westbrook and H. Conrad, Eds. (American Soc. Metals, 1973) 55.

8.0 Future Work

Measurements will be made of the physical properties of Cu-Be-Ni

9.0 Publications

Most of this report was presented in a paper by the same authors entitled "Correlation of the Yield Strength and Microhardness of High-Strength, High-Conductivity Copper Alloys", 1st Intern. Conf. on Fusion Reactor Materials, Tokyo, December 1984, to be published in J. Nucl. Mater.

EXTERNAL DISTRIBUTION

UC-20 (112), 20c (66)

DOE-HQ/Office of Fusion Energy
ER-62
Washington, DC 20545

SE Parket

DOE-HQ/Office of
International Security Affairs
DP-33, Mail Stop 41-024
Washington, DC 20585

DW Dorn

Argonne National Laboratory (3)
9700 South Cass Avenue
Argonne, It 60439

LR Greenwood, CMT-205
A. Taylor, MST-712
BA Loomis, EST-212

Battelle
Pacific Northwest Laboratory (2)
P.O. Box 999
Richland, WA 99352

JL Brimhall 306W/210
TD Chikalla PSL/1277

Carneqie-Mellon University
Metallurgical Engineering
3325 Science Hall
Pittsburgh, PA 15213

WM Garrison Jr

Columbia University
School of Engineering & Applied Science
New York, NY 10027

RA Gross

Coinmission of the European Communities
Rue de la Loi 200
R-1049 Bruxelles, Belgium

J. Darvas

Commission of the European Communities
Joint Research Center
Materials Science Division
1-21020 Ispra, Varese, Italia

P. Schiller

Department of the Navy
Naval Research Laboratory (2)
Washington, DC 20375

JA Sprague, Code 6395
LE Steele, Code 6390

Energieonderzoek Centrum Nederland (2
Netherlands Energy Research Foundation
Westerduinweq 3, Postbus 1
NL-1755 ZG, Petten (NH), The Netherlands

R. vanderSchaaf
W. vanWitzenburg, Materials Dept

GA Technologies Inc (3)
P.O. Box 85608
San Dieqo, CA 92138

JR Gilleland
GR Hopkins
T. Lechtenberq

General Dynamics/Convair
P.O. Box 85377
San Diego, CA 92138

H. Gurol, MZ 92-1072

General Electric
Advanced Nuclear Technology Operation (2)
310 DeGuign Drive
Sunnyvale, CA 94088

ANTO Library, M/C F-02
S. Vaidyanathan, M/C 5-53

Hahn-Meitner Institut fur Kernforschung Berlin GmbH
Arbeitsgruppe C2
Glienickerstrasse 100
D-1000 Berlin 39, Federal Republic of Germany

H. Wollenberger

Hokkaido University (2)
Facility of Enqineering
Kita-hu, Sapporo, 060 Japan

Michio Kiritani, Precision Engineering
Taro Takeyama, Metals Research Institute

Institut fur Festkörperforschung der
Kernforschungsanlage Jülich GmbH
Postfach 1913
D-5170 Jülich 1, Federal Republic of Germany

P. Jung

Japan Atomic Energy Research Institute (2)
Physical Metallurgy Laboratory
Tokai Research Establishment
Tokai-mura, Naka-qun, Ibaraki-ken, 319-11 Japan

Tadao Iwata, Physics
Kensuke Shiraishi, Fuels Materials Research

Kernforschungszentrum Karlsruhe GmbH
Institut fur Material und Festkorperforschunq II
Postfach 3640
D-7500 Karlsruhe 1, Federal Republic of Germany

K. Ehrlich

EXTERNAL DISTRIBUTION (Cont'd)

Kyushu University
Research Institute for Applied Mechanics
6 Kasuga-Koen, Kasuga-shi
Fukuoka, 816 Japan

Kazunori Kitajinia

Lawrence Livermore National Laboratory (2)
P.O. Box 808
Livermore, CA 94550

MW Guinan, L-396
DW Heikkinen

Lawrence Livermore National Laboratory
P.O. Box 5511
Livermore, CA 94550

EC Dalder, L-643

Los Alamos National Laboratory
P.O. Box 1663
Los Alamos, NM a7544

OJ Dudziak, S-41F611

Massachusetts Institute of Technology (2)
77 Massachusetts Avenue
Cambridge, MA 02139

I-Wei Chen, 13-5118
NJ Grant, 8-407

Massachusetts Institute of Technology
Nuclear Reactor Laboratory
138 Albany St
Cambridge, MA 02139

OK Harling, NW12-204

Max-Planck-Institüt fur Plasma Physik (2)
The NET Team, IPP/NET
D-8049 Garching bei München.
Federal Republic of Germany

DR Harries
R. Toschi

McDonnell-Douglas Astronautics Co
P.O. Box 516
St. Louis, MO 63166

JW Davis

Nagoya University
Institute of Plasma Physics
Furo-chyo, Chikusa-ku,
Nagoya, 464 Japan

Taijiro Uchida

National Research Institute for Metals
Tsukuba Laboratories
1-2-1 Sengen, Sakura-mura,
Nihari-qun, Ibaraki, 305 Japan

H. Shiraishi

North Carolina State University
Box 7907
Materials Engineering Department
Raleigh, NC 27695-7907

JR Beeler Jr

Oak Ridge National Laboratory (7)
P.O. Box X
Oak Ridge, TN 37831

ML Grossbeck
MCG Hall
LK Mansur
PJ Maziasz
NH Packan
M. Roberts
RE Stoller

Oak Ridge National Laboratory (2)
P.O. Box Y
Oak Ridge, TN 37831

LA Berry
FW Wiffen, FEDC Bldg

Osaka University
2-1 Yamada-oka, Suita,
Osaka, 565 Japan

Kenji Sumita, Nuclear Engineering

Osaka University
8-1 Mihogaoka
Ibaraki, Osaka, 567 Japan

Toichi Okada, Institute of
Scientific & Industrial Research

Pacific Sierra Research Corp
11048 Camino Del Mar
Del Mar, CA 92014

RD Stevenson

Princeton University (2)
Plasma Physics Laboratory
Forrestal Campus
P.O. Box 451
Princeton, NJ 08544

JPF Conrads
Long-poe Ku

Risa National Laboratory
Postfach 49
DK-4000 Roskilde, Denmark

BN Singh

EXTERNAL DISTRIBUTION (Cont'd)

Rockwell International Corp
Rocketdyne Division
6633 Canoga Avenue
Canoga Park, CA 91304

DW Kneff, NA02

Sandia National Laboratories
Livermore, CA 94550

WG Wolfer

Science University of Tokyo
Faculty of Engineering
Kagurazaka, Shinjuku-ku,
Tokyo, 162 Japan

RR Hasiguti

Studiecentrum voor Kernenergie
Centre d'Etude de l'Energie Nucleaire
Boeretang 200
B-2400 Mol, Belgium

J. Nihoul

Swiss Federal Institute
for Reactor Research (2)
CH-5303 Wurenlingen, Switzerland

WV Green
M. Victoria

Tohoku University (2)
Research Institute for Iron,
Steel and Other Metals
2-1-1 Katahira, Sendai, 980 Japan

Katunori Abe
Hideki Matsui

Tokyo Institute of Technology
Research Laboratory for Nuclear Reactors
12-1, 2-chome, O-Okayama
Meguro-ku, Tokyo, 152 Japan

Karutaka Kawamura

United Kingdom Atomic Energy Authority
Atomic Energy Research Establishment (2)
Oxfordshire OX11 ORA, UK

R. Bullough, Theoretical Physics

United Kingdom Atomic Energy Authority
Culham Laboratory
Applied Physics & Technology Division
Abingdon, Oxfordshire OX14 3DB, UK

GJ Butterworth

University of California (2)
School of Engineering and Applied Science
Boelter Hall
Los Angeles, CA 90074

RW Conn, KL-98
NM Ghoniem, KH-01

University of Michigan
Nuclear Engineering
Ann Arbor, MI 48109

T. Kammash

University of Missouri
Mechanical & Aerospace Engineering
1006 Engineering Bldg
Columbia, MO 65211

M. Jolles

University of Missouri
Dept of Nuclear Engineering
Rolla, MO 65401

A. Kumar

University of Tokyo (3)
3-1, Hongo 7-chome,
Bunkyo-ku, Tokyo, 113 Japan

Naohira Igata, Met & Materials Science
Shiori Ishino, Nuclear Engineering
Shuichi Iwata, Nuclear Engineering

University of Virginia
Dept of Materials Science
Thornton Hall
Charlottesville, VA 22901

WA Jesser

Westinahouse
Advanced Energy Systems Division
Fuels Materials Technology
P.O. BOX 10864
Pittsburgh, PA 15236

A. Boltax, Manager

Westinghouse
Research and Development Center
310 Beulah Road
Pittsburgh, PA 15235

JA Spitznagel

INTERNAL DISTRIBUTION

DOE-RL/AME
Breeder Technology Division
Technology Development & Enaineering Branches
FED/210

KR Absher, Chief

HEDL (28)

SD Atkin	W/A-58	C. Martinez	W/A-58
HR Rrager	W/A-58	WN McElroy	W/C-39
LL Carter	W/B-47	EK Opperman	W/A-58
DG Doran	W/A-57	RW Powell	W/A-58
MJ Korenko	W/C-27	R J Puigh	W/A-58
FA Garner	W/A-58	FH Ruddy	W/C-39
DS Gelles	W/A-58	FA Schmittroth	W/A-58
R. Gold	W/C-39	WF Sheely	W/C-20
HL Heinisch	W/A-58	RL Simons	W/A-65
DL Johnson	W/B-41	JL Straalsund	W/A-61
GD Johnson	W/A-65	HH Yoshikawa	W/C-44
NE Kenny	W/C-115	Central Files (3)	W/C-110
FM Mann	W/A-58	Documentation Services	W/C-123